NONLINEAR FREQUENCY DOMAIN ANALYSIS AND DESIGN OF VEHICLE SUSPENSION SYSTEMS

CHEN YUE

M.Phil

The Hong Kong Polytechnic University

2013

The Hong Kong Polytechnic University

Department of Mechanical Engineering

Nonlinear Frequency Domain Analysis and Design of Vehicle Suspension Systems

CHEN YUE

A thesis submitted in partial fulfillment of the requirements for the degree of Master of Philosophy

July 2012

CERTIFICATE OF ORIGINALITY

I hereby declare that this thesis is my own work and that, to the best of my knowledge and belief, it reproduces no material previously published or written, nor material that has been accepted for the award of any other degree of diploma, except where due acknowledgement has been made in the text.

______________ (Signed)

CHEN YUE____ (Name of student)

ABSTRACT

In the analysis and design of vehicle suspension systems, springs and dampers, which are usually inherently nonlinear, are the most crucial elements to improve the ride comfort, assure the stability and increase the longevity of spring to a large extent. Therefore, it is of great significance to determine proper stiffness and damping characteristics to meet various requirements in practice. In this study, a nonlinear frequency domain analysis method is introduced for nonlinear analysis and design of vehicle suspension systems. The explicit relationship between system output spectrum and model parameters is derived by using the nonlinear frequency domain analysis method and the characteristic parameters of interest can therefore be analyzed directly. The optimal nonlinear stiffness and damping characteristics of the nonlinear vehicle suspension system can then be achieved. Comparative studies indicate that the optimal nonlinear damping characteristics demonstrate obviously better dynamic performance than the corresponding linear counterparts and the existing nonlinear optimal damping characteristics. Simulation studies based on the full vehicle dynamic model verify the nonlinear advantages in terms of three different vehicle evaluation standards. The study shows that the nonlinear optimal damping characteristic obtained by using the nonlinear frequency domain analysis method is very helpful in the improvement of vehicle vibration performance and decrease of suspension stroke. Meanwhile, the optimal nonlinear damper will not cause any negative effect on the handling capability.

PUBLICATIONS

Yue Chen, Xingjian Jing, Li Cheng, Investigation of a Nonlinear Vehicle Suspension System Using Frequency Domain Analysis Method. Proceedings of the 14th Asia Pacific Vibration Conference, Hong Kong, pp.473-481, 5-8 December 2011

ACKNOELEDGEMENTS

I would like to express my deepest gratitude to my supervisors, Dr. Xingjian Jing and Prof. Li Cheng, for introducing me to the field of nonlinear system dynamics. Dr. Jing is an enthusiastic and responsible researcher, and he provided continuous support during the preparation of my thesis. Throughout my whole graduate study, he also provided encouragement, advice and the method for me to do good research. Meanwhile, I would like to give my special thanks to Prof. Cheng for sharing his academic experience and guidance whenever possible. The period of study with Dr. Jing and Prof. Cheng has significantly influenced my future development.

Besides my supervisors, I would like to thank my colleague Mr. Zhenlong Xiao, for his suggestions on my study.

Finally, I wish to thank my family and all friends.

Table of Contents

LIST OF FIGURES

LIST OF TABLES

Chapter 1 Introduction

Vehicle suspension is the combination of springs, shock absorbers and linkages. It plays an important role in connecting the vehicle chassis to its wheels. For a vehicle suspension system, it has three main purposes. First, transmit the force and torque to the chassis to make sure the vehicle works well. Second, reduce and isolate the vibration by using its springs and dampers. Third, make sure the wheels jump as a given trajectory by using its guide components and control its travel. An ideal vehicle suspension system should be able to reduce the acceleration and displacement of the vehicle body to meet the requirement of the ride comfort quality. Meanwhile, the suspension system should also achieve the requirement of the handling ability [1]. To achieve a desired performance, the vehicle suspension system has been widely investigated and studied for a long time. Previous studies in the design and analysis of the vehicle suspension system show that the suspension system can be divided into three main groups, passive suspension, semi-active suspension and active suspension according to the force generation mode [2].

For an active suspension system, it consists of sensors and actuators to generate the force according to the vehicle working conditions. It can provide the achievable performance by generating the optimal force continuously which cannot be obtained by the passive suspensions, such as achieving a significant reduction of the sprung mass acceleration in its natural frequency and avoiding high frequency harshness [3]. However, the disadvantages of the active suspension systems are also obvious. The cost of its sensors and actuators is very high, and it also needs rather frequent maintenance and considerable energy, especially when applied to the heavy vehicles. Furthermore, the design of the active suspension systems is also very complex due to the need for an external power source, and it will reduce the system reliability.

Passive suspensions are the most common systems and still be widely used in the current vehicles because they are simpler, more reliable and inexpensive than the other two types. In the passive suspensions, the characteristic of two main elements, spring and damper, are fixed at the design period. By properly choosing the spring stiffness and damping value, the desired vehicle performance can be achieved. However, the design of the passive suspension systems also has a significant limitation as the vehicle work environment is various; the performance of the passive suspensions in different operating conditions is various. For example, when the suspension damping is large, it can suppress the vibration of sprung mass at low frequencies. However, it will make the performance worse at the second resonance perk. Lower damping can improve isolation in the high frequency range but it will have a bad effect on the low frequency range [4].

Semi-active suspension system was proposed in the early 1970 and can be regarded as the compromise of the active suspension systems and the passive suspension systems [5]. It can achieve the performances as the active suspension systems by the continuously changing the damping characteristics, such as the magneto rheological (MR) damper [6], electro rheological (ER) damper [7] and twin tube variable orifice damper [3], or switch between different discrete characteristics. Compared with active suspension systems, the semi-active suspension system has the following advantages, lower implementation cost, lower power consumption, simpler design and easier to control. Compared with the passive suspensions, the semi-active suspension systems can reach some performances which are difficult for the passive suspension systems. Furthermore, it is much more reliable as it can work with its passive components when the control implements or the actuators break down. In the semi-active suspensions, some control strategies have been proposed, which contains sky hook control method [8-10], ground hook control method [11, 12] and sliding mode control method [13].

It is obvious that each type of suspension system has its advantages and disadvantages. The active and semi-active suspension systems can show better performance in the vehicle vibration performance, but the passive suspension systems still dominate the market [14]. Despite of the numerous advanced technologies and control strategies in the vehicle suspension system, it is of significant importance to investigate the spring and damper inherent nonlinear properties for passive suspension systems, such as the spring stiffness and damping characteristics. In this study, the nonlinear stiffness and damping characteristics will be systematically analyzed using a frequency domain method and the relationship with various vehicle performances will be discussed.

Previous studies often regard the suspension system as the model which is consisted of the spring and damper. As it is well known that an important characteristic of any spring is the fact that it can store energy from bumps and acceleration easily. However, these vehicle springs, such as leaf spring, coil spring and rubber spring, cannot release energy in a wanted way and this may cause an issue that it will not permit an acceptable life before failure [15]. Therefore, a damper should be well designed in suspension systems and it plays an important role in the suppression of vehicle vibration as it can damp out the vertical motion of its everyday environment and increase the spring's life. With a proper damping level, the car will have a good ride comfort and handling ability. How to design a proper and realistic damper is of great significance in the vehicle suspension system, especially the damping coefficient. In most vehicle dynamic analysis, the damping coefficient is based on the assumption that the damping force is proportional to the velocity of the damper piston, which mainly considers the fact of simplicity, and easiness in implementation and computer simulation [3, 15-17]. However, the relationship between the damping force and piston velocity in both of the desired and realistic damper is not proportional in the both low and high velocities. In reality, the characteristic curves for a suspension damper can be approximately obtained as shown in Figure 1.1.

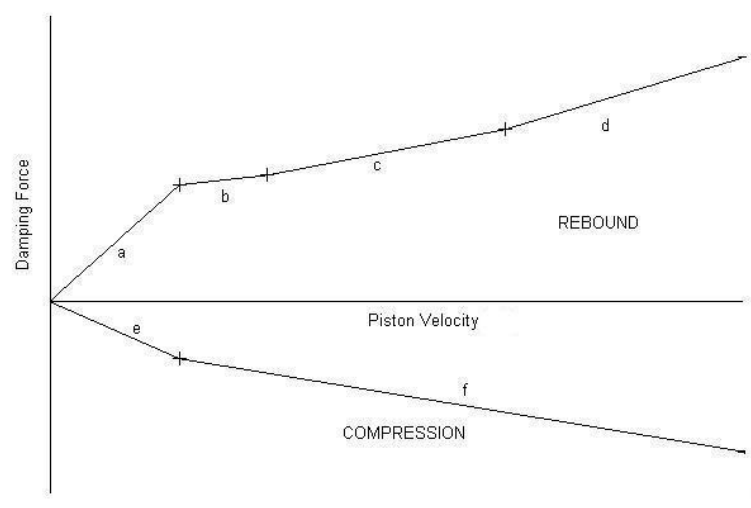

Figure 1.1 Characteristic curve for a suspension damper [15]

From Figure 1.1, it is obvious that the damping force is a piecewise linear instead of a single linear function of the damping coefficient and damper piston velocity. Meanwhile, with the wide usage of some novel dampers, such as MR fluid dampers, ER fluid dampers, and some other smart materials, the analysis and design of the damping characteristics cannot be simply regarded as a linear relationship. For example, the viscoelastic damper is not only affected by the piston velocity but also exhibits a complex nonlinear function between the damping force and the deformation [18, 19]. The spring system also has nonlinear characteristics, for example, the air suspension system has the quadratic and cubic nonlinearities after calculation [20]. The characteristics of rubber components which are widely used in the vehicle suspension system are also nonlinear [21]. Therefore, in the analysis of vehicle vibration performance, the nonlinear effects need to be taken into consideration to make sure the accuracy of the suspension system.

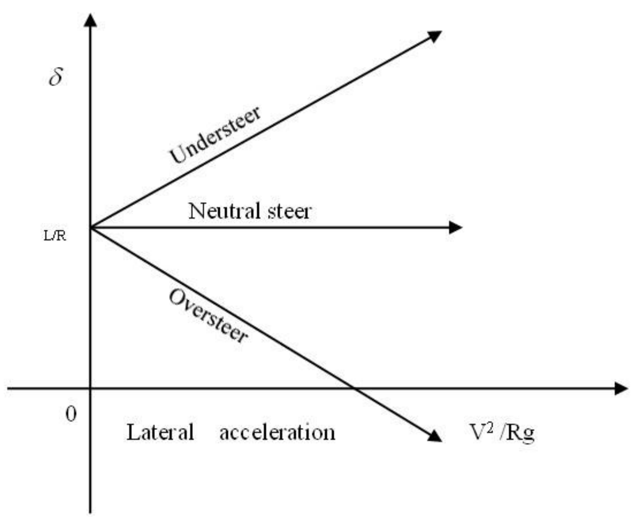

Figure 1.2 Evaluation standards of handling ability

The vehicle suspension system also has a significant influence on the suspension stroke and vehicle handling ability [17]. According to the previous study, the vehicle handling capability can be evaluated by using the under-steer (US), over-steer (OS) and neutral-steer (NS) conditions [17]. And it can be defined as

$$\delta_f = \frac{L}{R} + \left(\frac{W_f}{C_{\alpha f}} - \frac{W_r}{C_{\alpha r}}\right)\frac{V^2}{gR} \tag{1.1}$$

In the equation above, if the value of $(\frac{W_f}{C_{\alpha f}} - \frac{W_r}{C_{\alpha r}})$ is larger than zero, then the system will be under-steer; if the value of $(\frac{W_f}{C_{\alpha f}} - \frac{W_r}{C_{\alpha r}})$ is equal to zero, then the system will be neutral-steer; if the value of $(\frac{W_f}{C_{\alpha f}} - \frac{W_r}{C_{\alpha r}})$ is smaller than zero, the system will be over-steer. In the analysis of handling ability, the desired vehicle suspension system should keep the vehicle under-steered in order to make sure the stability during the turn movement. The neutral-steer can also be accepted while over-steer should be avoided. This is because an over-steered vehicle will decrease the steer angle, which can operate at the steer angle smaller than the Ackerman steer angle and it can cause the vehicle spin. The handling ability standards can be seen in Figure 1.2.

As presented above, the nonlinear effect of the vehicle suspension system needs to be taken into consideration during the analysis and design of the vehicle system. In order to analyze nonlinear suspension systems, some methods will be adopted in the study. There are several analysis methods especially for nonlinear systems, such as harmonic balance methods [22], describing function methods [23, 24] and averaging methods [25, 26]. The harmonic balance method is based on the assumption that the solution can be represented in the form of a Fourier series. The describing function method is based on quasi-linearization, which is the approximation of the nonlinear system under investigation by a linear system transfer function that depends on the amplitude of the input waveform. The averaging method is based on the averaging principle when the exact differential equation of the motion is replaced by an averaged equation. However, these methods cannot well reflect the relationship between the vehicle performance and system parameters. Therefore, a systematic frequency domain method based on Volterra series expansion for nonlinear systems which has been developed in recent years was adopted in this study [27-33]. This method is to determine the generalized frequency response functions (GFRFs) for the nonlinear system which can be described by the Volterra series. Based on this concept, many works have been done to analyze the dynamic characteristics of nonlinear systems in the frequency domain. By using this method, the system output spectrum can be derived to analyze the effect of nonlinear parameters on the output spectrum. Numerical methods to determine the nonlinear output spectrum of a nonlinear system are also developed using a parametric characteristic analysis method, which can greatly facilitate the analysis and design of important physical parameters in the nonlinear system [32, 33]. The main advantage of this numerical determination approach is that it can explain how the system output frequency response is affected by the system nonlinear parameters. By using the numerical method, the system output frequency response can be derived easily and engineers can analyze the system in terms of any model parameters of interest [33]. This frequency domain analysis method makes the nonlinear system analysis much more straightforward and easy to be understood. Meanwhile, it also provides the accessibility to study the system output frequency response with respect to the system parameters. The accuracy and reliability of this method have been studied in [34] by comparing with the harmonic balance method.

The main objective of this work is to employ the nonlinear frequency domain analysis method together with existing knowledge of the vehicle suspension system to investigate the relationship between the performance of vehicle suspension systems and its inherent parameters or some added artificial parameters in order to meet different requirements. According to the previous result [35], by properly introducing the nonlinearities and determining the model parameter of interest the system may suppress vibration and achieve a better output. As the relationship between the system output and system parameters can be derived, it provides a useful tool by which the optimal value of system parameters can be designed to achieve different performance requirements.

The rest of the chapter is organized as follows.

Chapter 2: In this chapter the mathematical model of the vehicle suspension system will be given. Then the evaluation standard of the vehicle performance will be presented. In this chapter, the theory of the nonlinear frequency domain analysis method will be introduced in detail. The system output will be derived according to the knowledge of the nonlinear frequency domain analysis method. The optimal value of the nonlinear parameters will be derived in this chapter. Some discussions will be given in this part.

Chapter 3: The existing optimal nonlinear damping characteristics was adopted from [36] and the detailed function of the nonlinear characteristic was derived from the fitting method. In the present study, another nonlinear optimal damping characteristics will be obtained by using the nonlinear frequency domain analysis method. Then the comparative study between these two nonlinear damping characteristics will be conducted to show which one will be better in the suppression of the vibration performance. The dynamic model of the spring damper system is built to verify the accuracy of the result.

Chapter 4: In this chapter, the full vehicle dynamic model will be built in Adams/ View. The detailed steps of how to build the vehicle dynamic model are also presented in this part. Then the nonlinear damping characteristics will be imported into this dynamic model and the comparative studies will be made to show its effect on the vehicle ride comfort, suspension stroke and the handling ability.

Chapter 5: In this part, the conclusion will be given and the future work will also be presented.

Chapter 2 System modeling and the OFRF method

In this chapter, the vehicle suspension model will be presented firstly. Then the relationship between the system output and system parameters will be derived by using the nonlinear frequency domain analysis method. Finally the optimal value of the system parameters will be obtained and some discussion will be presented.

2.1 System modeling

The vehicle suspension system can be investigated by using the following three different types of models, which are the quarter vehicle suspension model [3, 15], half vehicle suspension model [37] and the full vehicle suspension model [38]. Quarter vehicle suspension is the simplest one and it is mainly used for the analysis of vehicle vertical movement and vibration. The half vehicle suspension system and the full vehicle suspension system are mainly used for the analysis of the coupling relationship between the vehicle body and the components. For a half vehicle suspension system, it can well reflect the vertical vibration and pitch motion. The full vehicle suspension system can be used to investigate all the vehicle movements under road disturbances, including the vertical vibration, pitch motion, yaw movement and roll behavior. In the present study, the quarter suspension system is adopted to be the system model.

2.1.1 Linear system model

In this study, the research model is chosen to be the quarter vehicle suspension system. The model is very simple and sometimes cannot reflect the detailed vehicle motions, but it contains efficient and accurate information for the vertical movement [8, 22]. As stated above, the objective is to investigate the nonlinear effect occurs in the vehicle vibration performance. Therefore, it is possible to use the 1 degree of freedom (1DOF) model to reflect the basic dynamic concept of vehicle vertical motion. Then the vehicle model can be seen in Figure 2.1.

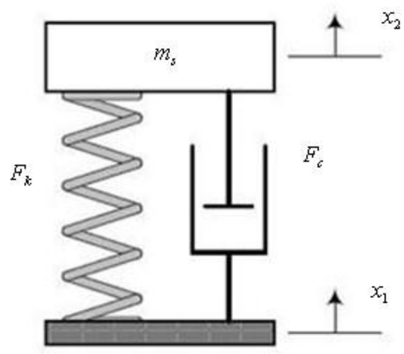

Figure 2.1 1 DOF quarter vehicle suspension model

The mass m_s represent the quarter of body mass. The vertical displacement of the sprung mass is x_2 and the base excitation displacement is x_1. In the linear suspension model, the damping force can be described as $F_c = c\dot{x}$ and the spring force can be written as $F_k = kx$. Here, k is the linear stiffness and c is the linear damping, x is the relative displacement between the sprung mass and the base excitation which can be defined as

$$x = x_2 - x_1 \tag{2.1}$$

Then the governing equation for this suspension system can be written as

$$m_s\ddot{x}_2 + F_k + F_c = 0 \tag{2.2}$$

Substituting x, F_k, F_c, then Eq. (2.2) can be written as

$$m_s\ddot{x} + kx + c\dot{x} = -m_s\ddot{x}_1 \tag{2.3}$$

Assuming that the base excitation is considered to be a sinusoidal function which can be written as

$$x_1 = Y\sin(\omega t) \tag{2.4}$$

where ω is the frequency and Y is the magnitude of the base motion. Then Eq. (2.3) can be written as

$$m_s\ddot{x} + kx + c\dot{x} = Ym_s\omega^2\sin(\omega t) \tag{2.5}$$

In order to conduct an analysis which is not specific to particular choices of system initial parameters, such as the mass and the spring stiffness, the non-dimensional form of the governing equation can be derived as:

$$\ddot{y}(\tau)+y(\tau)+\xi\dot{y}(\tau)=Y\sin(\Omega\tau) \tag{2.6}$$

where

$$\tau=\omega_0 t,\omega_0=\sqrt{k/m_s},\Omega=\frac{\omega}{\omega_0},\bar{Y}=m_s\omega^2,z(\tau)=x(t)=x\left(\frac{\tau}{\omega_0}\right),y(\tau)=\frac{kz(\tau)}{\bar{Y}},\xi=\frac{c}{\sqrt{km_s}} \tag{2.7}$$

2.1.2 Nonlinear system model

In the present study, the nonlinear effects will be taken into consideration in terms of the vehicle vibration performance. According the previous discussion in part 1.1, the damping force is neither proportional to the velocity in the low velocities nor a simple linear function of piston velocity in the whole velocity range. In this study, the damping force is $F_c = c\dot{x} + c_1\dot{x}^3 + c_2\dot{x}^2x + c_3\dot{x}x^2$ and the spring force is $F_k = kx + c_4x^3$, c_1, c_2, c_3, c_4 are the nonlinear values. In the present study, these four nonlinear parameters are introduced purposely. Some of them related to the velocity and some of them related to the velocity. And these four parameters will be taken as an example to investigate the nonlinear influence on the vehicle performances. Then the nonlinear system governing equation can be written as

$$m_s\ddot{x}+kx+c\dot{x}+c_1\dot{x}^3+c_2\dot{x}^2x+c_3\dot{x}x^2+c_4x^3=-m_s\ddot{x}_1 \tag{2.8}$$

And the non-dimensional model can be derived as

$$\ddot{y}(\tau)+y(\tau)+\xi\dot{y}(\tau)+\xi_1\dot{y}(\tau)^3+\xi_2\dot{y}(\tau)^2y(\tau)+\xi_3\dot{y}(\tau)y(\tau)^2+\xi_4y(\tau)^3=Y\sin(\Omega\tau) \tag{2.9}$$

where,

$$\xi_1=\frac{c_1\bar{Y}^2}{\sqrt{(km_s)^3}},\xi_2=\frac{c_2\bar{Y}^2}{k^2m_s},\xi_3=\frac{c_3\bar{Y}^2}{\sqrt{k^5m_s}},\xi_4=\frac{c_4\bar{Y}^2}{k^3} \tag{2.10}$$

The other parameters have the same definition in Eq. (2.7).

2. 2 Evaluation standard

In the design and analysis of a vehicle suspension system, there are different evaluation standards, such as the quality of ride comfort, handling ability and suspension stroke, to check the effect of suspension systems. Different performances will lead to different analysis of the suspension system. In this study, the ride comfort evaluation standard is the main objective of the analysis of vehicle suspension systems. There are many methods to evaluate the ride comfort in the world. For example, the ISO 2631 is used in Europe and while United Kingdom uses the British Standard BS 6841 [39]. In this study, the evaluation standard is mainly based on the British Standard BS 6841. Therefore, the vehicle ride comfort is evaluated by the transmissibility in this study, which can be defined as the ratio of the vertical maximum acceleration and road-induced vibration. The transmissibility for the non-dimensional 1 DOF quarter suspension system can be calculated as

$$\eta = \left| \frac{\ddot{y}(\tau)}{Y} \right| \tag{2.11}$$

For the linear system, the transmissibility can be calculated easily. However, the transmissibility of nonlinear systems is much more complicated than the linear system and it will be investigated in the present study. The objective of this study is to improve the vehicle ride comfort, and other evaluation standards will not be introduced and analyzed in detail in the present study. For the evaluation of suspension stroke, it can be reflected by the mean square relative displacement between the sprung mass and the unsprung mass [16]. The handling ability of vehicle is another important factor and it can be evaluated by the difference of the front slip angle and the rear slip angle. These two evaluation standards will be discussed in detail in Chapter 4.

The main objective of this study is to analyze the nonlinear effect on the vibration performance. According to the discussion above, the vibration performance can be evaluated by the vehicle body acceleration. In the present study, let the output be the transmitted force F. Then the objective function is to minimize the transmitted force. As the system output spectrum will reach the maximum value at the resonance frequency point, therefore the input frequency is chosen to be system natural frequency and thus $\Omega = 1$. The detailed form of the transmitted force can be measured by

$$F = y(\tau) + \xi \dot{y}(\tau) + \xi_1 \dot{y}(\tau)^3 + \xi_2 \dot{y}(\tau)^2 y(\tau) + \xi_3 \dot{y}(\tau) y(\tau)^2 + \xi_4 y(\tau)^3 \tag{2.12}$$

Therefore, the vehicle suspension system can be described as a non-dimensional model as

$$\begin{cases} \ddot{y}(\tau) + y(\tau) + \xi \dot{y}(\tau) + \xi_1 \dot{y}(\tau)^3 + \xi_2 \dot{y}(\tau)^2 y(\tau) + \xi_3 \dot{y}(\tau) y(\tau)^2 + \xi_4 y(\tau)^3 = Y \sin(\Omega \tau) \\ F = y(\tau) + \xi \dot{y}(\tau) + \xi_1 \dot{y}(\tau)^3 + \xi_2 \dot{y}(\tau)^2 y(\tau) + \xi_3 \dot{y}(\tau) y(\tau)^2 + \xi_4 y(\tau)^3 \end{cases} \tag{2.13}$$

Then, the objective of this study is to analyze the effect of the nonlinear terms with coefficients $\xi_1, \xi_2, \xi_3, \xi_4$ on the system output spectrum. To determine the nonlinear parameters' effect on the output, the system output spectrum needs to be obtained firstly. In section 2.3, two approaches based on the frequency domain analysis method will be given to derive the system output spectrum.

2.3 Determination of the system OFRF

In this section, a brief review about the theory of nonlinear frequency domain analysis method is introduced firstly and then an efficient numerical approach is discussed for the determination and optimization of nonlinear output spectrum in terms of system parameters. By using the steepest descent method, the optimal value of the nonlinear system parameters will be obtained.

2.3.1 Nonlinear output spectrum: the theory

For nonlinear systems, the output $f(t)$ can be expressed by a Volterra functional polynomial of the input $u(t)$ [40] as

$$f(t) = \sum_{n=1}^{N} f_n(t) \tag{2.14}$$

where N is the maximum order of the system nonlinearity, and then the $\mathrm{n^{th}}$-order output of the system is given by

$$f_n(t)=\int_{-\infty}^{\infty}\cdots\int_{-\infty}^{\infty}h_n(\tau_{1,\cdots}\tau_n)\prod_{i=1}^{n}u(t-\tau_i)d\tau_i \tag{2.15}$$

where $h_n(\tau_1 \dots \tau_n)$ is the real function of $\tau_1 \dots \tau_n$ and is defined as the n$^{\text{th}}$-order kernel of the system. Then the system n$^{\text{th}}$-order transfer function (GFRF) can be derived by using the multi-dimensional Fourier transform of the n$^{\text{th}}$-order impulse response, which can be written as

$$H_n(j\omega_1,\cdots j\omega_n)=\int_{-\infty}^{\infty}\cdots\int_{-\infty}^{\infty}h_n(\tau_1,\cdots\tau_n)\exp(-j(\omega_1\tau_1+\cdots+\omega_n\tau_n))d\tau_1\cdots d\tau_n \tag{2.16}$$

And when the system is subjected to a input such that

$$u(t)=\sum_{i=1}^{K}\left|A_i\right|\cos\left(\omega_i+\angle A_i\right) \tag{2.17}$$

According to[28], the system output spectrum can be written as

$$F(j\omega)=\sum_{n=1}^{N}\frac{1}{2^n}\sum_{\omega_1+\ldots+\omega_n=\omega}H_n\left(j\omega_1,\cdots,j\omega_n\right)A\left(\omega_{k_1}\right)\cdots A\left(\omega_{k_n}\right) \tag{2.18}$$

where

$$A\left(\omega_{k_i}\right)=\left|A_{k_i}\right|e^{j\angle A_{|k_i|}\cdot\operatorname{sgn}(k_i)}\text{for } k_i\in\left\{\pm1,\cdots,\pm\bar{K}\right\},\operatorname{sgn}(a)=\begin{cases}1 & a\geq 0\\ -1 & a<0\end{cases},\ \omega_{k_i}\in\left\{\pm\omega_1,\cdots,\pm\omega_{\bar{K}}\right\}$$

In this study, the existing nonlinear output frequency response function method will be adopted to analyze the nonlinear effect on the system output. By using the probing method, the following result is obtained according to [41]

$$\begin{aligned}L_n&\left(j\omega_1+\cdots+j\omega_n\right)\cdot H_n\left(j\omega_1,\cdots,j\omega_n\right)=\sum_{k_1,k_n=1}^{K}c_{0,n}\left(k_1,\cdots,k_n\right)\left(j\omega_1\right)^{k_1}\cdots\left(j\omega_n\right)^{k_n}\\&+\sum_{q=1}^{n-1}\sum_{p=1}^{n-q}\sum_{k_1,k_{p+q}=0}^{L}c_{p,q}\left(k_1,\cdots,k_{p+q}\right)\times\left(\prod_{i=1}^{q}\left(j\omega_{n-q+i}\right)^{k_{p+i}}\right)\cdot H_{n-q,p}\left(j\omega_1,\cdots,j\omega_{n-q}\right)\\&+\sum_{p=2}^{n}\sum_{k_1,k_p=0}^{K}c_{p,0}\left(k_1,\cdots,k_p\right)H_{n,p}\left(j\omega_1,\cdots,j\omega_n\right)\end{aligned} \tag{2.19}$$

$$H_{n,p}(\cdot)=\sum_{i=1}^{n-p+1}H_i(j\omega_1,\cdots,j\omega_i)\times(j\omega_{i+1},\cdots,j\omega_n)(j\omega_1+\cdots+j\omega_i)^{k_p} \tag{2.20}$$

$$H_{n,1}(j\omega_1,\cdots,j\omega_n)=H_n(j\omega_1,\cdots,j\omega_n)(j\omega_1+\cdots+j\omega_n)^{k_1} \tag{2.21}$$

where $L_n(j\omega_1+\cdots+j\omega_n)=-\sum_{k_1=0}^{K}c_{1,0}(k_1)(j\omega_1+\cdots+j\omega_n)^{k_1}$. From Eq. (18) and Eq. (2.19), the system output polynomial can be derived.

For a single input two output systems, the output response can also be seen in [42]. To be noted that the convergence of the system should be analyzed in advance of obtaining the system nonlinear output frequency response function. The author in [32] has defined a ratio function to evaluate the convergence for the system OFRF in terms of the system nonlinear parameters and this study will not present the detailed steps here. In this study, the non-dimensional system output frequency response is calculated up to the fifth order. and the detailed expression can be written as

(1) The first order frequency response is

$$H_1^{2:1}(j\omega_1)=\frac{\xi(j\omega_1)+1}{(j\omega_1)^2+\xi(j\omega_1)+1} \tag{2.22}$$

(2) The third order frequency response is

$$H_3^{1:111}(j\omega_1,j\omega_2,j\omega_3)=-\frac{H_1(j\omega_1)H_2(j\omega_2)H_3(j\omega_3)\begin{bmatrix}\xi_4+\xi_3(j\omega_3)\\+\xi_2(j\omega_3)(j\omega_2)\\+\xi_1(j\omega_1)(j\omega_2)(j\omega_3)\end{bmatrix}}{(j\omega_1+j\omega_2+j\omega_3)^2+\xi(j\omega_1+j\omega_2+j\omega_3)+1} \tag{2.23.a}$$

$$H_3^{2:111}(j\omega_1,j\omega_2,j\omega_3)=\left(-(j\omega_1+j\omega_2+j\omega_3)^2\right)H_3^{1:111}(j\omega_1,j\omega_2,j\omega_3) \tag{2.23.b}$$

(3) The fifth order frequency response is much more complicated and symbolic and will not be given in this chapter in order to save space. See Appendix A for the detailed expression for $H_5^{2:11111}(j\omega_1,\ldots,j\omega_5)$.

Then the system output can be derived according to Eq. (2.18), which can be written as

$$
\begin{aligned}
F(j\omega) &= \sum_{n=1}^{5}\frac{1}{2^n}\sum_{\omega_1+\ldots+\omega_n=\omega} H_n^2\left(j\omega_1,\cdots,j\omega_n\right)A\left(\omega_{k_1}\right)\cdots A\left(\omega_{k_n}\right) \\
&= \frac{1}{2}H_1^{2:1}\left(j\omega_1\right)A\left(\omega\right)+\frac{1}{2^3}\sum_{\omega_1+\ldots+\omega_3=\omega} H_3^{2:111}\left(j\omega_1,\cdots,j\omega_3\right)A\left(\omega_{k_1}\right)\cdots A\left(\omega_{k_3}\right) \\
&+\frac{1}{2^5}\sum_{\omega_1+\ldots+\omega_5=\omega} H_5^{2:11111}\left(j\omega_1,\cdots,j\omega_5\right)A\left(\omega_{k_5}\right)\cdots A\left(\omega_{k_5}\right)
\end{aligned} \tag{2.24}
$$

2.3.2 Numerical determination of nonlinear output spectrum

In section 2.3.1, the analytical computation of the nonlinear output spectrum has been discussed. In practice, a more efficient numerical method can be adopted, which allow nonlinear output spectrum to be determined directly in terms of system physical parameters. To this end, the system output spectrum can be written into a more explicit polynomial form as follows [32, 33, 43]

$$
F(j\omega) = \sum_{n=1}^{N} CE(H_n(.))\phi_n(j\omega)^T \tag{2.25}
$$

where

$$
\phi_n(j\omega) = \frac{1}{\sqrt{N}(2\pi)^{n-1}}\int_{\omega_1+\cdots+\omega_n=\omega} f_n(j\omega_1,\cdots,j\omega_n)\prod_{i=1}^{n}U(j\omega_i)d\sigma_\omega. \tag{2.26}
$$

$CE(.)$is a coefficient extraction operator which has two fundamental operations '$\otimes$'and '$\oplus$'. The detailed definitions were given in [43], and $CE(H_n(.))$ is the parametric characteristics of the n$^{\text{th}}$-order GFRF $H_n(.)$, which can be written as

$$
CE(H_n(\cdot)) = C_{0,n}\oplus\left(\mathop{\oplus}_{q=1}^{n-1}\mathop{\oplus}_{p=1}^{n-q} C_{p,q}\otimes CE(H_{n-q-p+1}(.))\right)\oplus\left(\mathop{\oplus}_{p=2}^{n} C_{p,0}\otimes CE(H_{n-p+1}(.))\right) \tag{2.27}
$$

Obviously, Eq. (2.25) can be written as

$$
F(j\omega) = \psi\varphi(j\omega)^T \tag{2.28}
$$

where

$$\psi = \bigoplus_{n=1}^{N} CE(H_n(.)), \ \varphi(j\omega) = [\varphi_1(j\omega), \varphi_2(j\omega), \cdots, \varphi_n(j\omega)] \tag{2.29}$$

Therefore, the determination of the output spectrum by using the numerical determination method in this study can be carried out by the following steps:

(1) Determination of the parametric characteristics of OFRF

The first step of this task is to determine the largest order N. This can be done by evaluating the magnitude of the $\mathrm{n^{th}}$-order output frequency response $F_n(j\omega)$. If the magnitude bond of $F_n(j\omega)$ is less than a predefined value, then the largest order N can be obtained. The second step is to determine the parametric characteristics according to Eq. (2.27). For a given system which can be described in Eq. (2.13), the nonlinear parameters of interest are $\xi_1, \xi_2, \xi_3, \xi_4$ and all the other parameters are zero. According to [32], the parametric characteristics of OFRF can be shown as below

$$\psi = [1, \xi_1, \xi_2, \xi_3, \xi_4, \xi_1^{\ 2}, \xi_1\xi_2, \xi_1\xi_3, \xi_1\xi_4, \xi_2^{\ 2}, \xi_2\xi_3, \xi_2\xi_4, \xi_3^{\ 2}, \xi_3\xi_4, \xi_4^{\ 2} \cdots] \tag{2.30}$$

(2) Determination of $\phi(j\omega)$ for the OFRF

The first step of this task is to construct a non-singular matrix which should cover a large range. Then the Second step is to obtain the output frequency response $F(j\omega)$ of the system for different combinations of nonlinear parameters $\xi_1, \xi_2, \xi_3, \xi_4$. This can be achieved by using FFT on the time domain output response. Then $\phi(j\omega)$ for the OFRF can be written as

$$\varphi(j\omega)^T = \left(\psi^T\psi\right)^{-1}\psi^T F\left(j\omega\right) \tag{2.31}$$

Therefore, the OFRF of the system with respect to nonlinear parameters $\xi_1, \xi_2, \xi_3, \xi_4$ can be obtained according to Eq. (2.28).

In conclusion, the main idea of the numerical determination method is that, given a nonlinear model, $CE(H_n(.))$ can be derived according to Eq. (2.27) and $\phi_n(j\omega)$ can be obtained by the numerical method which will be discussed in detail in the next section. Then the system output spectrum will be achieved according to Eq. (2.28), and finally frequency domain analysis can be conducted.

2.4 Optimization and system analysis

In this section, the relationship between the system output and the system parameters of interest will be derived. Then the optimal value of the system nonlinear parameters will be obtained by using the steepest descent method. Finally some conclusions about the advantage of system nonlinearity on the system vibration control will be given.

2.4.1 Computation of the nonlinear output spectrum

With the nonlinear output spectrum of vehicle suspension system derived above, parameter optimization can then be conducted to find the optimal nonlinear parameters $\xi_1, \xi_2, \xi_3, \xi_4$ to achieve the best vibration suppression in the system output. To understand the nonlinear output spectrum with respect to any nonlinear parameters of interest in the system, consider the output spectrum with respect to only two parameters ξ_1, ξ_2. Following the numerical method above, it can be eventually obtained that

$$\begin{aligned}
F(j\Omega)\Big|_{\Omega=1} &= (1.5599\text{e}-001 + 1.6160\text{e}-001\text{i}) + (-2.4599\text{e}-002 + 5.7895\text{e}-004\text{i})*\xi_1 \\
&+ (4.8410\text{e}-002 - 3.1037\text{e}-002\text{i})*\xi_2 + (2.5315\text{e}-003 - 2.1792\text{e}-003\text{i})*\xi_1^2 \\
&+ (-1.2208\text{e}-002 + 1.0914\text{e}-002\text{i})*\xi_1*\xi_2 + (-3.4105\text{e}-003 - 1.5597\text{e}-003\text{i})*\xi_2^2 \\
&+ (1.5519\text{e}-004 - 9.5445\text{e}-005\text{i})*\xi_1^3 + (2.9229\text{e}-004 - 6.2336\text{e}-005\text{i})*\xi_1^2*\xi_2 \\
&+ (2.0404\text{e}-003 - 1.8717\text{e}-003\text{i})*\xi_1*\xi_2^2 + (-5.2480\text{e}-004 + 1.0759\text{e}-003\text{i})*\xi_2^3 \\
&+ (-2.4643\text{e}-005 + 2.5870\text{e}-005\text{i})*\xi_1^4 + (4.5495\text{e}-005 - 6.8368\text{e}-005\text{i})*\xi_1^3*\xi_2 \\
&+ (-1.1712\text{e}-004 + 1.1884\text{e}-004\text{i})*\xi_1^2*\xi_2^2 + (-4.6285\text{e}-005 + 4.7699\text{e}-005\text{i})*\xi_1*\xi_2^3 \\
&+ (4.5823\text{e}-005 - 7.5763\text{e}-005\text{i})*\xi_2^4
\end{aligned} \tag{2.32}$$

where the frequency Ω can be chosen at any values, for example here $\Omega = 1rad/s$. In order to well reflect the relationship between the system output spectrum the initial damping value is $\xi = 0.01$ and the magnitude of the system is $\overline{Y} = 0.2$. The result is shown in Figure 2.2.

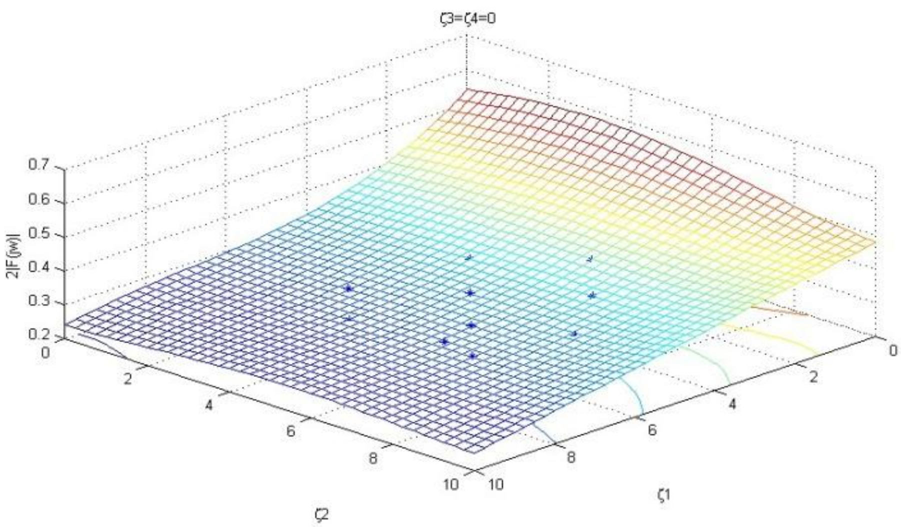

Figure 2.2 Nonlinear output spectrum with respect to ξ_1, ξ_2 (The stars were obtained by the theoretical approach)

From Figure 2.2, it can be seen that the output spectrum is a typical nonlinear function of nonlinear parameters ξ_1, ξ_2. The nonlinear output spectrum provides a straightforward and powerful insight into the analytical relationship between system output response and physical parameters.

In order to find the optimal parameter values for $\xi_1, \xi_2, \xi_3, \xi_4$, the nonlinear output spectrum with respect to all these four parameters can be derived by following the procedure in the section 2.3. It should be noted that the range of the nonlinear parameters should be sufficiently large in order to get a globally optimal solution. However, when the parameters cover a large range, the matrix inverse in Eq. (2.30) is easy to be ill-conditioned. To solve this problem, matrix ψ can be written as [32]

$$\begin{aligned}\psi = [&1, \alpha(\xi_1/\alpha), \alpha(\xi_2/\alpha), \alpha(\xi_3/\alpha), \alpha(\xi_4/\alpha), \alpha^2(\xi_1^2/\alpha^2), \alpha^2(\xi_1\xi_2/\alpha^2),\\ &\alpha^2(\xi_1\xi_3/\alpha^2), \alpha^2(\xi_1\xi_4/\alpha^2), \alpha^2(\xi_2^2/\alpha^2), \alpha^2(\xi_2\xi_3/\alpha^2), \alpha^2(\xi_2\xi_4/\alpha^2),\\ &\alpha^2(\xi_3^2), \alpha^2(\xi_3\xi_4/\alpha^2), \alpha^2(\xi_4^2/\alpha^2)]\end{aligned} \tag{2.33}$$

Then Eq. (2.28) can be written as

$$F(j\omega)=\psi\varphi(j\omega)^T=[1,(\xi_1/\alpha),(\xi_2/\alpha),(\xi_3/\alpha),(\xi_4/\alpha),(\xi_1{}^2/\alpha^2),(\xi_1\xi_2/\alpha^2),$$
$$(\xi_1\xi_3/\alpha^2),(\xi_1\xi_4/\alpha^2),(\xi_2{}^2/\alpha^2),(\xi_2\xi_3/\alpha^2),(\xi_2\xi_4/\alpha^2),(\xi_3{}^2/\alpha^2),(\xi_3\xi_4/\alpha^2),$$
$$(\xi_4{}^2/\alpha^2)][\varphi_0(j\omega),\alpha\varphi_1(j\omega),\alpha\varphi_2(j\omega),\alpha\varphi_3(j\omega),\alpha\varphi_4(j\omega),\alpha^2\varphi_5(j\omega),\alpha^2\varphi_6(j\omega), \quad (2.34)$$
$$\alpha^2\varphi_7(j\omega),\alpha^2\varphi_8(j\omega),\alpha^2\varphi_9(j\omega),\alpha^2\varphi_{10}(j\omega),\alpha^2\varphi_{11}(j\omega),\alpha^2\varphi_{12}(j\omega),\alpha^2\varphi_{13}(j\omega),$$
$$\alpha^2\varphi_{14}(j\omega)]^T$$

Using this scaling method, the parameters could not only cover a large range, but also ensure the non-singularity of the matrix in Eq. (2.30).

2.4.2 Parameter optimization

According to Eq. (2.28), the polynomial with respect to all the nonlinear parameters can be derived. To this end, the following points should be noted.

(a) The matrix ψ should cover a large range to make sure the optimal results can be found as mentioned above. However, usually when the range of the nonlinear parameter is too large, the matrix inverse in Eq. (2.30) would be ill-conditioned. To solve this problem, the range of the variables can also be divided into several parts. For example, the range of $[0,100]$ can be divided into $[0,1],[1,10],[10,100]$. Using this subsection method, together with the scaling method discussed in Eq. (2.33-2.34), the matrix will be easy to be non-singular and the accuracy of the solution can be guaranteed.

(b) The optimal solution should be the optimal one within all the sub-ranges.

(c) The nonlinear parameters ξ_1,ξ_2,ξ_3,ξ_4 have their physical meaning. Therefore some parameters can be negative while the others cannot.

Moreover, in practice to further restrict the searching space, two new variables a,b can be introduced which are defined as

$$\xi_1=a,\xi_2=3ab,\xi_3=3ab^2,\xi_4=ab^3 \quad (2.35)$$

Therefore, Eq. (2.11) can be written as

$$F=y(\tau)+\xi\dot{y}(\tau)+a\left[\dot{y}(\tau)+by(\tau)\right]^3 \quad (2.36)$$

Then the system output spectrum is a function with respect to two variables a, b and can be obtained by the frequency domain analysis method. In this study, the range of a, b is $[0,10]$ and $[-1,0]$ respectively. The system output frequency response with respect to nonlinear variables was obtained in this study.

$$\begin{aligned}
F(j\Omega)\big|_{\Omega=1} &= (1.2297\text{e-}001 + 2.6101\text{e-}001i) + (1.4043\text{e-}002 - 2.1368\text{e-}002i) * a \\
&+ (3.1627\text{e-}002 + 3.7759\text{e-}003i) * 3ab + (-7.5741\text{e-}003 + 2.3285\text{e-}002i) * 3ab^2 \\
&+ (4.8602\text{e-}003 + 1.7763\text{e-}001i) * ab^3 + (-1.8905\text{e-}003 + 1.9025\text{e-}003i) * a^2 \\
&+ (-2.8603\text{e-}003 + 9.4444\text{e-}004i) * 3a^2b + (6.9260\text{e-}005 - 8.4367\text{e-}004i) * 3a^2b^2 \\
&+ (-1.2002\text{e-}002 + 1.3644\text{e-}002i) * a^2b^3 + (1.5270\text{e-}003 - 9.8513\text{e-}004i) * 9a^2b^2 \\
&+ (1.6447\text{e-}003 - 2.7494\text{e-}004i) * 9a^2b^3 + (-2.2671\text{e-}003 + 2.4648\text{e-}002i) * 3a^2b^4 \\
&+ (5.7254\text{e-}003 - 3.0388\text{e-}003i) * 9a^2b^4 + (3.5859\text{e-}003 + 2.4658\text{e-}002i) * 3a^2b^5 \\
&+ (-7.3119\text{e-}002 + 2.0120\text{e-}001i) * a^2b^6
\end{aligned} \tag{2.37}$$

Note that the parameter here is dimensionless. Therefore, a value for $a = 0.1$ for example is equivalent to the value $c_1 = a\sqrt{(km_s)^3}/Y^2 = 75248.3$ (for example, $k = 16000$, $m_s = 240$ and $Y = 100$). Also, note that the parameter a takes very small values, the scaling method and the subsection method above can still be applied similarly in order to avoid matrix singularity. Using the steepest descent method, the optimal solution can be obtained. For the first polynomial, the optimal value is

$$a = 3.89, b = -0.77, 2|F(j\omega)| = 0.251 \tag{2.38}$$

According to Eq. (2.6), the definition of Ω is the ratio of the input frequency to the system nature frequency. In this study, the range of Ω is $[0.1,10]$, and then the realistic road input frequency is $[0.1\omega_0, 10\omega_0]$ which can cover the normal working frequency range [17]. For an optimal value, it should not only suppress the vibration in the resonance frequency, but also is helpful in other frequency range. In the present study, the system output spectrum with respect to a and b will be given in Figure 2.3.

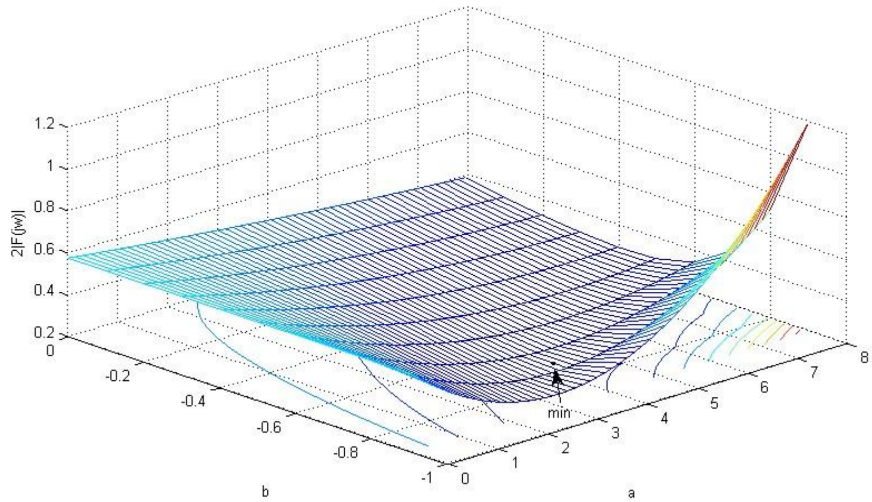

Figure 2.3 Nonlinear output spectrum with respect to a, b

2.4.3 Comparison with linear systems

For pure linear system, the system spring force is $F_k = kx$ and the damper force is $F_c = c\dot{x}$. The system governing equation can be seen in Eq. (2.6). Then according to Eq. (2.22), the system transfer function can be written

$$H(j\Omega) = \frac{\xi(j\Omega)+1}{(j\Omega)^2 + \xi(j\Omega)+1} \tag{2.39}$$

According to the [15, 17], the magnitude of the transfer function is

$$|H(j\Omega)| = \sqrt{\frac{1+(\xi\Omega)^2}{\left(1-\Omega^2\right)^2 + (\xi\Omega)^2}} \tag{2.40}$$

And the phase of the transfer function is

$$\theta = \arctan\left[-\frac{\xi\Omega^3}{\left(1-\Omega^2\right)+\xi^2\Omega^2}\right] \tag{2.41}$$

Therefore, the system output response for a sinusoidal input can be written as

$$F=\sqrt{\frac{1+(\xi\Omega)^2}{\left(1-\Omega^2\right)^2+(\xi\Omega)^2}}\sin(\Omega\tau-\theta) \tag{2.42}$$

The output spectrum of the linear system under different values of ξ is given in Figure 2.4

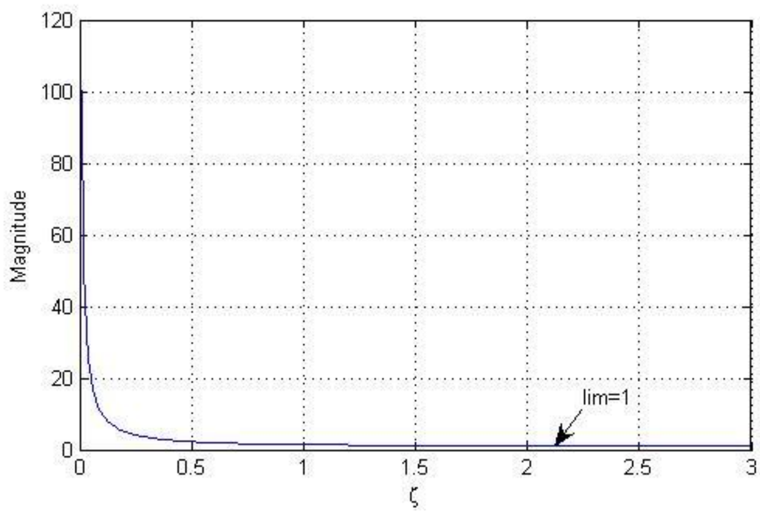

Figure 2.4 Magnitude with respect to ξ

From Figure 2.4, it is obvious that the magnitude of the output response is a monotonically decreasing function and the minimum of the output response can be derived as

$$\min\sqrt{\frac{1+\xi^2}{\xi^2}}=\lim_{\xi\to\infty}\sqrt{\frac{1+\xi^2}{\xi^2}}=1 \tag{2.43}$$

From Eq. (2.43), it can be shown that when the input frequency $\Omega = 1rad/s$, the transfer function is a decreasing function and the minimum is 1 when the linear damping ξ is as large as possible. However, the vehicle suspension linear damping usually gets the value of $\xi = 0.25$ [17]. In this study, the recommended linear damping will be used to compare with the nonlinear optimal damping. And the system spectrum of the system with respect to different system values can be shown in Table2.1

Table 2.1 The system output spectrum

ξ	a	b	$2\|F(j\Omega)\|$
0.01	0	0	20
0.25	0	0	0.825
0.01	3.89	-0.77	0.251

In order to verify whether the nonlinear optimal value has a positive effect on the system output spectrum in the whole frequency range, the system transmissibility was introduced in this study according to [31] as the figure of the system transmissibility can well reflect how the system parameters affect the system output just as the transfer function does in the linear theory. In this study, the system transmissibility can be defined as the system output divided by input which can be written as

$$T = \frac{F}{Y} \tag{2.44}$$

And the system transmissibility can be plotted in Figure 2.5

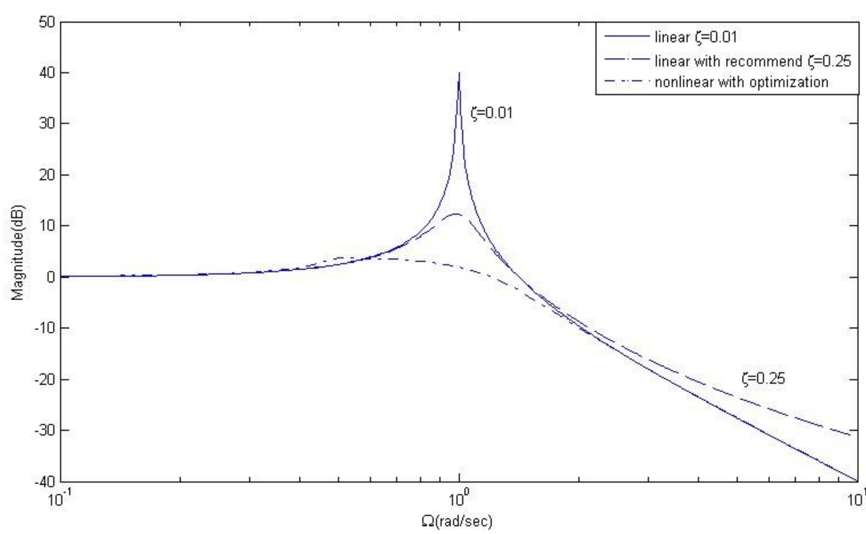

Figure 2.5 The force transmissibility for different systems

By further inspection of Figure 2.5, here are some conclusions:

1. It is obvious that when the nonlinear parameters get an optimal value, the system transmissibility at the frequency of $\Omega = 1$ is more excellent than the initial linear system. In Figure 2.5, the peak at the frequency of $\Omega = 1$ means the maximum transmissibility. It can be shown that the nonlinear optimal system can get the smallest transmissibility at the frequency of $\Omega = 1$, which means that when the system under the same input signal, the system output spectrum with the nonlinear optimal value will get the lowest output spectrum. Therefore, it can be concluded that the system vibration is well suppressed at the system resonant frequency when the nonlinear system get the optimal value.

2. From Figure 2.5, it is also clear that the optimal nonlinear value can not only minimize the transmissibility in the resonant frequency, but also be helpful for the system vibration suppression in other frequency ranges. In the high frequency range, the nonlinear optimal value can keep the transmissibility unchanged just as the curve obtained from the initial linear damping value, which is much better than the curve obtained from the recommended damping value. In the low frequency range, the transmissibility does not vary with the change of the linear damping value, the three curves match very well. However, at the frequency of about $\Omega = 0.5$, the transmissibility obtained by the optimal nonlinear system is bigger than the other two systems and there exists a peak. This is because that in this study, the nonlinear stiffness term was also introduced. This will decrease the system stiffness, and then the resonant frequency will be decreased. Therefore, the nonlinear system transmissibility will get a maximum value below the system nature frequency of $\Omega = 1$. This will also be helpful as the vehicle suspension system resonance frequency can be changed by introducing the nonlinear terms, which can be used to design the suspension system in order to avoid some important frequency points, such as the human sensitive frequency or the engine resonant frequency.

In this study, the area which was combined by the three output spectrum curves $x = 0.1, x = 10, y = 0$ can be calculated to show the effect of optimal nonlinearity in the whole frequency range. The detailed steps of calculating the output spectrums can be seen in [17]. To be noted that the unit of y-label is N and the unit of x-label is rad/s, so in this study the unit of the area here is N.rad/s. The areas of different systems can be seen in Table 2.2.

Table 2.2 The area of different systems

System	Area (N.rad/s)
Linear $\xi = 0.01$	1.3091
Linear$\xi = 0.25$	0.7112
Nonlinear optimal system	0.4728

From Table 2.2 it can be shown that the area obtained by the nonlinear system is the smallest one in the three different systems above. Therefore, the optimal nonlinear system is much more competitive than the linear system as it can successfully suppress vibration in the resonant frequency range.

2.4.4 Optimal nonlinear stiffness and damping characteristics

Based on the discussion above, the system transmitted force can be obtained in this study. Submit the optimal nonlinear value in Eq. (2.11), and then the system transmitted force can be derived as

$$F = y + 0.01\dot{y} + 3.89\dot{y}^3 - 8.9589\dot{y}^2 y + 6.9161 y\dot{y}^2 - 1.7759 y^3 \tag{2.45}$$

The vehicle damping characteristics and spring force can be plotted under the optimal nonlinear parameters respectively. For the suspension damping force, it can be obtained according to Eq. (2.11) and Table 2.1, and then the nonlinear damping force with respect to the displacement and velocity can be written as

$$F_d = 0.01\dot{y} + 3.89\dot{y}^3 - 8.9589\dot{y}^2 y + 6.9161 y\dot{y}^2 \tag{2.46}$$

And the nonlinear spring force with respect to the displacement and velocity can be written as

$$F_s = y - 1.7759 y^3 - 8.9589\dot{y}^2 y + 6.9161 y\dot{y}^2 \tag{2.47}$$

In this study, the range of velocity $\dot{y}$ is chosen to be $[-1.5, 1.5]$ and the range of displacement y is chosen to be $[-0.04, 0.04]$. To be noted that both of these are dimensional ranges and the non-dimensional ranges can be obtained according to Eq. (2.9) and Eq. (2.10) when given a specific mass, linear stiffness and input frequency. In this part, the system parameters can be written as:

$$m_s = 1kg, k = 1N / m, \Omega = 1rad / s \tag{2.48}$$

In this study, the non-dimensional units of displacement and velocity are $m^2/s^2$and m^2/s^3 and the dimensional range is the same as the non-dimensional range. Then the system nonlinear damping force after optimization was taken as an example to further investigation and it can be clearly shown in Figure 2.6.

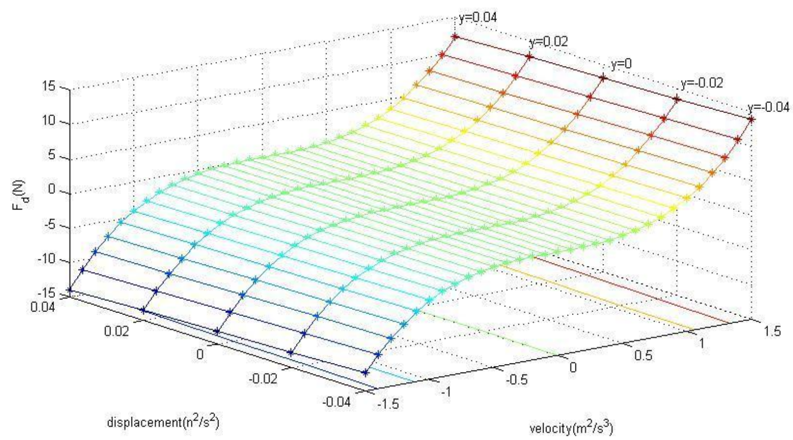

Figure 2.6 Damping force

Figure 2.6 is the suspension damping characteristics under different displacements and velocities. It can be concluded that in this study, the damping force is not only a function of velocity but also affected by the displacement. From Figure 2.6, it can be shown that when the relative displacement gets different value, the curve of the damping force will change. In some real systems, for example, the viscoelastic damper is not only affected by the piston velocity but also exits a complex nonlinear function between the damping force and the deformation [19]. In this study, the damping characteristics obtained by the frequency domain method can reflect the detailed relationship between the force and velocity-displacement. Similarly, Eq. (2.47) shows that the velocity also has an influence on the spring force. For different values of velocity, the spring versus displacement curve is different.

2.5 Conclusion

Based on some previous work, a brief introduction about the nonlinear frequency domain analysis method was given in this chapter. The output spectrum obtained by the analytical determination approach and the numerical determination approach was conducted to analyze the effect of the model parameters on the nonlinear vehicle suspension system. It can be seen that the system output spectrum varies with respect to different system parameters according to the results above. Then the output spectrum derived from the numerical determination approach was used to find the optimal solution because of its advantage in computational cost. The nonlinear optimal solution was obtained and compared with the initial linear system and the system with recommended damping values. The results show that when the system nonlinear parameters are set to the optimal value, the output spectrum can be much better than the linear system at the resonant frequency range. This is very useful in the application of the suppressing vibration. The damping characteristics obtained in this study demonstrates that the damping force can also be affected by the displacement. In this chapter the system parameters are the artificially determined but it is coinciding with the study [44] to some extend as it reflects the relationship between the damping force and the velocity and displacement. To be noted that, the optimal value of the system parameters presented in this study is obtained at a given input signal. The corresponding optimal value will be different when the input signal is changed. Therefore, the system vibration performance will be improved by properly determining the model parameters when the system input is given. In the next chapter, the OFRF based analysis method will be used to find the optimal value of a realistic suspension system. Different evaluation standards will be adopted to analyze the effects of system nonlinearity.

Chapter 3 Comparative studies

In this chapter, the nonlinear frequency domain analysis method will be applied to obtain the nonlinear optimal damping characteristics, and the comparative studies between two nonlinear optimal damping characteristics will be conducted to verify the advantage of the nonlinear frequency domain analysis method. In the first section, existing optimal vehicle damping characteristics [36] will be derived by using a curve fitting method. The second section will analyze the relationship between the system output spectrum and the system nonlinearities. In the third section, comparative studies between these two optimal damping characteristics will be conducted. Finally a dynamic model of the spring damper system will be built to verify the effectiveness of the result derived from the theoretical analysis.

3.1 The existing nonlinear damping characteristics

In the analysis of vehicle suspension systems, the damping and stiffness are generally considered to be the constant value [45-47]. And the vehicle suspension system can be regarded as the linear suspension system when the damping and stiffness are constant values. This type of suspension system has been widely studied in the past decades and it is mainly considering its advantages of simple calculation and easily to be understood. However, as mentioned in Chapter 1 and Chapter 2, the real damping and stiffness are not the linear relationship with respect to piston velocity and the distance respectively. For example, the air suspension system can be seen in the commercial vehicles now [20, 48]. After some calculations, the spring stiffness can be described as a function as

$$F_s = k_1 \Delta x + k_2 \Delta x^2 + k_3 \Delta x^3 \tag{3.1}$$

where Δx is the relative displacement and k_1 k_2 k_3 are the nonlinear stiffness respectively. The detailed steps of how to derive Eq. (3.1) can be seen in [20]. Other reasons may also cause spring nonlinearity, such as the bumping stop of the vertical movement and the effect of strut bushing [13]. In addition, the damping characteristics can also reflect some nonlinear effect in some studies of suspension systems. One example is that the damping characteristics is described as a piecewise curve in [15]. The relationship between the damping force and piston velocity in both of the desired and the realistic damper is not proportional in the both low and high velocities. Another example is the fact that the rubber has been widely used in the design of vehicle suspension systems, while the rubber can reflect some nonlinear effects [49]. Furthermore, the nonlinear damping can be introduced by different diameters of holes which are drilled in the hydraulic shock absorbers to obtain the desired damping force in the vehicle suspension system [36].

In this study, an existing nonlinear optimal damping characteristics is adopted to make the comparative study and it is obtained from [36]. The authors consider the ride comfort and the safety as the main criteria and the weighted criteria method is adopted in the paper. The objective function can be written as

$$\Psi = w_c \Psi_c + w_s \Psi_s \tag{3.2}$$

where w_c and w_s are the weight values for ride comfort and safety respectively, while Ψ_c and Ψ_s are the criteria for the ride comfort and safety and Ψ is the overall evaluation function. The optimal damping characteristics, as example, can be seen in Figure 3.1

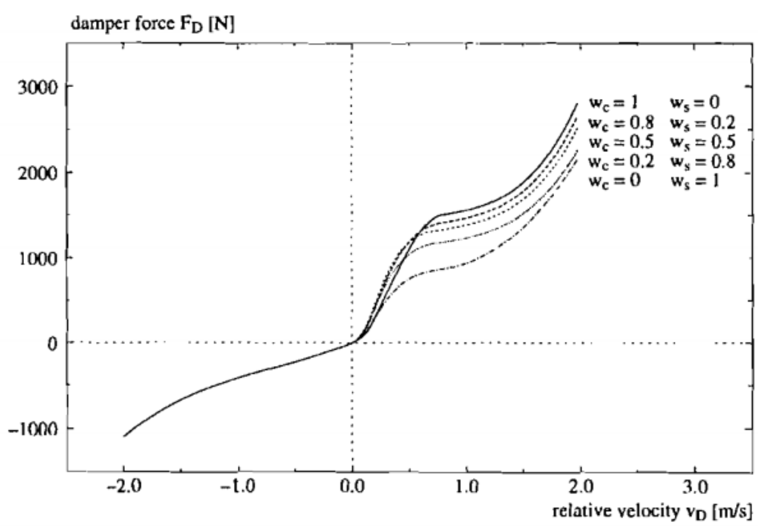

Figure 3.1 Optimal damping characteristics [36]

In the figure above, the curves are the optimal damping characteristics of a suspension system. But the complete set of data, such as the detailed function of the damping characteristics, has not been given. In order to make a comparative study, one method is to fit the data from Figure 3.1. By using the fitting method, the optimal damping characteristics can be obtained and the damping force can be described as the function with respect to the velocity according to Figure 3.1. The detailed steps of fitting the curve above can be seen in the following parts.

3.1.1 Data obtain

In Figure 3.1, it consists of several different curves, which is mainly determined by the different criteria. According to the description of w_c and w_s, the range of these two variables should be $[0,1]$. For example, if the value of w_c is 1 and the value of w_s is 0, then the main criteria is ride comfort; if the value of w_s is 1 and the value of w_c is 0, the then main criteria is safety; if both of these two values are 0.5, then the ride comfort and safety hold the same importance during the optimization. In the present study, the main objective is to reduce the vertical vibration. Therefore, the curve obtained under the condition of $w_c = 1, w_s = 0$ is the objective curve that will be used to obtain the data.

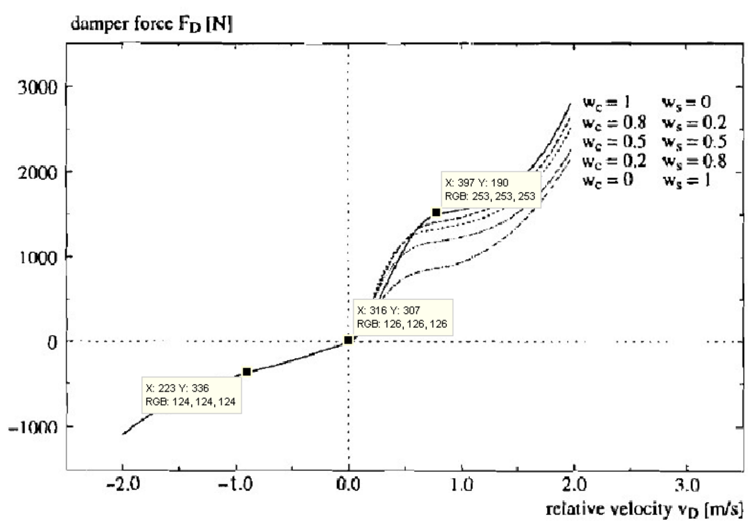

Figure 3.2 Data acquisition by Matlab

In this study, it is important to make sure that the data is accurate as it can significantly affect the results. In order to solve this problem, the damping characteristics curve is imported in the Matlab by using the 'imread' and 'imshow' function firstly; then the coordinate of the curves will be added automatically and values of all the points in the curve can be read from Matlab directly, which is much more accurate and efficient. The description of how to use Matlab to get the data can be seen in Figure 3.2.

By using Figure 3.2 above, the data which will be used to fit the damping characteristics can be obtained. In this study, the number of the data is 103 and it can be seen in Appendix B. In Figure 3.2, it is also clear that the range of the x-axis obtained in the Matlab is $[108,521]$ and the range of the y-axis is $[89,392]$. However, the real range of the x-axis is $[-2.0,2.0]$. Therefore, it can be inferred that the data obtained by Matlab is enlarged to some extent. The real value of the x-axis can be determined by

$$x_{real} = \frac{x_{Malab}-108}{103.25} - 2 \tag{3.3}$$

where x_{Malab} means the value of each point obtained in the Matlab figure while the x_{real} means the real velocity after some calculations. And the value of the y-axis can be determined by

$$y_{real} = \frac{308-y_{Matlab}}{303} * 3895 \tag{3.4}$$

where y_{Malab} means the value of each point obtained in the Matlab figure while the y_{real} means the real velocity after some calculations. After finishing the steps above, the real damping characteristics data can be obtained and all these data can be seen in Appendix B.

In conclusion, the data of the damping characteristics can be obtained according to the above steps. First, the enlarged value of the damping value can be achieved by using Matlab efficiently and actually. Second, the real damping value can be derived according to the relationship between the rough data and real data. To be noted that, in order to make sure the accuracy of the fitting result, the number of the data should be large enough. Meanwhile, during the process of obtaining the rough data, the points should be distributed homogeneously on the curve so that the points can reflect the tendency of damping curve.

3.2 Data fitting

In this section, the data which are obtained in section 3.1 will be used to fit the polynomial of the damping characteristics. Firstly, the least square fitting method will be discussed briefly. Secondly, the detailed steps of how to use this method to get the polynomial will be given.

3.2.1 Data fitting method

There are many techniques can be used to fit the data, such as least square fitting method [50], interpolation method [51] and nonlinear least square fitting method [50]. In the present study, the least square method is adopted to fulfill this objective mainly due to the fact that the present data is relatively simple. The method is to find the best polynomial for a set of points by minimizing the sum of the squares of the offsets which are obtained from the given curve [52], which can be written as

$$min \sum [y_i - f(x_i, a_1, a_2, \dots, a_n)]^2,$$

where y_i are the points in the curve and the $f(x_i, a_1, a_2, \dots, a_n)$ are the values of the polynomial derived by fitting method respectively. In the present study, the fitting process is finished by Matlab and the damping force can be described as the n^{th}degree polynomial

$$y = a_n x^n + a_{n-1} x^{n-1} + a_{n-2} x^{n-2} + \cdots + a_1 x + a_0 \tag{3.5}$$

where a_n is the coefficient and y is the final polynomial. In equation 3.5, x is the velocity, a_n is the relative damping value and y is the damping force. In this form, the damping force is the function with respect to the velocity. To be noted that, when the velocity $x = 0$, the damping force should be 0. The reason is that when there is no velocity, the damper could not produce any damping force in the real applications.

3.2.2 Data fitting steps

As mentioned above, the value of a_0 in Eq. (3.5) should be equal to 0. However, it is hard to use the polyfit or the polyval function to realize this objective in Matlab even though the order of the polynomial is large. In order to obtain the desired polynomial, the fitting process is finished by using Matlab GUI and the basic theory of GUI fitting technique is the same as polyfit or polyval. However, GUI can be used to fit the polynomial based on the customer's command. For example, in this part, the form which is used to fit the data is

$$y = a_n x^n + a_{n-1} x^{n-1} + a_{n-2} x^{n-2} + \cdots + a_1 x \tag{3.6}$$

In this way, the value of a_0 is 0 before fitting, which can make sure the accuracy of the final result. By choosing different orders of Eq. (3.6), the polynomial can be achieved. However, in Figure 3.2 the range of the velocity is$[-2.0,2.0] m/s$, but the velocity range of some real dampers is only$[-0.5,0.5] m/s$. For example, the damping characteristics of a real damper which is made by the ZF Sachs AG Company can be shown in Adams/View

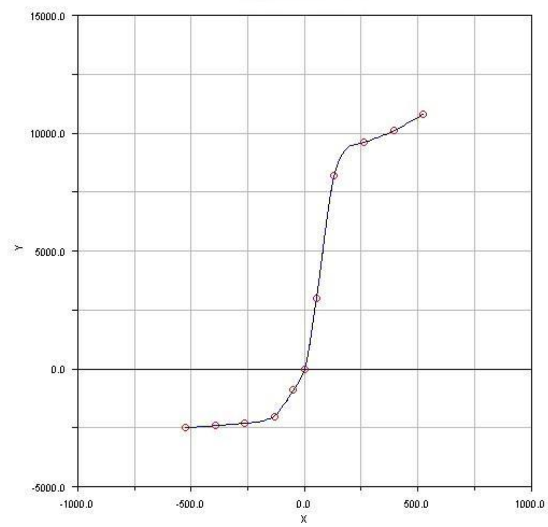

Figure 3.3 Damping characteristics of a real damper (unit of x_axis is mm/s, y_axis is N)

Therefore, in the present study, the velocity is chosen to be$[-0.5,0.5] m/s$. And only part of the whole data will is used to fit the polynomial. Then the polynomial of the damping characteristics can be achieved and it can be written as

$$F_{fit} = 1641\dot{x}^3 + 1882\dot{x}^2 + 937.2\dot{x} \tag{3.7}$$

where F_{fit} is the damping force and $\dot{x}$ is the velocity. In Eq. (3.7), the last term is the linear damping and the first two terms are the nonlinear damping effect. The comparison between the fitted curve and the initial curve can be seen in Figure 3.3

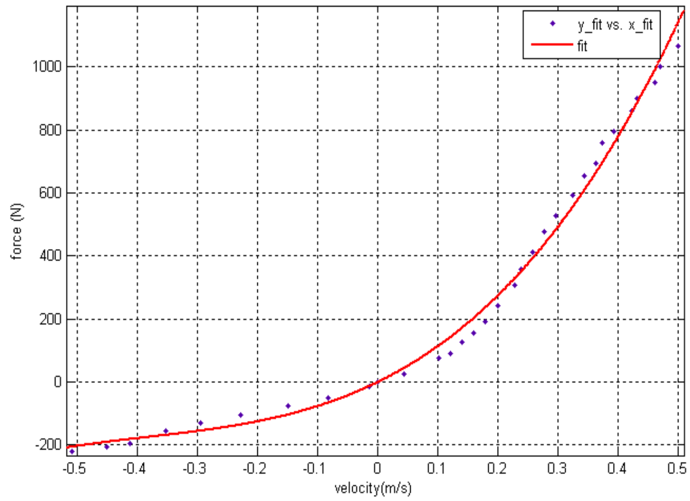

Figure 3.4 Comparison between the fitted curve and the initial optimal curve (3rd order)

From Figure 3.4, it can be shown that the fitted curve can match the initial curve very well. If the order is increased, the performance will not increase too much. In some cases, the tendency of the fitted curve is not true when the order of the function is increased. For example, when the order of the polynomial is 4 then the comparison can be seen in Figure 3.5.

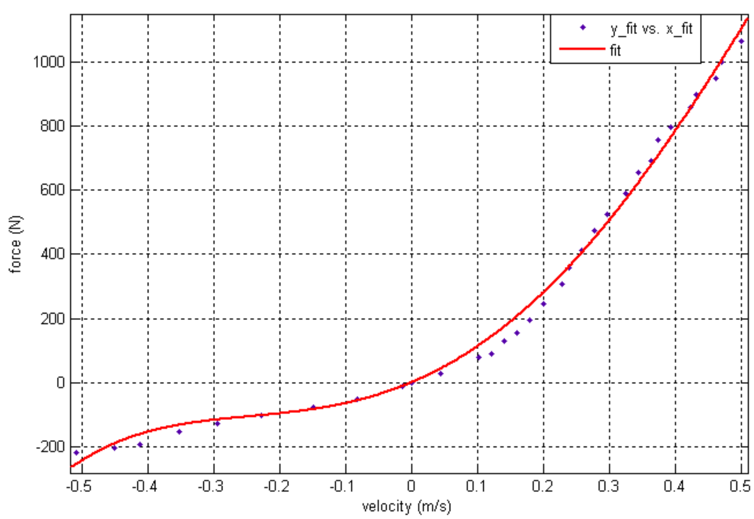

Figure 3.5 Comparison between the fitted curve and the initial optimal curve (4th order)

In Figure 3.5, it can be shown that when the velocity is less than $-0.4m/s$, the gradient of the damping force will be increased. That is to say there exists an inflection point at the velocity of $-0.4m/s$ while there is no obvious inflection point in the compressed period of the initial curve. Therefore, this order will not match the tendency of the initial data when the order of the function is 4.

3.3 Damping characteristics obtained by the OFRF-based analysis method

In this section, the nonlinear optimal damping characteristics will be obtained by the nonlinear frequency domain analysis method. The detailed steps of how to use this method have been presented above and some brief descriptions will be given here.

3.3.1 Derivation of the optimal damping characteristics

In this part, the model is the same as the model presented in section 2.1 and it can be seen in Figure 3.6

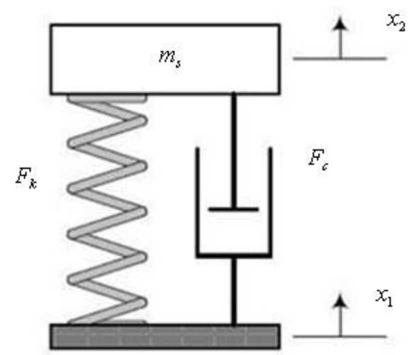

Figure 3.6 1 DOF quarter vehicle suspension model

The definitions can be seen in section 2.1 except the nonlinear damping force F_c. In this part, the main objective is to compare the optimal damping characteristics obtained by the OFRF-based analysis method with the previous optimal damping curve. The nonlinear damping force is $F_c = c\dot{x} + a\dot{x}^2 + b\dot{x}^3$ and therefore the governing equation can be written as

$$m_s\ddot{x} + kx + c\dot{x} + a\dot{x}^2 + b\dot{x}^3 = -m_s\ddot{x}_1 \tag{3.8}$$

where a and b are the nonlinear damping parameters which need to be determined in this study. The transmitted force can be written as

$$F = kx + c\dot{x} + a\dot{x}^2 + b\dot{x}^3 \tag{3.9}$$

According to [36] and [46], the detailed value of the stiffness and mass are $m_s = 290kg, k = 16812N/m$. Then the system natural frequency can be obtained as

$$f = \sqrt{\frac{k}{m_s}} = 7.6rad/s \tag{3.10}$$

The input signal is assumed to be a sine wave and the amplitude is $50\ mm$, which can be approximately regarded as the real road amplitude [53]. The input frequency is chosen to be same as the vehicle natural frequency. Therefore, the system input signal can be written as

$$x_1 = 0.05\, sin(7.6t)\, m/s \tag{3.11}$$

Substituting equations above and system parameters in the equation (3.8) and it can be written as

$$290\ddot{x} + 16812x + 937.2\dot{x} + a\dot{x}^2 + b\dot{x}^3 = 840.6084\ddot{x}_1 \tag{3.12}$$

Finally, after some calculations and simplifications, the system governing equation can be written as

$$\begin{cases} 290\ddot{x} + 16812x + 937.2\dot{x} + a\dot{x}^2 + b\dot{x}^3 = 840.6084\ddot{x}_1 \\ F = 16812x + 937.2\dot{x} + a\dot{x}^2 + b\dot{x}^3 \end{cases} \tag{3.13}$$

In this study, the objective is to reduce the transmitted force between the sprung mass and the base excitement. In order to realize this objective, the system output frequency response function should be obtained. The steps to derive the system output spectrum have been discussed in Chapter 2 and thus are not given here in order to save space. The Simulink block diagram of the system can be seen in Figure 3.7.

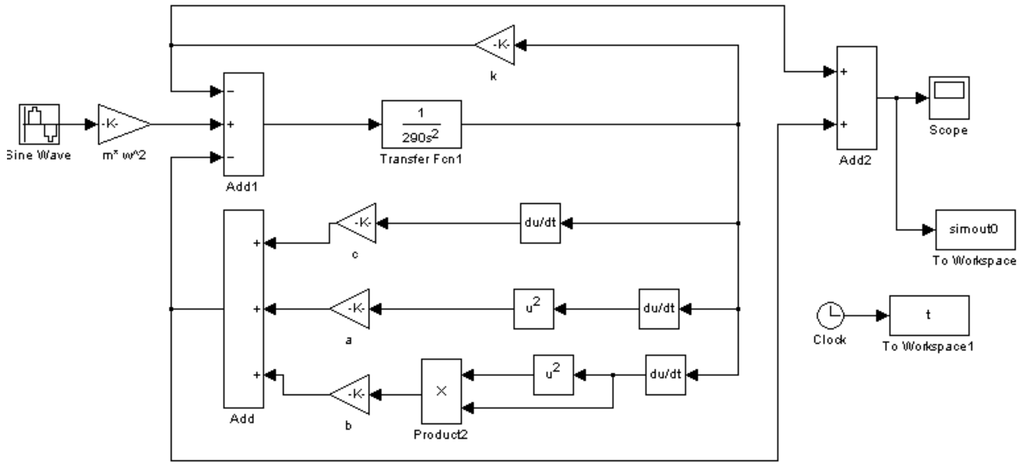

Figure 3.7 System Simulink model

Then the system output spectrum with respect to system parameters a, b can be seen in Figure 3.8

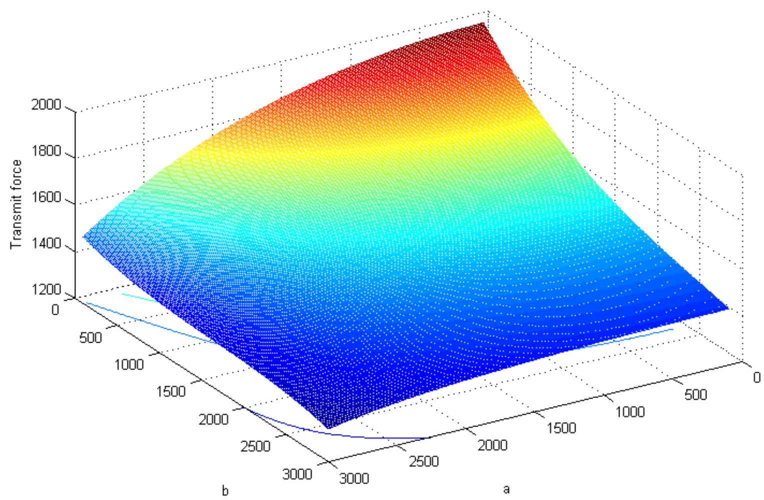

Figure 3.8 Nonlinear output spectrum with respect to a and b

In Figure 3.8, it is clear that when the value of a and b increase, the system output spectrum will decrease, which means that the transmitted force will be decreased. If the objective is to reduce the transmitted force, the value of the a and b should be large. However, this does not mean that in order to get the minimum transmit force, the value of a and b should be large enough or infinite. There are two reasons. The first reason is that when the value of a and b is very large, then the equivalent damping will also become very large. And the second reason is that if the value of a and b is very large, the damping force in the compression period will be positive and this is not acceptable. Taking the case of $a = 4000$ and $b = 4000$ as an example, the damping characteristics will become as

$$F_d = 937.2\dot{x} + 4000\dot{x}^2 + 4000\dot{x}^3 \tag{3.17}$$

Then the system damping characteristics of Eq. (3.17) can be seen in Figure 3.9.

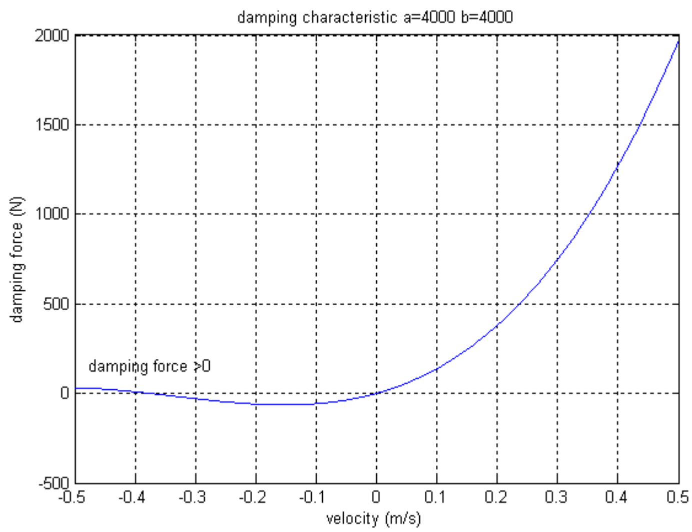

Figure 3.9 Damping characteristics ($a = 4000, b = 4000$)

In Figure 3.9, it is clear that when the velocity is in the period of $[-0.5, -0.4]m/s$, the damping force will be larger than 0. The gradient of the damping characteristics curve in this velocity range will be negative, which cannot be achieved by the real damping system. Meanwhile, in the real vehicle suspension system, the damper should absorb energy in order to reduce vibration. Therefore, the damping characteristics is not useful theoretically and practically when the nonlinear damping parameters get the value of $a = 4000, b = 4000$.

By analyzing the problem above, the main reason is that the value of parameter a is too large. For a given value of b, the value of a can be determined properly. In Figure 3.9, the system damping characteristics at the value of $b = 4000$ and the values of $a = [500,1000,2000,3000,4000,5000]$ are given as follows respectively.

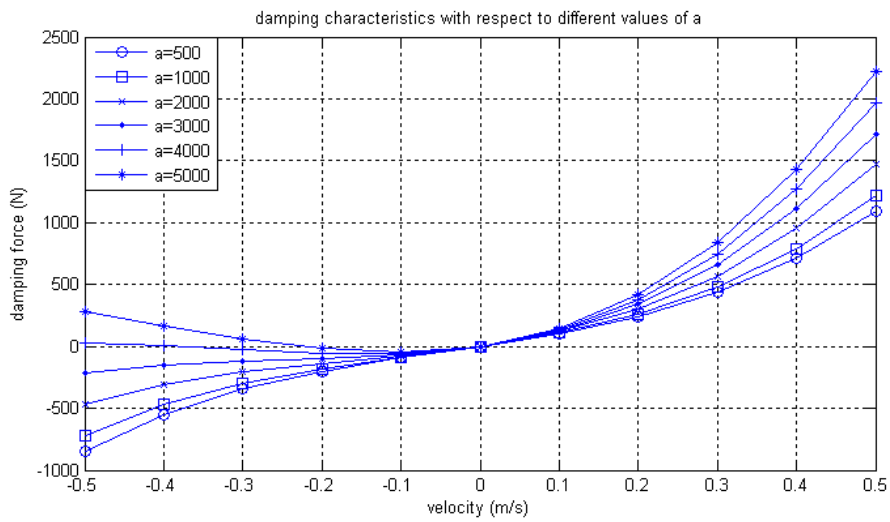

Figure 3.10 Damping characteristics with respect to the different values of a

From Figure 3.10, it is clear that the damping characteristics curves vary with respect to the values of a. Based on the discussions above, it can be concluded that

1. In order to reduce the system output the values of parameter a and b should be large enough.
2. The maximum value of a should be determined by the value of b in order to make sure the damping characteristics is accurate.

In some real vehicle suspension system, the damping characteristics are determined by many different evaluation standards, such as the ride comfort, suspension stroke and handling ability. Meanwhile, the damping characteristics should also be restricted by the real application. In this study, as the main objective is vertical vibration reduction, therefore a relatively large damping value is regarded as the optimal damping characteristics. Here the combination of $a = 3800, b = 4000$ is regarded as the optimal damping value obtained by the OFRF-based analysis method and the damping characteristics will become

$$F_d = 937.2\dot{x} + 3800\dot{x}^2 + 4000\dot{x}^3 \tag{3.18}$$

3.4 Comparative studies

According to section 3.1, section 3.2 and section 3.3 above, the two optimal damping characteristics are obtained. The first one is the damping characteristics fitted from an existing literature and it can be written as

$$F_{fit} = 937.2\dot{x} + 1882\dot{x}^2 + 1641\dot{x}^3 \tag{3.19}$$

The second one is obtained by using the OFRF-based analysis method and it can be written as

$$F_d = 937.2\dot{x} + 3800\dot{x}^2 + 4000\dot{x}^3 \tag{3.20}$$

In this study, these two damping characteristics will be used to make several comparative studies to show their effects in suppression of the vibration. And the system performance under different input signals will be given in the following parts.

3.4.1 The input frequency is changed

In this case, the input frequency is chosen as the variables and the system transmitted force of the linear system and two nonlinear optimal systems are given as follows

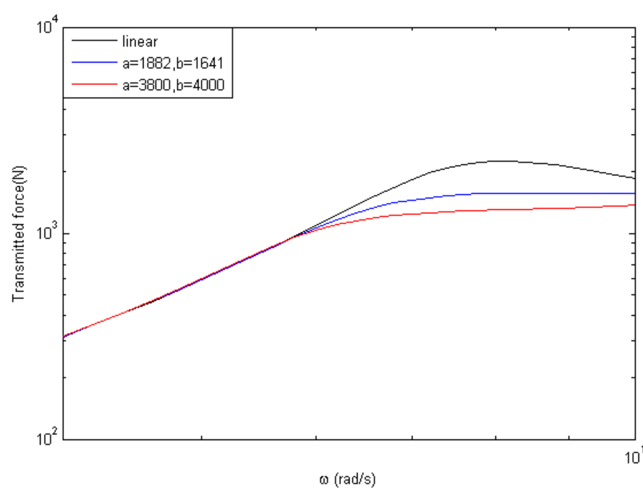

Figure 3.11 Transmitted force with respect to different systems

In Figure 3.11, the transmitted forces of three different systems are given. The frequency of the input signal is chosen from 4 $\mathrm{rad/s}$ to 10 $\mathrm{rad/s}$. It can be shown that in the low frequency range, the vibration performance of the nonlinear system does not have significant improvement when compared with the linear system. In the resonant frequency, the vibration can be suppressed significantly. Some specific cases are given as follows.

1. The input signal is $x_1 = 0.05\,sin(7.6t)$

Table 3.1 System output when the input frequency is $7.6rad/s$

Damping characteristics	System output (N)
$F_d = 937.2\dot{x}$	2159.9
$F_{fit} = 937.2\dot{x} + 1882\dot{x}^2 + 1641\dot{x}^3$	1536.4
$F_d = 937.2\dot{x} + 3800\dot{x}^2 + 4000\dot{x}^3$	1278.0

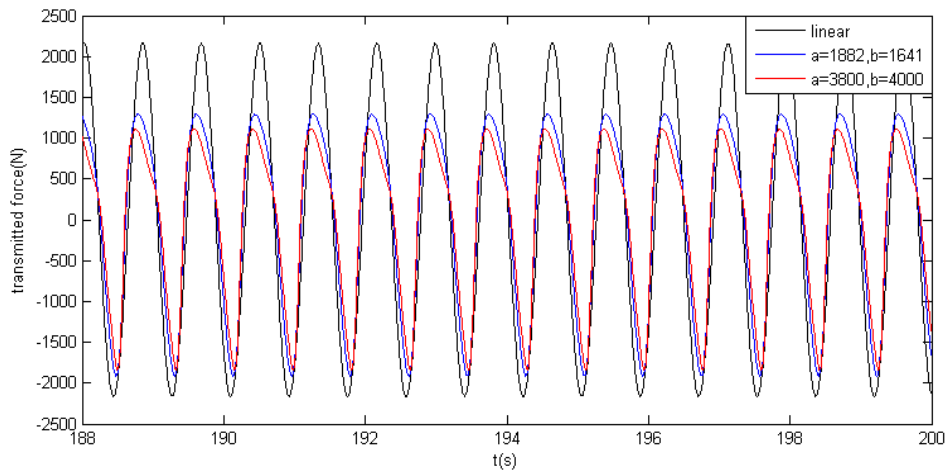

Figure 3.12 Transmitted force when the input frequency is $7.6rad/s$

2. The input signal is $x_1 = 0.05\,sin(6t)$

Table 3.2 System output when the input frequency is $6rad/s$

Damping characteristics	System output (N)
$F_d = 937.2\dot{x}$	1087.5
$F_{fit} = 937.2\dot{x} + 1882\dot{x}^2 + 1641\dot{x}^3$	1056.4
$F_d = 937.2\dot{x} + 3800\dot{x}^2 + 4000\dot{x}^3$	1027.7

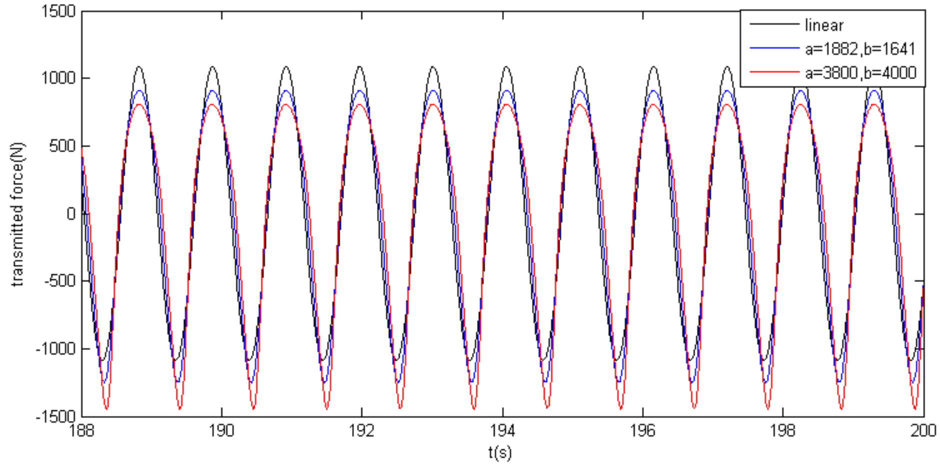

Figure 3.13 Transmitted force when the input frequency is $6rad/s$

3. The input signal is $x_1 = 0.05\,sin(10t)$

Table 3.3 System output when the input frequency is $10rad/s$

Damping characteristics	System output (N)
$F_d = 937.2\dot{x}$	1851.6
$F_{fit} = 937.2\dot{x} + 1882\dot{x}^2 + 1641\dot{x}^3$	1552.9
$F_d = 937.2\dot{x} + 3800\dot{x}^2 + 4000\dot{x}^3$	1369.9

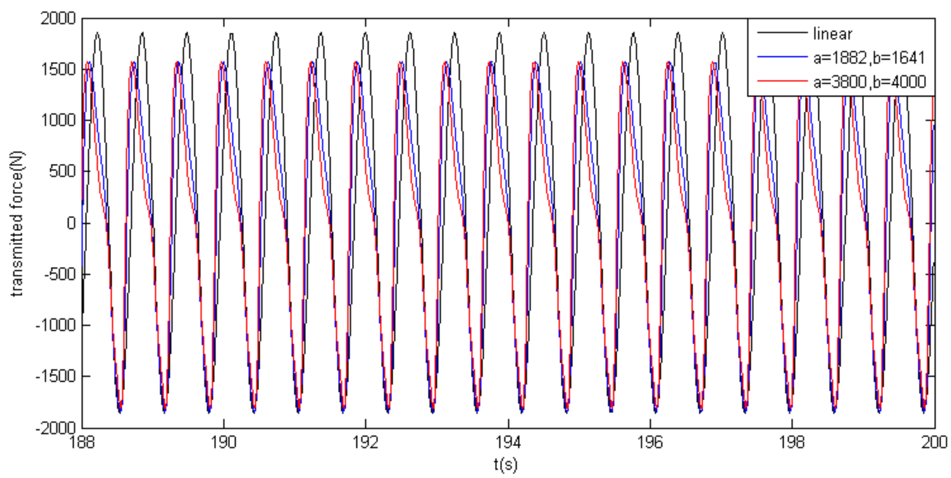

Figure 3.14 Transmitted force when the input frequency is $10rad/s$

From Figure 3.11 to Figure 3.14, it is obvious that in the resonant frequency range, the optimal damping characteristics obtained by the OFRF-based analysis method demonstrates better performance than the existing nonlinear optimal damping characteristics and the linear damping characteristics. In the low or high frequency range, the optimal damping characteristics are still better than the fitted optimal damping value. But the vibration performance will not improve too much. Therefore, it can be concluded that at the resonant frequency range, the nonlinear damping characteristics are better than the linear damping characteristics in the vibration suppression; the nonlinear optimal damping characteristics obtained by using the nonlinear frequency domain analysis method is better than the previous optimal nonlinear damping characteristics.

3.4.2 The input magnitude is changed

In this case, the input magnitude is chosen to be variables and the system transmitted force of the linear system and two nonlinear optimal systems are given in Figure 3.15.

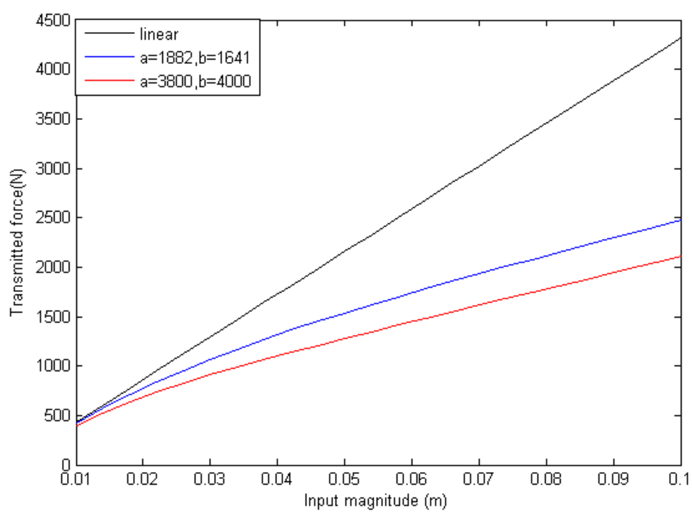

Figure 3.15 Transmitted force with respect to different systems

In Figure 3.15, the transmitted force of three different systems is given. The magnitude of the input signal is chosen from $0.01m$ to $0.1m$ to show the effect of nonlinearities on the system vibration suppression. It is clear that when the magnitude is large, the vibration performance obtained by the nonlinear damping characteristics will be more obvious. Meanwhile, the damping characteristics obtained by using the nonlinear frequency domain analysis method are better than the existing optimal damping characteristics. Some specific cases are given as follows.

1. The input signal is $x_1 = 0.07\,sin(7.6t)$

Table 3.4 System output when the input magnitude is $0.07m$

Damping characteristics	System output (N)
$F_d = 937.2\dot{x}$	3023.8
$F_{fit} = 937.2\dot{x} + 1882\dot{x}^2 + 1641\dot{x}^3$	1931.5
$F_d = 937.2\dot{x} + 3800\dot{x}^2 + 4000\dot{x}^3$	1611.7

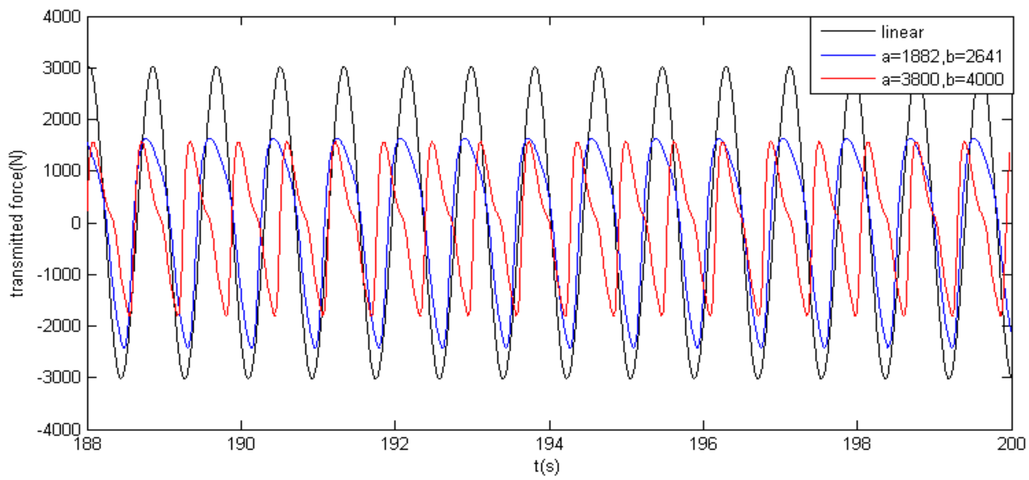

Figure 3.16 Transmitted force when the input magnitude is $0.07m$

2. The input signal is $x_1 = 0.1\,sin(7.6t)$

Table 3.5 System output when the input magnitude is $0.1m$

Damping characteristics	System output (N)
$F_d = 937.2\dot{x}$	4319.8
$F_{fit} = 937.2\dot{x} + 1882\dot{x}^2 + 1641\dot{x}^3$	2468.6
$F_d = 937.2\dot{x} + 3800\dot{x}^2 + 4000\dot{x}^3$	2105.6

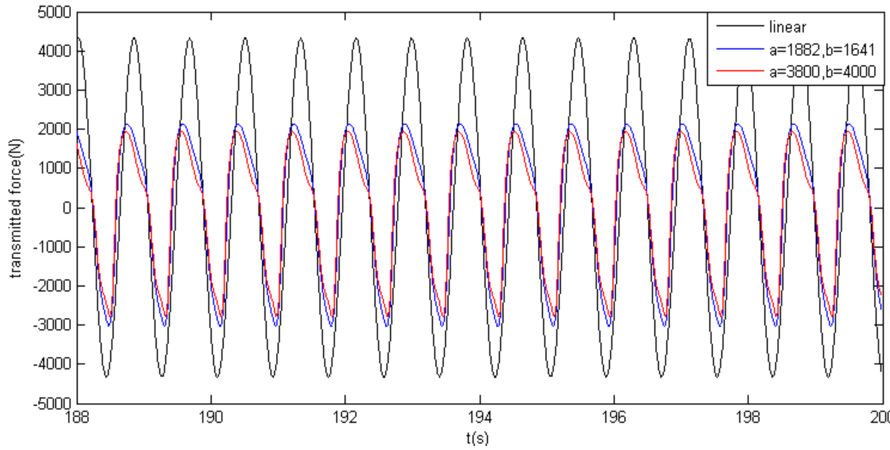

Figure 3.17 Transmitted force when the input magnitude is $0.1m$

3. The input signal is $x_1 = 0.03\,sin(7.6t)$

Table 3.6 System output when the input magnitude is $0.03m$

Damping characteristics	System output (N)
$F_d = 937.2\dot{x}$	1295.9
$F_{fit} = 937.2\dot{x} + 1882\dot{x}^2 + 1641\dot{x}^3$	1065.9
$F_d = 937.2\dot{x} + 3800\dot{x}^2 + 4000\dot{x}^3$	913.9

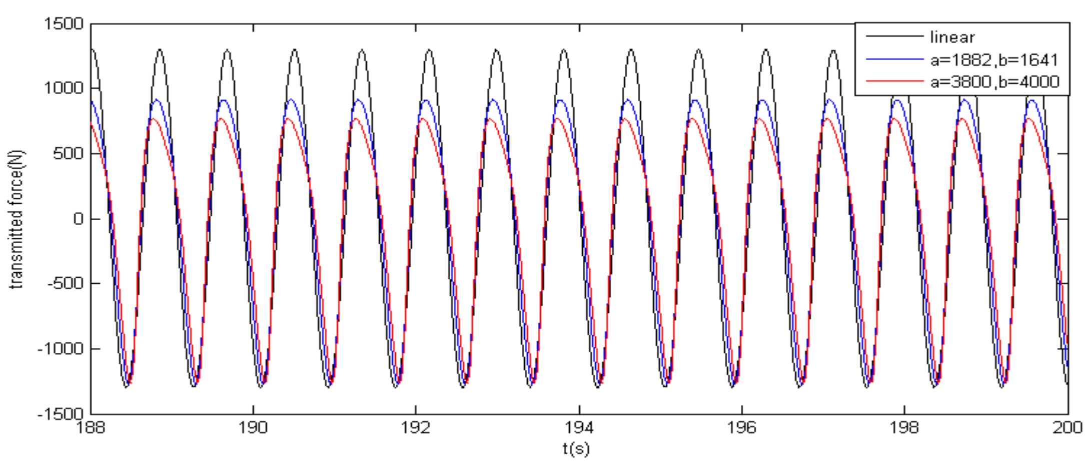

Figure 3.18 Transmitted force when the input magnitude is $0.03m$

4. The input signal is $x_1 = 0.01\, sin(7.6t)$

Table 3.7 System output when the input magnitude is $0.01m$

Damping characteristics	System output (N)
$F_d = 937.2\dot{x}$	432.0
$F_{fit} = 937.2\dot{x} + 1882\dot{x}^2 + 1641\dot{x}^3$	417.4
$F_d = 937.2\dot{x} + 3800\dot{x}^2 + 4000\dot{x}^3$	399.0

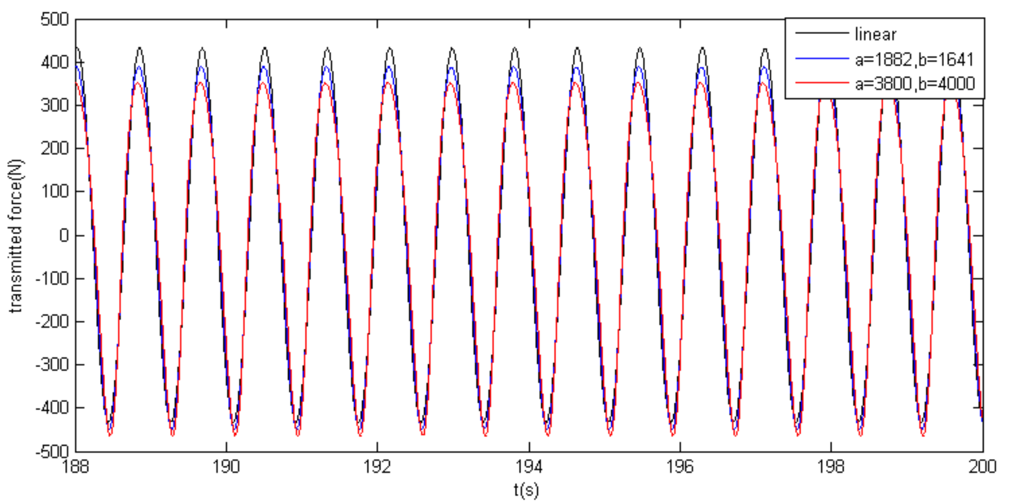

Figure 3.19 Transmitted force when the input magnitude is $0.01m$

From Figure 3.15 to Figure 3.19, all the studies are conducted under the condition of input frequency is equal to the resonance frequency. It can be shown that the both of these two nonlinear optimal damping characteristics are better than the linear damping characteristics. To be more specific, the nonlinear optimal damping characteristics obtained by the nonlinear frequency domain analysis method is much more competitive than the existing optimal damping value when the signal input magnitude ranges from $0.01m$ to $0.1m$. When the input magnitude is larger, the performance of the damping characteristics obtained by nonlinear frequency domain analysis method will be better than the fitted optimal damping characteristics. When the input magnitude is relatively small, the damping characteristics obtained by nonlinear frequency domain analysis method is still better than the fitted optimal damping characteristics. Therefore, it can be concluded that the damping characteristic obtained by nonlinear frequency domain analysis method will be more effective than the existing optimal damping characteristics when the input magnitude changes.

3.4.3 The input magnitude and frequency is changed

1. The input signal is $x_1 = 0.03\, sin(10t)$

Table 3.8 System output when the input signal is $x_1 = 0.03\, sin(10t)$

Damping characteristics	System output (N)
$F_d = 937.2\dot{x}$	1110.9
$F_{fit} = 937.2\dot{x} + 1882\dot{x}^2 + 1641\dot{x}^3$	1002.7
$F_d = 937.2\dot{x} + 3800\dot{x}^2 + 4000\dot{x}^3$	887.8

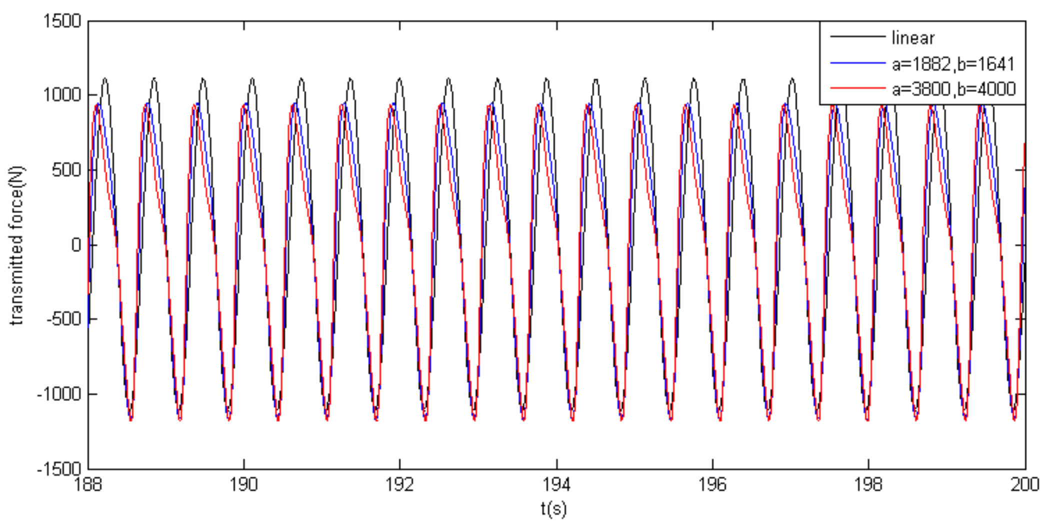

Figure 3.20 Transmitted force when the input signal is $x_1 = 0.03\, sin(10t)$

2. The input signal is $x_1 = 0.03\, sin(6t)$

Table 3.9 System output when the input signal is $x_1 = 0.03\, sin(6t)$

Damping characteristics	System output (N)
$F_d = 937.2\dot{x}$	652.5
$F_{fit} = 937.2\dot{x} + 1882\dot{x}^2 + 1641\dot{x}^3$	646.3
$F_d = 937.2\dot{x} + 3800\dot{x}^2 + 4000\dot{x}^3$	646.1

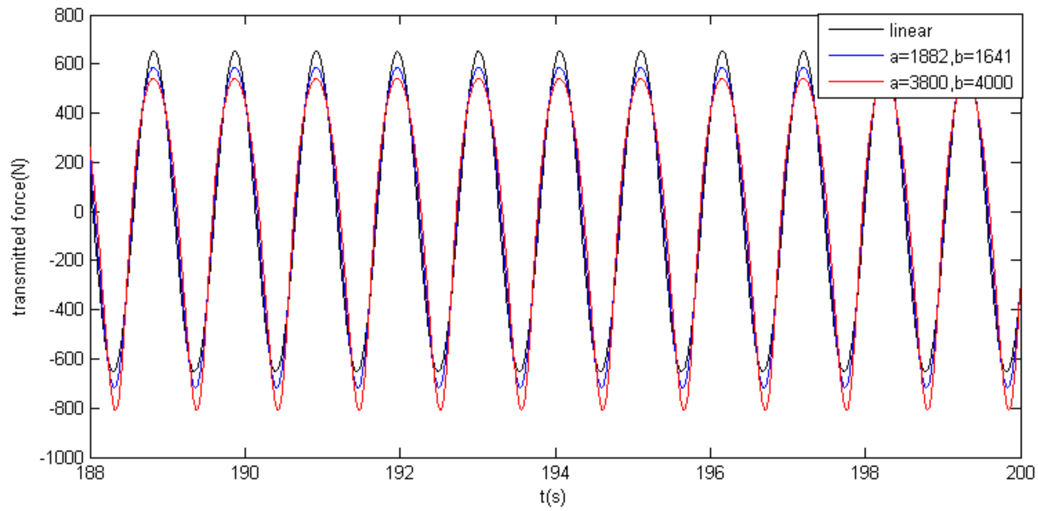

Figure 3.21 Transmitted force when the input signal is $x_1 = 0.03\, sin(6t)$

3. The input signal is $x_1 = 0.1\, sin(10t)$

Table 3.10 System output when the input signal is $x_1 = 0.1\, sin(10t)$

Damping characteristics	System output (N)
$F_d = 937.2\dot{x}$	3703.1
$F_{fit} = 937.2\dot{x} + 1882\dot{x}^2 + 1641\dot{x}^3$	2884.2
$F_d = 937.2\dot{x} + 3800\dot{x}^2 + 4000\dot{x}^3$	2701.4

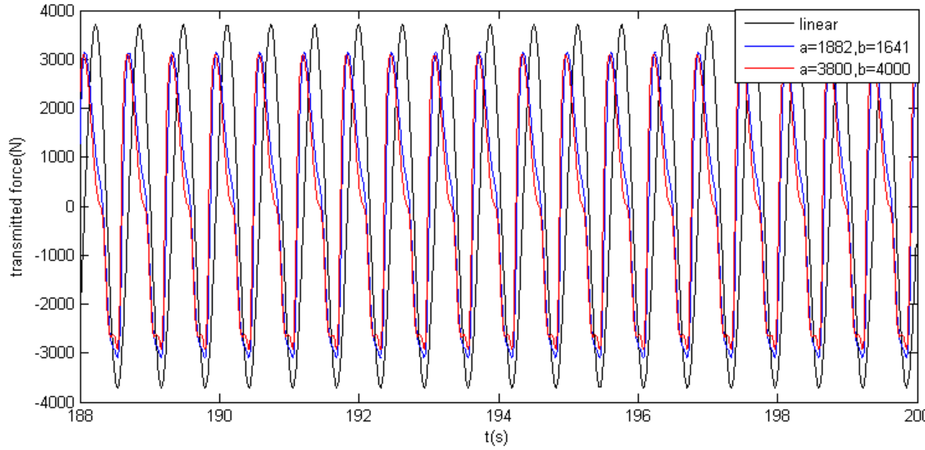

Figure 3.22 Transmitted force when the input signal is $x_1 = 0.1\, sin(10t)$

4. The input signal is $x_1 = 0.1\, sin(6t)$

Table 3.11 System output when the input signal is $x_1 = 0.1\, sin(6t)$

Damping characteristics	System output (N)
$F_d = 937.2\dot{x}$	2174.9
$F_{fit} = 937.2\dot{x} + 1882\dot{x}^2 + 1641\dot{x}^3$	1926.3
$F_d = 937.2\dot{x} + 3800\dot{x}^2 + 4000\dot{x}^3$	1725.9

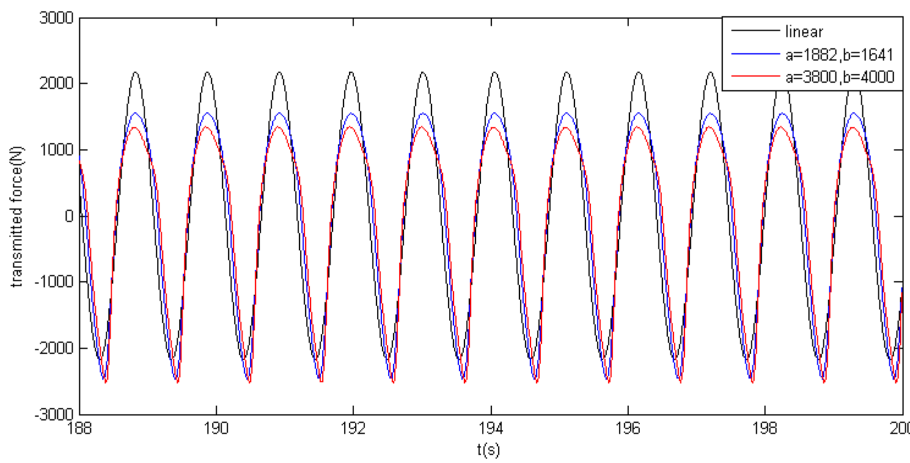

Figure 3.23 Transmitted force when the input signal is $x_1 = 0.1\, sin(6t)$

In this part, the system is simulated under different input signals. The input signal frequency is $6\, rad/s$ and $10\, rad/s$, while the input magnitude is $0.1m$ and $0.03m$, thus generates four combinations. From those combinations, it can be shown that the nonlinear optimal damping characteristics obtained by the nonlinear frequency domain analysis method are better than the fitted optimal damping characteristics.

3.4.4 Comparison between small damping system and nonlinear damping system

The comparative study between the system with small linear damping and the system with small linear damping and nonlinear damping is conducted to show the effect of system nonlinearities. Here, the system mass and spring stiffness are the same as the values in section 3.3 and the linear damping value are $c = 552N.s/m$ and $c = 100N.s/m$. The nonlinear system is obtained by adding some nonlinear terms on the linear ones. In order to show the effect of system nonlinearity on the vibration performance, the nonlinear term values of both systems are assumed to be$100\dot{x}^2 + 1000\dot{x}^3$. The system input is $x_1 = 0.05\, sin(7.6t)$ .Then the system transmitted force at the resonant frequency can be obtained respectively.

1. $c = 552N.s/m$

Table 3.12 System output when the linear damping is $c = 552N.s/m$

Damping characteristics	System output (N)
$F_d = 552\dot{x}$	3471.5
$F_{fit} = 552\dot{x} + 100\dot{x}^2 + 1000\dot{x}^3$	1975.4

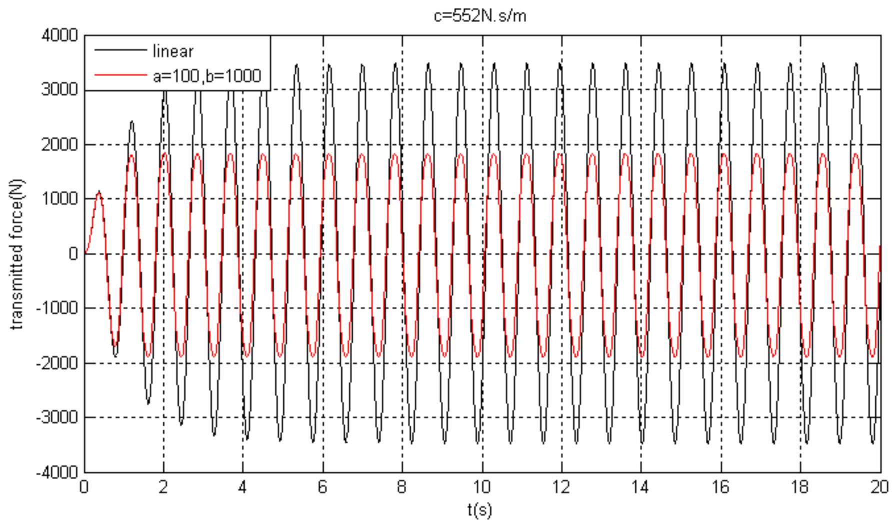

Figure 3.24 Transmitted force when the linear damping is $c = 552N.s/m$

2. $c = 100N.s/m$

Table 3.13 System output when the linear damping is $c = 100N.s/m$

Damping characteristics	System output (N)
$F_d = 100\dot{x}$	1846.8
$F_{fit} = 100\dot{x} + 100\dot{x}^2 + 1000\dot{x}^3$	2343.7

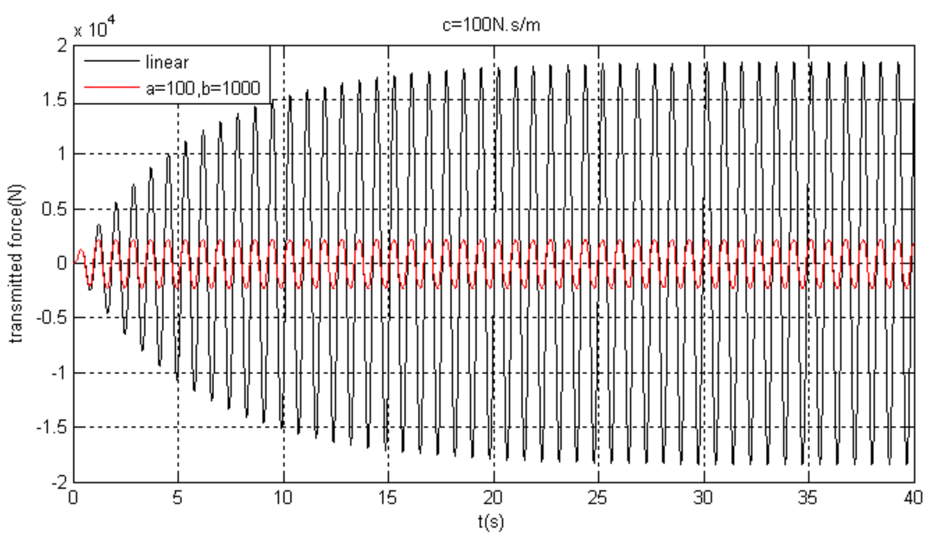

Figure 3.25 Transmitted force when the linear damping is $c = 100N.s/m$

From the two case studies above, it can be concluded that the system nonlinearities can be effective in suppressing the system vibration for the small damping system. In addition, when the system damping value is small, the effect of nonlinearities will be more obvious. Meanwhile, the system nonlinearities can also be helpful in reducing transient state and make the system become stable quickly.

3.4.5 Comparison between large damping system and nonlinear damping system

The comparative study between the system with large linear damping and the system with large damping and nonlinear damping are conducted to show the effect of system nonlinearities. Here, the system mass and spring stiffness are the same as the values in section 3.3 and the linear damping value is $c = 5000N.s/m$. The nonlinear system is obtained by adding some nonlinear terms on the linear ones. In order to show the nonlinearity on the system performance, the nonlinear term values of the system are assumed to be $5000\dot{x}^2 + 8000\dot{x}^3$. The system input is $x_1 = 0.05\,sin(7.6t)$ .Then the system transmitted force at the resonant frequency can be obtained respectively.

Table 3.14 System output when the linear damping is $c = 5000N.s/m$

Damping characteristics	System output (N)
$F_d = 5000\dot{x}$	921.6
$F_{fit} = 5000\dot{x} + 5000\dot{x}^2 + 8000\dot{x}^3$	916.5

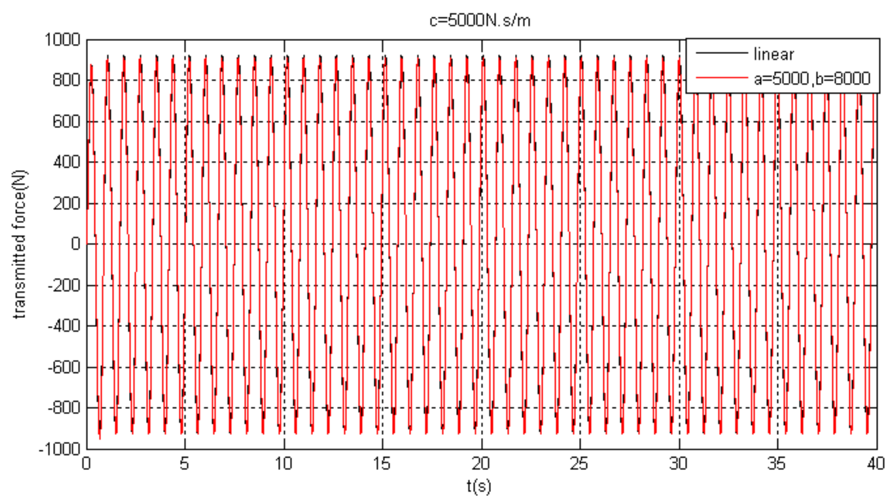

Figure 3.26 Transmitted force when the linear damping is $c = 5000N.s/m$

From Figure 3.26, it can be concluded that the vibration performance of the nonlinear large damping system cannot improve significantly when compared with the linear system. The time from transient state to stable state for both systems is almost the same. In this case, the system nonlinearities could not show any improvement than the linear system.

3.5 Dynamic model verification

In section 3.4, it can be shown that the nonlinear damping characteristics obtained by the nonlinear frequency domain analysis method is better than the previous optimal damping characteristics and both of these two damping characteristics are better than the linear one. However, these results are obtained based on the theoretical and mathematical study, and it is necessary to conduct some experiments to verify whether the result is accurate on the real dynamic model. In this study, the experiment is replaced by the simulation study based on Adams. The dynamic model of the spring damper system can be built by using Adams and it can be seen in Figure 3.27.

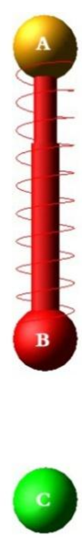

Fig 3.27 Dynamic model of the 1 degree of freedom spring damper system

In Figure 3.27, there are three balls and each ball has different meanings. A ball represents the body mass and it has the mass of $290kg$. B ball represents the base excitation. In the present study, the base excitation is a sine function and this can be readily realized in Adams by using the motion function. C ball is regarded as the reference and it is added to ground directly. To be noted that the distance between A ball and B ball should be reasonable, otherwise the simulation study will fail. A simple case is that if the magnitude of the movement of A ball is larger than the distance between A and B, then A will move to the location lower than B and this is not reasonable. Meanwhile, the distance between A ball and B ball has not influence on the result. Here two examples are given to show this effect.

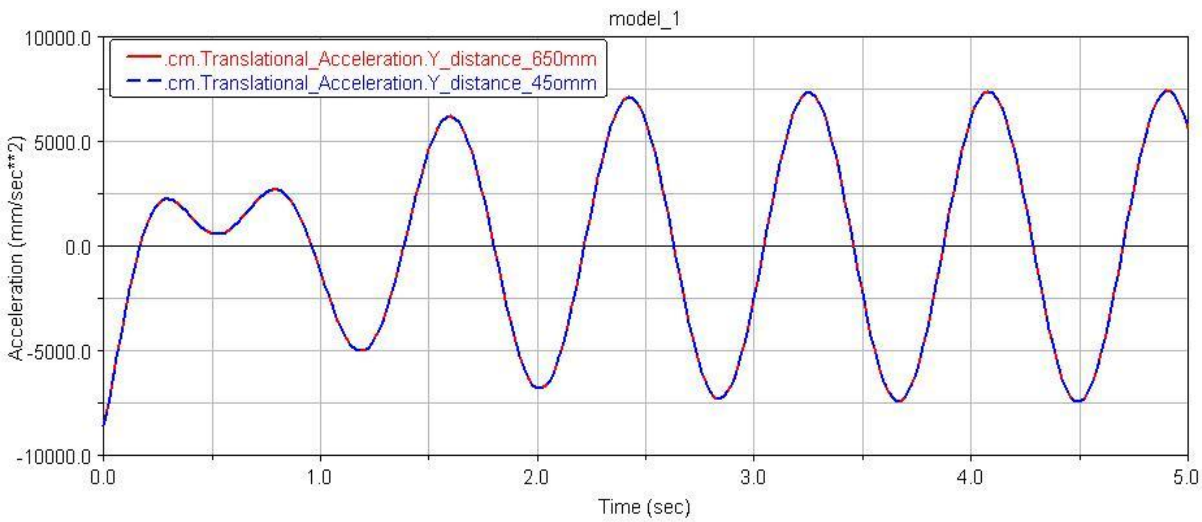

Figure 3.28 Vertical acceleration of the body mass

In the Figure above, x-axis is time and y-axis is vertical acceleration, which can be obtained directly from Adams. In Figure 3.25, the red solid line is the acceleration obtained when the initial relative displacement between A ball and B ball is $650mm$ and the blue dotted line is the acceleration obtained when the initial relative displacement is $450mm$. It can be shown that the displacement between A and B has no effect on the vibration performance. Importing the linear damping, nonlinear damping obtained by fitting method and the OFRF based analysis method, the vertical acceleration can be achieved. The stiffness and mass are mentioned in section 3.3. In this case, the base excitation in the Adams model can be written as

$$x_1 = 50\, sin(7.6 * time)mm \tag{3.26}$$

By using the base excitation above, the system vertical accelerations of three different systems with linear damping, the nonlinear damping obtained in the literature and that obtained by the nonlinear frequency domain analysis method can be obtained respectively and shown in Figure 3.29.

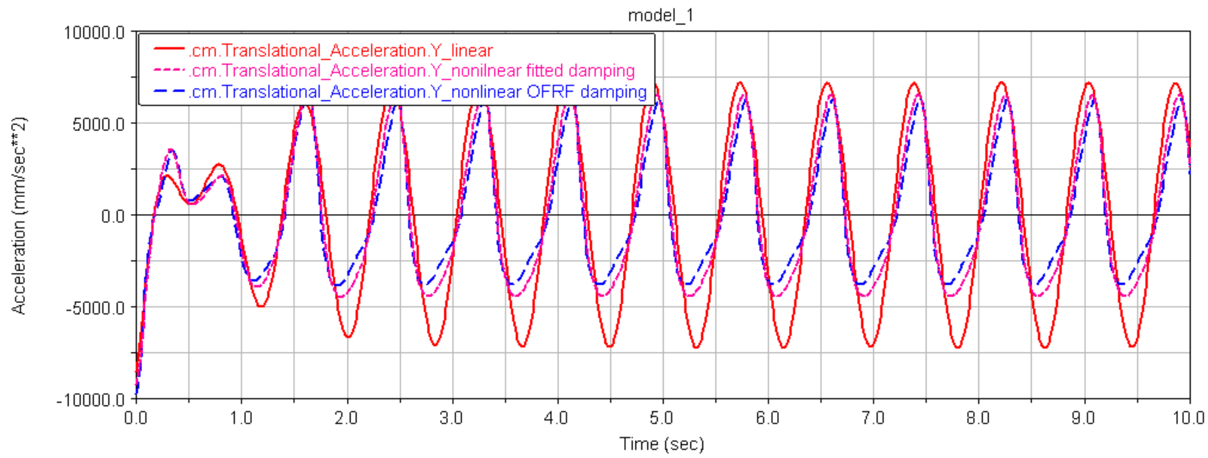

Figure 3.29 Vertical acceleration with respect to three different damping values

Table 3.15 RMS and maximum of the vertical acceleration

	Vertical acceleration RMS (mm/s^2)	Maximum vertical acceleration of stable period (mm/s^2)
Linear damping	7198	5084
Nonlinear damping by fitting method	6634	3878
Nonlinear damping by OFRF method	6331	3368

From Figure 3.29 and Table 3.15, it is clear that the nonlinear damping is more effective in suppressing the vertical vibration. Meanwhile, the nonlinear damping characteristics obtained by the nonlinear frequency domain analysis method is better than the fitted curve, which means that the nonlinear frequency domain analysis method is effective in the analysis and design of the damping characteristics.

3.6 Conclusion

In this chapter, the comparative results show that the nonlinear optimal damping characteristics obtained by using the nonlinear frequency domain analysis method are more effective than the existing nonlinear optimal damping characteristics. By using the nonlinear frequency domain analysis method, the relationship between the system output spectrum and system nonlinear parameters can be derived. Through further analyzing the system output, it can be concluded that

1. The system output spectrum is a decreasing function with respect to nonlinear parameter a and b.

2. The value of the nonlinear parameter a and b need to be determined properly in order to make sure the real damping characteristics accurate and reasonable

From the comparative studies above, it is clear that the nonlinear damping characteristics obtained by using the nonlinear frequency domain analysis method demonstrate better performance than the existing optimal damping characteristics. However, it is also necessary to do some studies to analyze its effect on the vehicle dynamic models. Meanwhile, it is still unknown whether the induced nonlinearities can have some negative effects on the vehicle other evaluation standards, such as the handling ability and suspension stroke. In the next chapter, a full vehicle dynamic model will be built to analyze the induced nonlinear effects on these evaluation indexes.

Chapter 4 Application on a dynamic vehicle model

In this study, it is hard to realize the proposed nonlinear optimal damping characteristics in a real vehicle. Therefore, the simulation study is adopted and it is mainly based on the model built in Adams/View. To be noted that, the full vehicle dynamic model built in this study is mainly to verify the nonlinear effect on the vehicle vibration performance. Meanwhile, some other performances are also obtained in this study, such as the suspension stroke and handling ability. In this part, the detailed parameters of the vehicle system are from [54], such as mass, inertia, kinematics parameter. The description of the vehicle dynamic model will be given in brief. And finally the simulation studies will be conducted under different conditions to show the nonlinear effect on various vehicle evaluation standards.

4.1 The dynamic vehicle model

The dynamic vehicle model is divided into several sub-systems, which are the chassis system, front suspension system, steering system, rear suspension system, tire and road. In these sub-systems, the relationship between each component to the others can be reflected by the graphical topology and it can be seen in Appendix D in order to save space. The constructions and functions of each subsystem are given here as follows.

(a). Chassis system

Chassis system is one of the most important and complex system in the vehicle as it contains many subsystems. In the present study, in order to reduce the workload of system modeling and make the model simpler, the chassis is represented by a sphere with detailed mass and inertia. The graphical topology of the chassis system can be seen in Figure 4.1.

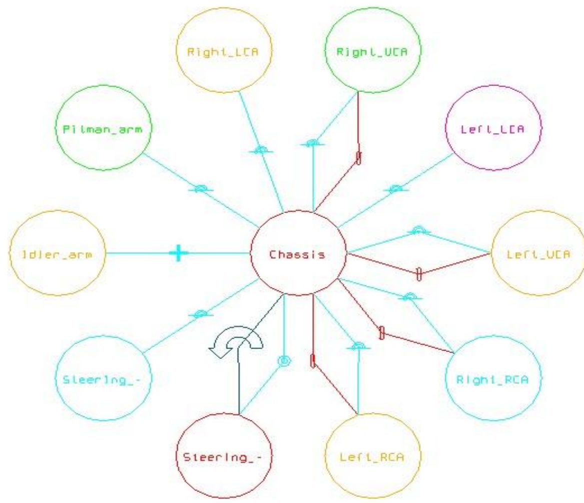

Figure 4.1 Graphical topology of chassis

In Figure 4.1, it can be found that the chassis is connected with different components of the vehicle through some detailed joints. For example, the connection style between the chassis and the low control arm is revolute joint while the connection between the chassis and the steering wheel is cylindrical joint. Meanwhile, a cylindrical motion is added in order to make sure the steering wheel works well. All these connections mentioned can be realized in Adams by properly choosing the constraint styles.

(b). Front suspension system

Front suspension part plays a role of connecting the wheels and vehicle chassis, controlling the relative movement between the chassis and the two front wheels and suppressing the vehicle vibration coming from the road input. In the theoretical study, the suspension system is approximately regarded as a spring and damper system as mentioned in Chapter 2 and Chapter 3 above. However, in the present chapter, the front suspension system contains the following parts, which are kingpin, up control arm, low control arm, pull arm, knuckle, tie rod, spring and damper. The detailed description of the front suspension system can be seen in Figure 4.2.

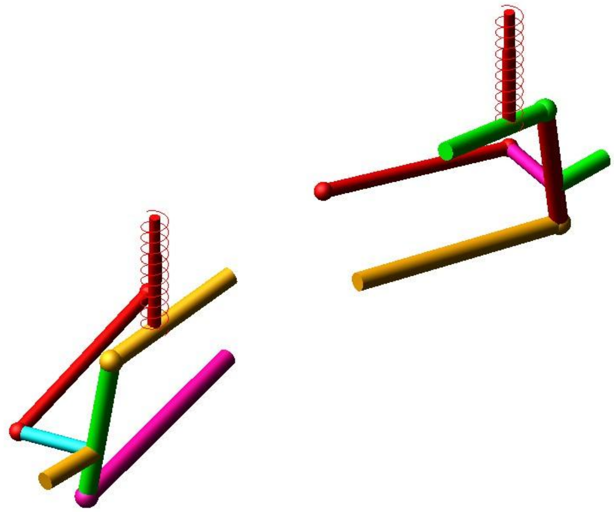

Figure 4.2 Front suspension system

In Figure 4.2, the spherical joint is used to connect the up control arm and the kingpin, and the fixed joint is adopted to connect the pull arm and knuckle. The revolute joint is used to connect the knuckle and the front wheel. While the Hooke joint is used to connect the tie rod and the center link which belongs to the steering system. In the suspension system, spring and damper are the key components in order to reduce vibration. Compared with the experimental study, the simulation study is more convenient in obtaining the specific spring and damping characteristics. It can be realized by changing the damping coefficient and stiffness coefficient in Adams, which can be seen in Figure 4.3

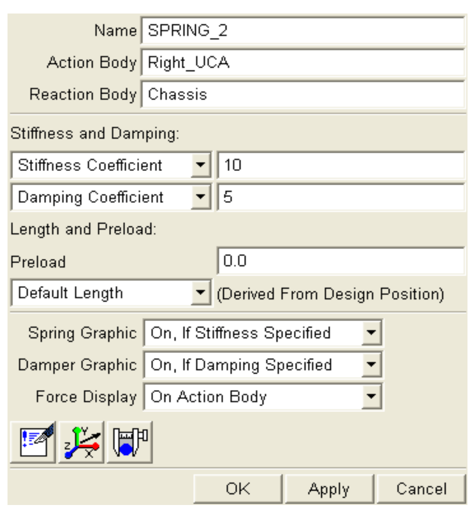

Figure 4.3 The realization for a specific damping and stiffness

For example, in order to obtain a given stiffness $k = 10N/mm$ and damping $C = 5\ N.S/mm$, then in the Adams/View setting, the value can be obtained by changing the stiffness coefficient and damping coefficient in Figure 4.3. In the present study, the nonlinear damping characteristics need to be taken into consideration. The nonlinear damping characteristics can be realized by changing to the Spline choice in the column instead of a specific value.

(c). Steering system

Steering system can make sure the driver's control input can be obtained by the two front wheels via the guide parts of the front suspension system. In a real vehicle, the steering system often contains the tie rod, pitman arm, idler arm, steering shaft, steering column and steering wheel. The construction of the steering system and front suspension system in Adams/view can be seen in Figure 4.4

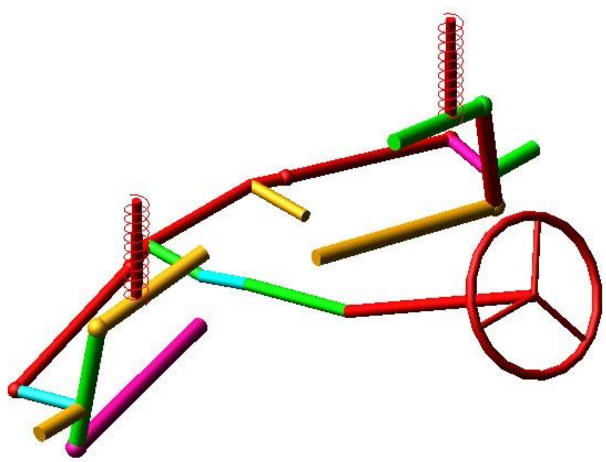

Figure 4.4 Steering system and front suspension system

(d). Rear suspension system

The rear suspension system is similar to the front suspension and it is much simpler compared with the front suspension. The spring and damper system is the same as the front suspension. However, there is no steering system anymore and a tie rod is adopted to connect the rear suspension to the chassis. In some real vehicle systems, the rear suspension is much more complicated as some vehicle will have a differential gear train on the rear axle. But in the Adams/View model, the construction of the rear suspension system can be seen in Figure 4.5

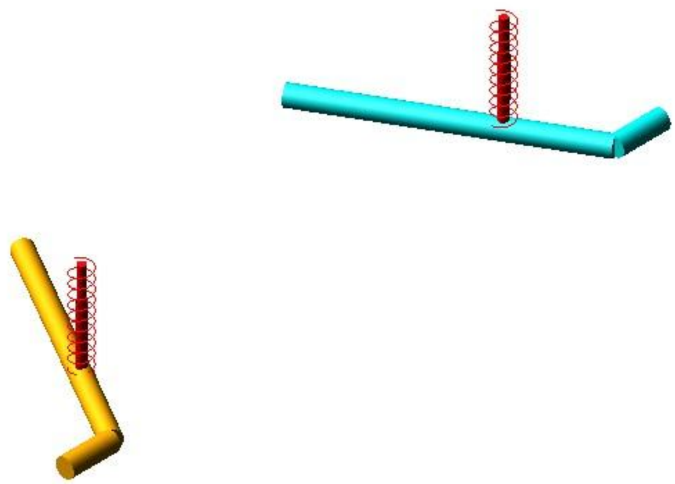

Figure 4.5 Rear suspension system

In Figure 4.5, the revolute joint is used to connect the rear suspension system and the chassis to make sure the rear suspension has the revolute freedom. The revolute joint is also adopted in the connection between the rear suspension and tire so that the tire suspension can work well.

(e). Tire

In the design and analysis of vehicle dynamic system, the tire system can be used to support the vehicle body and contact with the ground. Adams/View provides four types of tire and each type of tire has specific applications. The detailed application of each tire can be seen in Table 4.1

Table 4.1 Different types of tire [54]

Tire type	Application
Fiala	• Handling analysis • Pure slip
UA	• Handling analysis • Complex slip
Smithers	• Handling • Pure slip
Delft	• Handling • Complex slip

In this study, the fiala tire was adopted to conduct the dynamic simulation study [55]. The tire property is designed by its dimension, parameter and shape. The detailed description of the fiala tire file can be seen in Appendix E. During the process of the model building, the connection between the tire and the road should be very precise to make sure the model work well.

(f). Road

During the simulation of the full vehicle dynamic model, the road effects need to be taken into consideration. There are different types of road in Adams software, such as drum, flat, flank, polyline, pothole, ramp, roof, sine, sweep and stochastic uneven. In the present study, the sine road characteristic will be adopted in the simulation study. The parameters of the road file can be modified easily, such as the road amplitude and wave length. The wave length can affect the road input frequency and the detailed description of the road file can be seen in Appendix F.

(g). Full vehicle dynamic model

In the discussions above, the detailed steps of building the chassis system, suspension system, steering system, tire and road have been given. Each part’s function has been discussed in brief and connection style has also been clarified. Then the full vehicle system model can be seen in Figure 4.6

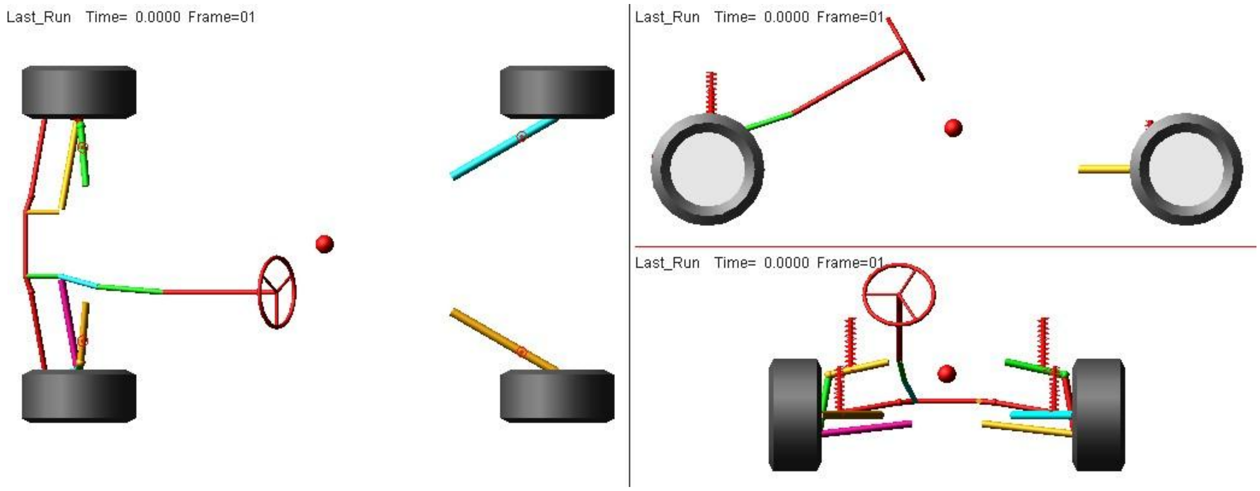

Figure 4.6 Full vehicle dynamic model

In this model, the basic components of a vehicle system have been given. The detailed characteristics of the components, such as the mass, inertia, length and width will be given in the next section. This model can be used to analyze the vibration performance of a vehicle under different working conditions. Meanwhile, other evaluation performances and the vehicle characteristics can also be studied by using this model.

4.2 Vehicle system parameters

In this study, the three-dimensional vehicle dynamic model is built above. The detailed characteristic of the components, such as the mass, inertia, length and width can be described in Figure 4.7

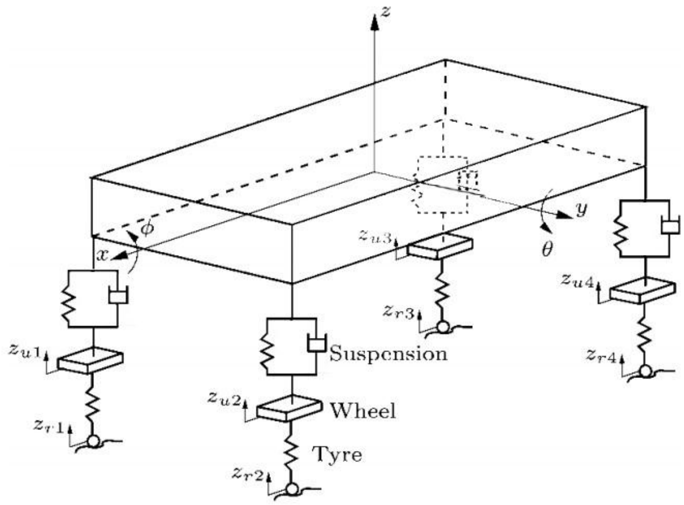

Figure 4.7 Full vehicle suspension mathematical model [38]

In Figure 4.7, $m_s, m_{11}, m_{12}, m_{21}, m_{22}$ are the masses of the vehicle body and the four wheels' mass,$c_{11}, c_{12}, c_{21}, c_{22}$ are the damping coefficients of the suspension systems and $k_{11}, k_{12}, k_{21}, k_{22}$ are the spring stiffness of the suspension system. In the real working conditions of the vehicle, z_{r1} z_{r2} z_{r3} z_{r4} are the road input respectively and $z_{u1}, z_{u2}, z_{u3}, z_{u4}$ are the displacement of the wheel. θ is the pitch movement and ϕ is the roll movement. In this study, the system parameters are obtained from the previous work [54], which can be seen in Table 4.2.

Table 4.2 System parameters

$m_s = 2010kg$	$k_{t11} = 310KN/m$	$k_{s12} = 129.8KN/m$	$c_{s21} = 1000N.s/m$
$m_{11} = 29.2kg$	$k_{t12} = 310KN/m$	$k_{s21} = 129.8KN/m$	$c_{s22} = 1000N.s/m$
$m_{12} = 29.2kg$	$k_{t21} = 310KN/m$	$k_{s22} = 129.8KN/m$	
$m_{21} = 29.2kg$	$k_{t22} = 310KN/m$	$c_{s11} = 1000N.s/m$	
$m_{22} = 29.2kg$	$k_{s11} = 129.8KN/m$	$c_{s12} = 1000N.s/m$	

In Table 4.2, it is clear that the values of the system mass, stiffness and damping are different from those referred in Chapter 3. This is because that it is very difficult to get the relevant data from the existing articles to build the vehicle dynamic model. Meanwhile, it is also not reliable to import the system parameters referred in Chapter 3 into the vehicle dynamic model directly as the vehicle in Chapter 3 is a sedan while the vehicle in this chapter is likely to be an SUV according to the value of the system parameters. Therefore, the vehicle dynamic model has not chosen the same parameters in Chapter 3. In this study, the vehicle dynamic model built according to the parameters listed in Table 4.2 will be used to conduct the simulation studies. In this study, the system main parameters are given in Table 4.2 and these system parameters can be realized by changing the property of the components in the dynamic model. The example about how to revise the mass and inertia of the chassis system will be given in Figure 4.8.

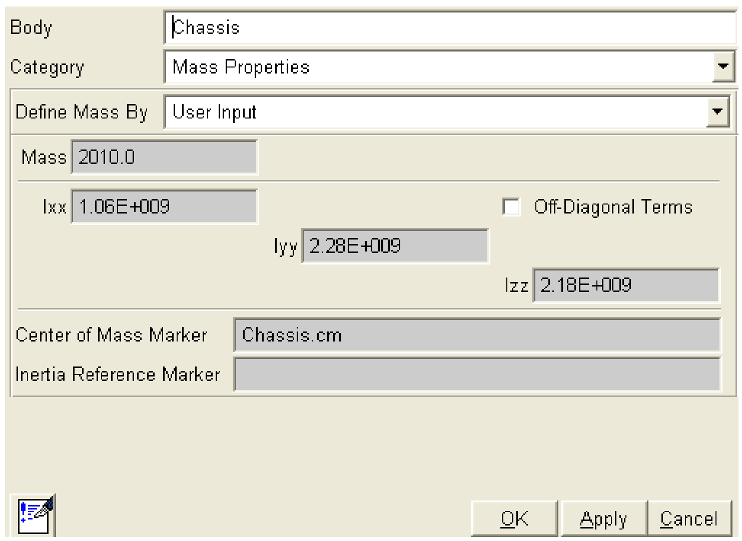

Figure 4.8 Modification of the mass of chassis system

4.3 Simulation conditions

In order to verify the nonlinear effects on the vehicle vibration performance, the simulation study needs to be conducted under different working conditions. The steps of building the road file have been discussed in section 4.1. The driving resource in the present study is chosen to be the point motion and it can be defined as the function of the velocity. For example if the vehicle runs at the speed at $10000mm/s$ then the function can be written as $velocity = 10000$ in Adams. The vehicle will run at this the velocity of $10000\mathrm{mm/s}$ when the simulation starts. However, in the vehicle dynamic model, it is difficult to make the vehicle runs at such a velocity while the initial velocity is zero as the vehicle needs to suffer a short period of accelerating and then the velocity will reach the desired value and finally the vehicle system will run at the constant velocity. In order to realize this type okf running progress, the real velocity of the vehicle body can be generated by using STEP function in Adams. By using this function, the vehicle will get the progress and the vehicle runs at the speed of $10000 mm/s$ can be seen in Figure 4.9.

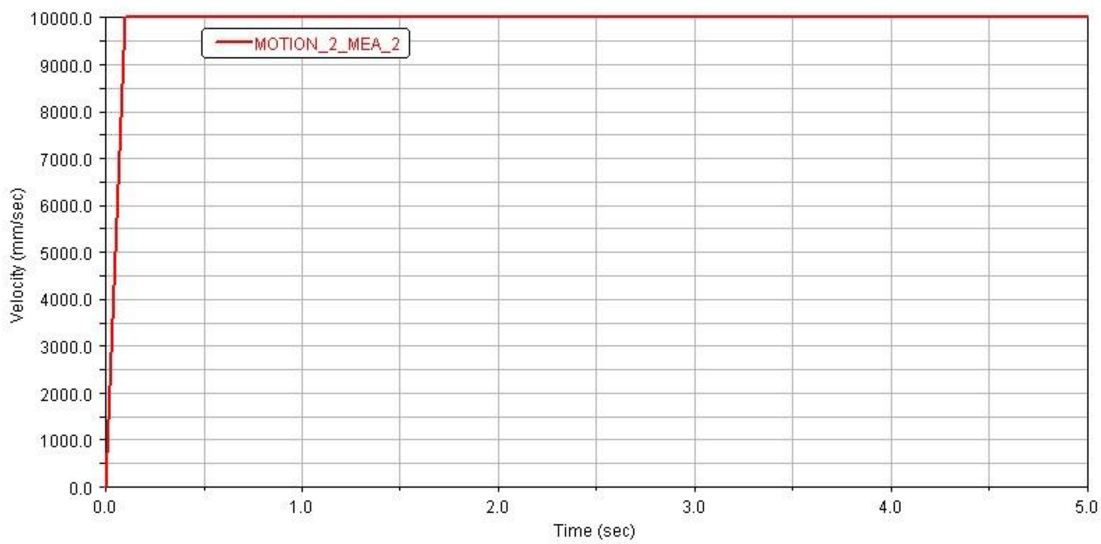

Figure 4.9 Vehicle velocity in Adams/View

In order to realize this velocity, the function of the point motion can be written as

$$velocity = STEP(\, time\, , 0\, , 0\, , 0.1\, , 10000\,) + STEP(\, time\, , 0.1\, , 0\, , 5\, , 0\,)$$

In the equation above, it means that the velocity will increase from 0 to 10000 in the time period of $0.1s$, and then it can get the constant velocity of 10000 in the next 4.9 seconds. By properly modifying the values in the STEP function, the vehicle will run at different velocities and thus can realize the desired velocity of the simulation study. In order to ignore the vibration during the acceleration period, the data related to vibration performance should be collected from the period with constant velocity.

4.4 Simulation study

In this section, several simulation studies will be conducted to show the effect of the nonlinear suspension system in terms of the vehicle vibration performance. By using the method proposed in Chapter 2, the optimal damping characteristics can be obtained easily. Then the comparative studies between the nonlinear suspension system and the linear suspension system will be conducted. The simulation studies based on three different evaluation standards are proposed. The result of the simulation study will be discussed in detail in the following parts.

4.4.1 Vehicle vibration study

As demonstrated in Chapter 3, the effect of system nonlinearity on the vehicle vibration suppression is different with respect to the input frequencies. The nonlinear suspension system will be helpful in the vibration suppression while in other cases it will not be helpful. In this part, several case studies to evaluate the vibration performance will be presented.

1. v=1m/s

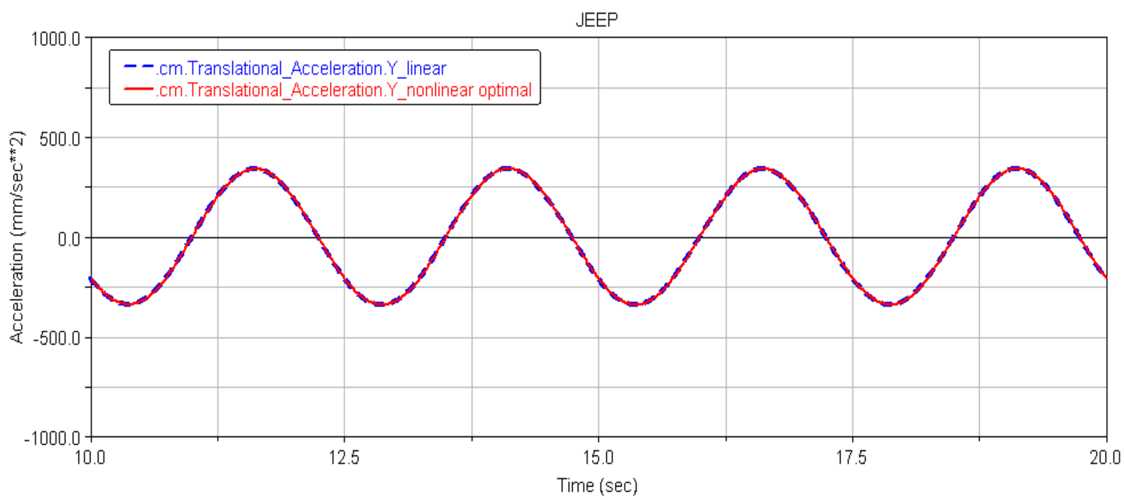

Figure 4.10 Vertical vibration at the speed of $1m/s$

Table 4.3 Vertical acceleration at the speed of $1m/s$

System	RMS (mm/s^2)	Max$\|a\|(mm/s^2)$
Linear	240	342
Nonlinear	240	342

2. v=5m/s

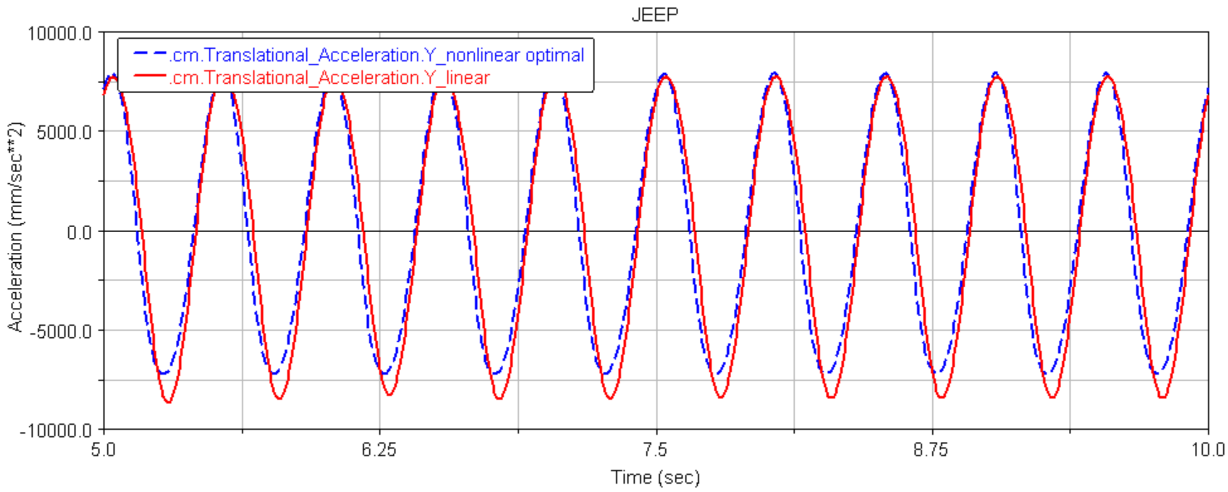

Figure 4.11 Vertical vibration at the speed of 5m/s

Table 4.4Vertical acceleration at the speed of 5m/s

System	RMS (mm/s^2)	Max$\|a\|$(mm/s^2)
Linear	5671	8641
Nonlinear	5463	7203

3. v=5.1m/s

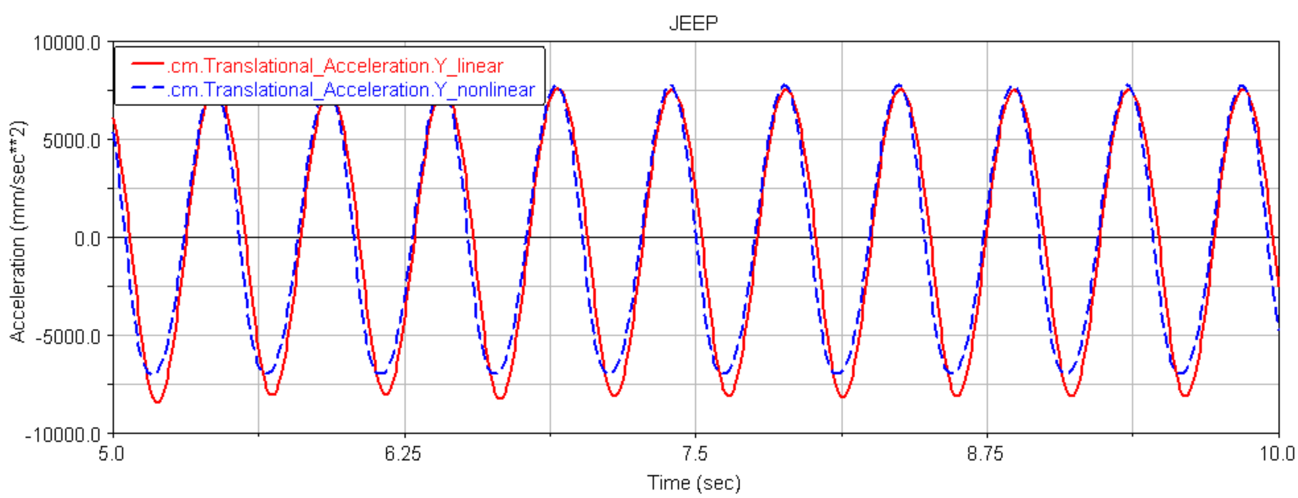

Figure 4.12 Vertical vibration at the speed of 5.1m/s

Table 4.5Vertical acceleration at the speed of $5.1m/s$

System	RMS (mm/s^2)	Max$\|a\|(mm/s^2)$
Linear	5554	8463
Nonlinear	5307	7008

4. v=5.2m/s

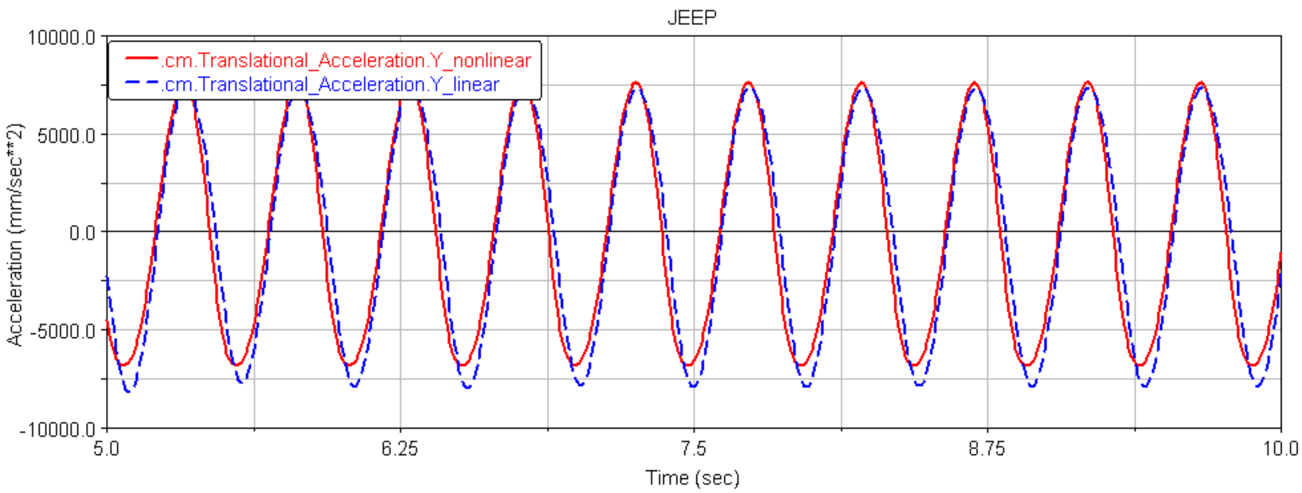

Figure 4.13 Vertical vibration at the speed of $5.2m/s$

Table 4.6 Vertical acceleration at the speed of $5.2m/s$

System	RMS (mm/s^2)	Max$\|a\|(mm/s^2)$
Linear	5450	8163
Nonlinear	5243	6827

5. v=5.5m/s

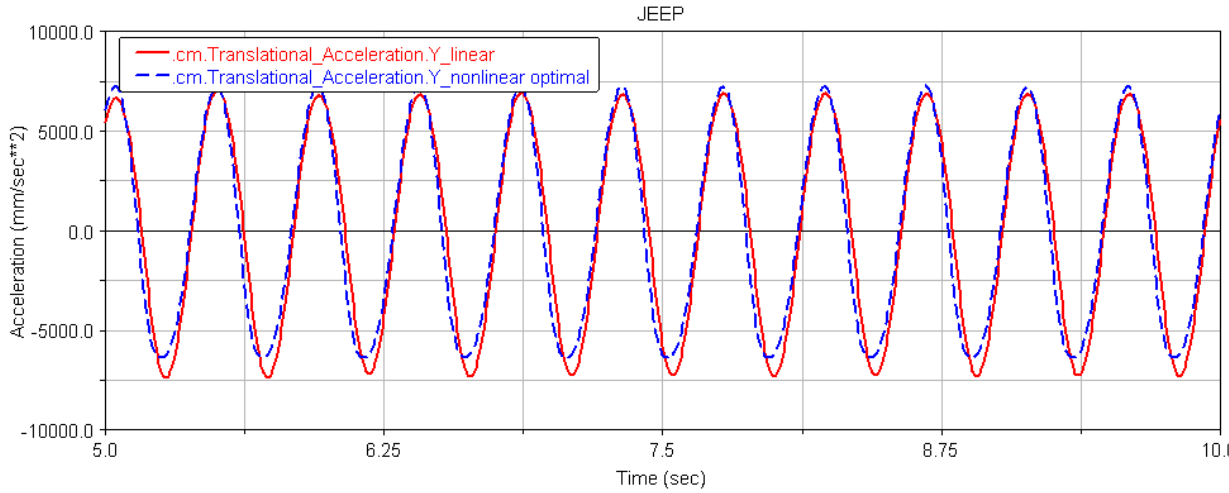

Figure 4.14 Vertical vibration at the speed of 5.5m/s

Table 4.7 Vertical acceleration at the speed of 5.5m/s

System	RMS (mm/s^2)	Max$\|a\|$(mm/s^2)
Linear	5030	7371
Nonlinear	4948	6379

6. v=6m/s

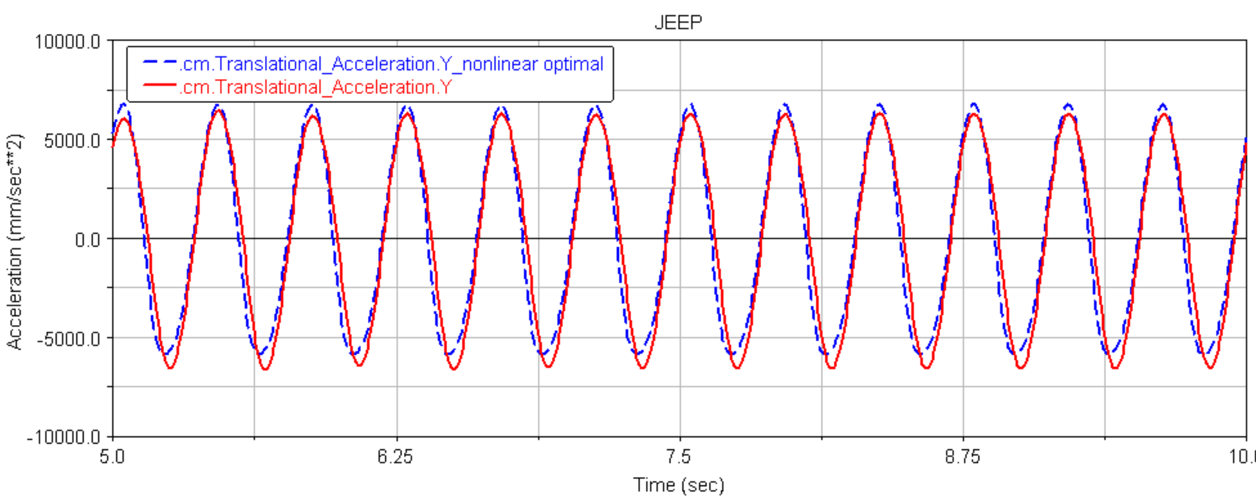

Figure 4.15 Vertical vibration at the speed of 6m/s

Table 4.8 Vertical acceleration at the speed of $6m/s$

System	RMS (mm/s^2)	Max$|a|$(mm/s^2)
Linear	4558	6660
Nonlinear	4588	6762

From Figure 4.10 to Figure 4.15, it can be shown that when the vehicle velocity is in a specific range around resonance frequency, the vehicle vibration performance obtained by the nonlinear optimal damping would be better than the linear suspension system. However, the nonlinear suspension system can bring some bad effects on the vibration performance when the velocity is very high. In the relatively low velocities, the vibration performance of the nonlinear vehicle suspension system will not be improved compared with the linear suspension system.

4.4.2 Suspension stoke

In the analysis of the vehicle suspension system, the distance of the sprung mass and the unsprung mass should be controlled. This is mainly due to the fact that it will strike the vehicle frame when the distance is large. In this study, the nonlinear effects on the vehicle suspension stroke need to be considered in order to make the result more reasonable. Some comparative studies between the linear suspension system and the nonlinear suspension system are conducted. As in the vehicle system, there are four independent suspension systems; the suspension stroke of the front right suspension system is given as an example. The figures of the suspension stroke under different velocities can be shown as follows.

1. v=1m/s

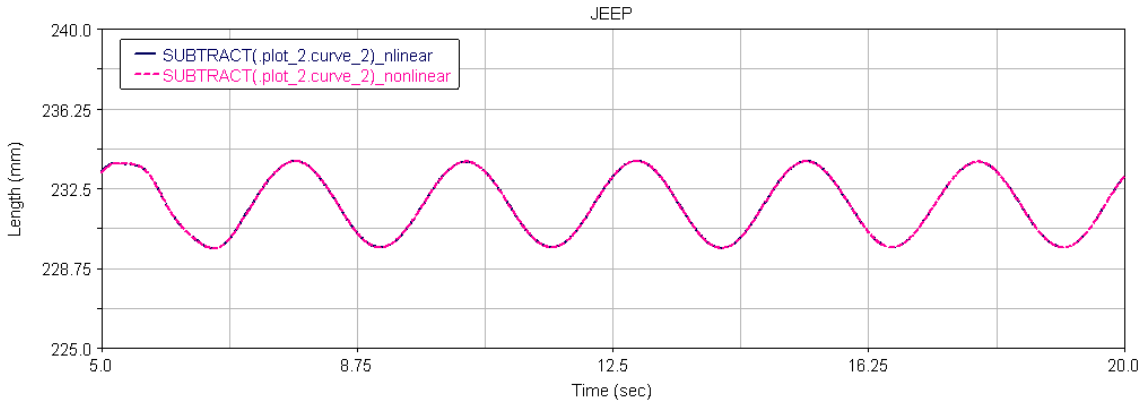

Figure 4.16 Suspension stroke at the velocity of $1m/s$

2. v=5m/s

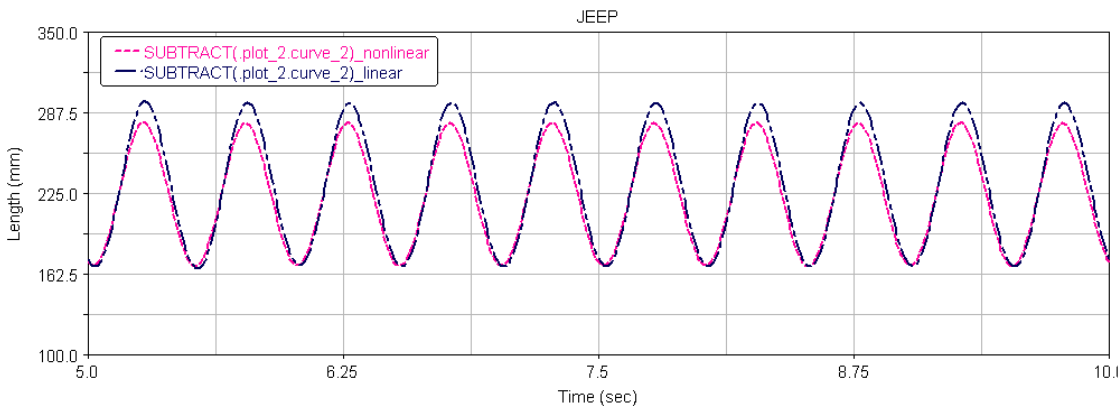

Figure 4.17 Suspension stroke at the velocity of $5m/s$

3. v=10m/s

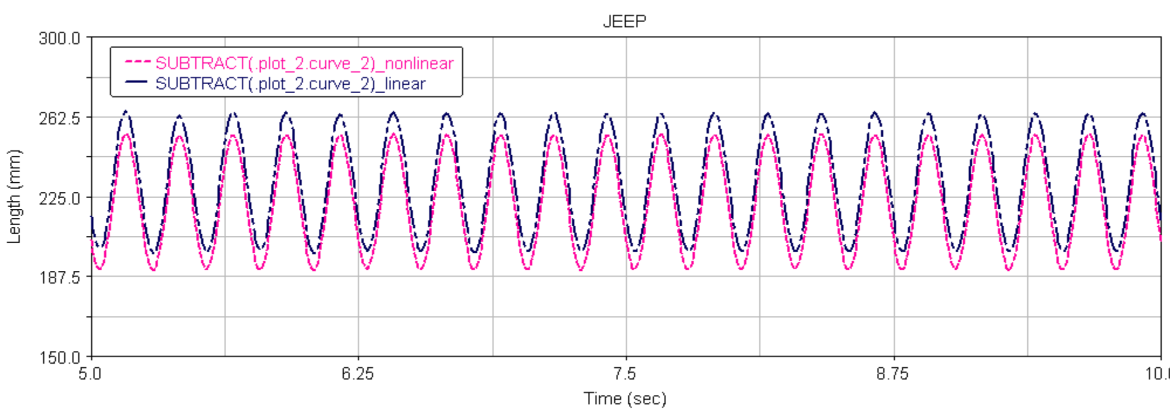

Figure 4.18 Suspension stroke at the velocity of $10m/s$

4. v=15m/s

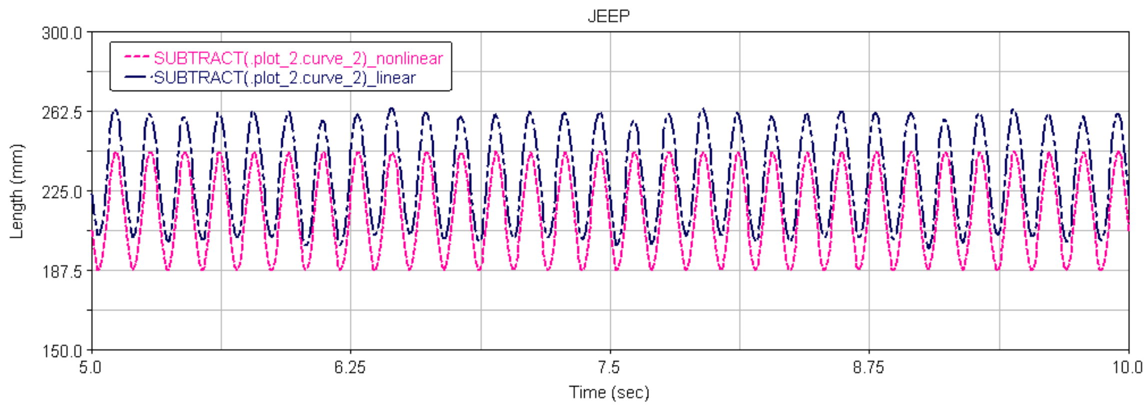

Figure 4.19 Suspension stroke at the velocity of $15m/s$

From the figures above, it can be shown that in the relatively low velocity range, the effect of nonlinearity on the suspension stroke is not obvious. However, in the high velocity range, such as 15m/s, the positive effect of system nonlinearity on the suspension stroke is extraordinarily obvious. Therefore, it can be concluded that the system nonlinearity can be helpful in the suppression of the relative displacement between the sprung mass and the unsprung mass.

4.4.3 Handling ability

In the analysis of the vehicle system, the handling ability is another important issue to consider. As is demonstrated in the previous work, the spring and damping characteristics often reach a compromise between the ride comfort and handling ability. In this study, the main evaluation standard is the vehicle vibration and the effect of the damping nonlinearity on the vibration performance has been discussed in 4.4.1. However, it is also worthwhile to evaluate the nonlinear effect on the handling ability to make sure the results more reasonable. Therefore, the simulation study based on the full vehicle dynamic model is conducted to evaluate the handling ability in this part. The evaluation index of the handling ability is given as

$$\alpha_1 - \alpha_2 = 57.3L(\frac{1}{R_0} - \frac{1}{R_i}) \tag{4.1}$$

In the equation above, α_1 is the front wheel slip angle, α_2 is the rear wheel slip angle. If the value of Eq. (4.1) is larger than zero, then the system will be under-steered and it is desired for the vehicle system; if the value of Eq. (4.1) is smaller than zero, then the system will be over-steered and it will have a bad effect on the handling ability; if the value of Eq. (4.1) is equal to zero, then the system will be neutral steer.

In this part, the simulation is conducted based on the GB/T6323.6-94 standard. Two different systems were used to make the comparative study, the first one is the vehicle suspension system with linear damping and the second one is the vehicle suspension system with the nonlinear damping. The result is shown in Figure 4.20

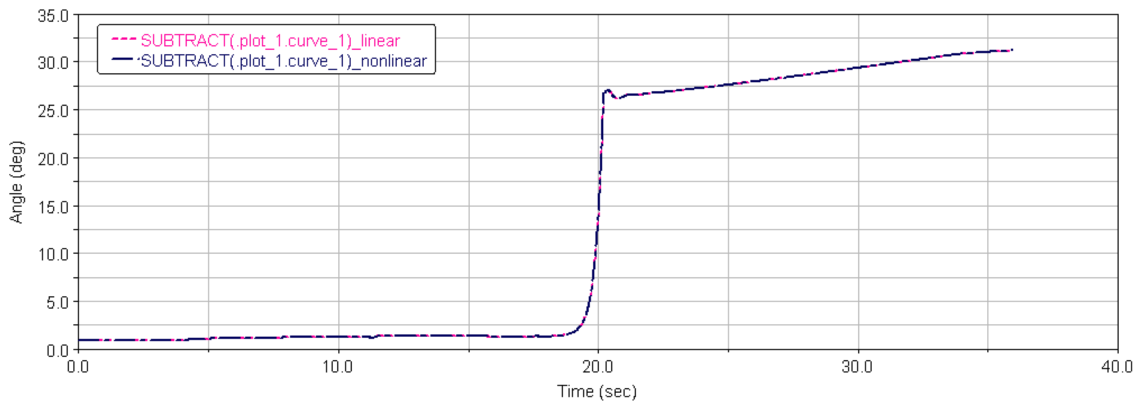

Figure 4.20 Lather slip angle of linear and nonlinear system

In Figure 4.20, it is obvious that the slip angle of these two systems is almost the same. Therefore, it can be concluded that the nonlinear damping characteristics will not have any effect on the performance of the vehicle handling ability.

4.5 Conclusion

In this chapter, the full vehicle dynamic model was built by using the Adams software to analyze the nonlinear effect on the vehicle performance, such as the ride comfort, suspension stroke and the handling ability. In the vehicle dynamic model, some realistic parameters are taken into consideration while conducting the simulation study, such as the mass, inertia, road input and the vehicle velocity and therefore the simulation results are more accurate and the reasonable. Three different types of simulation studies are conducted independently to evaluate the vehicle performance. For the vehicle vibration study, it can be seen that the vehicle suspension system with nonlinear damping can achieve a better ride comfort performance in the resonant frequency range. In relatively low and high frequency range, the system nonlinearity cannot induce some positive effects on the vibration performance. In the analysis of the suspension stoke, the results show that the system nonlinearity can be very helpful in the suppression of the suspension stroke. Unlike the vibration performance, in the relatively high velocity, the suspension stroke can also be suppressed with the nonlinear damping characteristics. The final part is the verification of the handling ability. The result in this part shows that if the damping characteristics are nonlinear, it basically has no effect on the vehicle handling ability when compared with the linear damping characteristics. Therefore, it can be concluded that the nonlinear damping characteristics will be helpful in the vibration suppression in many important practical situations, the performance of the suspension stroke will be improved and the handling ability is not affected by the nonlinearity.

Chapter 5 Conclusions and future work

In this study, the nonlinear output frequency response function method is adopted in the analysis and design of vehicle suspension systems. With this method, the relationship between the nonlinear suspension system output and system parameters can be obtained explicitly. In Chapter 2, it shows that the system parameters determined by the nonlinear frequency domain analysis method is very helpful in the suppression of vibration of vehicle systems. In this chapter, the main evaluation standard and the objective of the present study are given firstly. And the nonlinear frequency domain analysis method is introduced in detail. Then the system parameters can be analyzed and optimized by using the nonlinear frequency domain analysis method. In order to show the nonlinear effect, comparative studies between the nonlinear system, the linear system and a recommended linear system are conducted. The results show that the nonlinearities can be very beneficial in the suppression of system vibration around the resonant frequency. In Chapter 3, two different optimal nonlinear damping characteristics are presented. The first one is borrowed from existing results and the second one is obtained by using the nonlinear frequency domain analysis method. Comparative studies between these two damping characteristics show that the nonlinear damping characteristics designed by the mentioned nonlinear frequency domain analysis method demonstrates much better performance than the existing optimal nonlinear damping characteristics. A simple spring damper dynamic model is also built in Chapter 3. The result of the dynamic model simulation study is consistent with the results obtained from the theoretical analysis. In Chapter 4, the nonlinear damping characteristics are applied to a full vehicle dynamic model, which is built by using the Adams software. In this chapter, the full vehicle dynamic model is divided into several subsystems and the detailed functions and connection styles of each subsystem are presented in detail. The road input, vehicle velocity and turning movement are all taken into consideration in the vehicle dynamic model. Simulation studies for two different vehicle dampers with the nonlinear damping characteristics and the linear damping characteristics are conducted. The results confirm again the conclusions made in Chapter 2 and Chapter 3 that the nonlinear damping characteristic demonstrates better performance than the linear damping characteristic around the resonant frequency range. Other vehicle evaluation standards, such as the suspension stroke, can also be improved with the help of the nonlinear damping characteristics. The simulation study based on the evaluation of the handling ability shows that the introduced nonlinearity does not have an obvious effect on the handling ability.

Future work would focus more on the following points. Firstly, the nonlinear stiffness should be considered in order to make the optimization more realistic. It has been shown that the spring nonlinearity does exist in the real system, and therefore, it is of significance to analyze the nonlinear spring effect on the vehicle performance. Meanwhile, as is demonstrated in Chapter 2, the introduced nonlinear spring will change the system resonant frequency. The proper nonlinear stiffness will take some important frequency ranges into consideration, such as the human sensitive frequency and the engine resonant frequency. Therefore, it is also meaningful to investigate the relationship between the system resonant frequency and nonlinear spring stiffness. Secondly, the present study focuses more on the vibration performance and the results were obtained based on the sine input signal. However, the real vehicle road working conditions are various. It contains the random input and pulse input et al. Therefore, it is necessary to study the nonlinear performance under these working conditions and to obtain the optimal nonlinear system parameters to meet different requirements. Thirdly, in the present study, the main results are obtained based on the numerical and simulation studies. However, the vehicle system is a complicated model and therefore it is necessary to conduct some experiments to make sure the accuracy of the current result on the real vehicle system.

Appendix A Theoretical derivation of the frequency response function

The detailed expression for $H_5\left(j\omega_1,\cdots,j\omega_5\right)$ can be written as

$$
\begin{aligned}
& H_{5,3}\left(j\omega_1,\cdots,j\omega_5\right)=H_1\left(j\omega_1\right)\left(j\omega_1\right)^{l_3}H_{4,2}\left(j\omega_2,\cdots,j\omega_5\right) \\
& +H_2\left(j\omega_1,j\omega_2\right)\left(j\omega_1+j\omega_2\right)^{l_3}H_{3,2}\left(j\omega_3,\cdots,j\omega_5\right) \\
& +H_3\left(j\omega_1,j\omega_2,j\omega_3\right)\left(j\omega_1+j\omega_2+j\omega_3\right)^{l_3}H_{2,2}\left(j\omega_4,j\omega_5\right) \\
& =H_1\left(j\omega_1\right)\left(j\omega_1\right)^{l_3}\begin{pmatrix} H_1\left(j\omega_1\right)\left(j\omega_1\right)^{l_2}H_{3,1}\left(j\omega_3,j\omega_4,j\omega_5\right) \\ +H_2\left(j\omega_2,j\omega_3\right)\left(j\omega_2+j\omega_3\right)^{l_2}H_{2,1}\left(j\omega_4,j\omega_5\right) \\ +H_3\left(j\omega_2,j\omega_3,j\omega_4\right)\left(j\omega_2+j\omega_3+j\omega_4\right)^{l_2}H_{1,1}\left(j\omega_5\right) \end{pmatrix} \\
& +H_2\left(j\omega_1,j\omega_2\right)\left(j\omega_1+j\omega_2\right)^{l_3}\begin{pmatrix} H_1\left(j\omega_3\right)\left(j\omega_3\right)^{l_2}H_{2,1}\left(j\omega_4,j\omega_5\right) \\ +H_2\left(j\omega_3,j\omega_4\right)\left(j\omega_3+j\omega_4\right)^{l_2}H_{1,1}\left(j\omega_5\right) \end{pmatrix} \\
& +H_3\left(j\omega_1,j\omega_2,j\omega_3\right)\left(j\omega_1+j\omega_2+j\omega_3\right)^{l_3}\left(H_1\left(j\omega_4\right)\left(j\omega_4\right)^{l_2}H_{1,1}\left(j\omega_5\right)\right) \\
& =H_1\left(j\omega_1\right)\left(j\omega_1\right)^{l_3}\begin{pmatrix} H_1\left(j\omega_1\right)\left(j\omega_1\right)^{l_2}\left[H_3\left(j\omega_3,j\omega_4,j\omega_5\right)\left(j\omega_3+j\omega_4+j\omega_5\right)^{l_1}\right] \\ +H_2\left(j\omega_2,j\omega_3\right)\left(j\omega_2+j\omega_3\right)^{l_2}\left[H_2\left(j\omega_4,j\omega_5\right)\left(j\omega_4+j\omega_5\right)^{l_1}\right] \\ +H_3\left(j\omega_2,j\omega_3,j\omega_4\right)\left(j\omega_2+j\omega_3+j\omega_4\right)^{l_2}\left[H_1\left(j\omega_5\right)\left(j\omega_5\right)^{l_1}\right] \end{pmatrix} \\
& +H_2\left(j\omega_1,j\omega_2\right)\left(j\omega_1+j\omega_2\right)^{l_3}\begin{pmatrix} H_1\left(j\omega_3\right)\left(j\omega_3\right)^{l_2}\left[H_2\left(j\omega_4,j\omega_5\right)\left(j\omega_4+j\omega_5\right)\right]\cdot \\ H_{2,1}\left(j\omega_4,j\omega_5\right)^{l_1} \\ +H_2\left(j\omega_3,j\omega_4\right)\left(j\omega_3+j\omega_4\right)^{l_2}\left[H_1\left(j\omega_5\right)\left(j\omega_5\right)^{l_1}\right] \end{pmatrix} \\
& +H_3\left(j\omega_1,j\omega_2,j\omega_3\right)\left(j\omega_1+j\omega_2+j\omega_3\right)^{l_3}\left(H_1\left(j\omega_4\right)\left(j\omega_4\right)^{l_2}\left[H_1\left(j\omega_5\right)\left(j\omega_5\right)^{l_1}\right]\right)
\end{aligned} \tag{A.1}
$$

According to Eq. (7), $H_5\left(j\omega_1,\cdots,j\omega_5\right)$ can be written as

$$
H_5^{1:11111}\left(j\omega_1,\cdots j\omega_5\right)=-\frac{c_{3,0}\left(l_1,l_2,l_3,\right)H_{5,3}\left(j\omega_1,\cdots,j\omega_5\right)}{\left(j\omega_1+\cdots+j\omega_5\right)^2+\xi\left(j\omega_1+\cdots+j\omega_5\right)+1} \tag{A. 2a}
$$

$$
H_5^{2:11111}\left(j\omega_1,\cdots j\omega_5\right)=\left(-m\left(j\omega_1+\cdots+j\omega_5\right)^2\right)H_5^{1:11111}\left(j\omega_1,\cdots j\omega_5\right) \tag{A. 2a}
$$

As $c_{30}(111)=\xi_1, c_{30}(110)=\xi_2, c_{30}(100)=\xi_3, c_{30}(000)=\xi_4$ is given, then input Eq. (A. 1) and all the nonlinear parameters and it's corresponding l_1, l_2, l_3 to the Eq. (A. 2), $H_5^{2:11111}\left(j\omega_1,\cdots j\omega_5\right)$ can be derived.

Appendix B Damping characteristics data

x_{Matlab}	y_{Matlab}	x_{Matlab}	y_{Matlab}	x_{Matlab}	y_{Matlab}	x_{Matlab}	y_{Matlab}
108	392	247	329	350	257	444	177
113	389	252	328	352	254	449	176
119	384	257	327	353	249	455	173
124	381	262	325	355	246	459	170
128	378	268	324	358	241	464	167
134	375	272	323	359	238	467	165
139	371	278	320	362	234	470	161
143	369	284	318	363	230	474	159
147	366	291	316	366	225	478	155
152	364	299	314	368	222	480	152
155	362	306	312	370	218	485	148
161	359	313	309	371	216	488	144
167	357	314.5	308	374	211	490	141
173	354	319	306	377	207	494	136
177	352	325	302	380	203	497	132
182	350	327	301	384	199	500	127
190	347	329	298	388	196	503	124
195	345	331	296	391	193	505	119
201	343	333	293	397	191	508	114
208	341	335	289	405	190	511	108
214	340	338	284	410	188	514	103
217	338	339	280	415	187	516	99
222	336	341	276	423	186	518	95
227	335	343	271	430	184	520	91
233	333	345	267	436	182	521	89
240	331	348	262	438	181		

The rough data of the damping characteristics (x_{Matlab} and y_{Matlab} means the data obtained from Matlab respectively)

x_{real}	y_{real}	x_{real}	y_{real}	x_{real}	y_{real}	x_{real}	y_{real}
-2.000	-1079.802	-0.654	-269.950	0.344	655.594	1.254	1683.977
-1.952	-1041.238	-0.605	-257.096	0.363	694.158	1.303	1696.832
-1.893	-976.964	-0.557	-244.241	0.373	758.432	1.361	1735.396
-1.845	-938.399	-0.508	-218.531	0.392	796.997	1.400	1773.960
-1.806	-899.835	-0.450	-205.677	0.421	861.271	1.448	1812.525
-1.748	-861.271	-0.412	-192.822	0.431	899.835	1.477	1838.234
-1.700	-809.851	-0.354	-154.257	0.460	951.254	1.506	1889.653

-1.661	-784.142	-0.295	-128.548	0.470	1002.673	1.545	1915.363
-1.622	-745.578	-0.228	-102.838	0.499	1066.947	1.584	1966.782
-1.574	-719.868	-0.150	-77.129	0.518	1105.512	1.603	2005.347
-1.545	-694.158	-0.082	-51.419	0.538	1156.931	1.651	2056.766
-1.487	-655.594	-0.015	-12.855	0.547	1182.640	1.680	2108.185
-1.429	-629.884	0.000	0.000	0.576	1246.914	1.700	2146.749
-1.370	-591.320	0.044	25.710	0.605	1298.333	1.738	2211.023
-1.332	-565.611	0.102	77.129	0.634	1349.752	1.768	2262.442
-1.283	-539.901	0.121	89.983	0.673	1401.172	1.797	2326.716
-1.206	-501.337	0.140	128.548	0.712	1439.736	1.826	2365.281
-1.157	-475.627	0.160	154.257	0.741	1478.300	1.845	2429.554
-1.099	-449.917	0.179	192.822	0.799	1504.010	1.874	2493.828
-1.031	-424.208	0.199	244.241	0.877	1516.865	1.903	2570.957
-0.973	-411.353	0.228	308.515	0.925	1542.574	1.932	2635.231
-0.944	-385.644	0.237	359.934	0.973	1555.429	1.952	2686.650
-0.896	-359.934	0.257	411.353	1.051	1568.284	1.971	2738.069
-0.847	-347.079	0.276	475.627	1.119	1593.993	1.990	2789.488
-0.789	-321.370	0.295	527.046	1.177	1619.703	2.000	2815.198
-0.722	-295.660	0.324	591.320	1.196	1632.558		

The real data of the damping characteristics (x_{real} and y_{real} mean the real value after calculation)

Appendix C Matlab program

FFT file

```
clc

t =simout1.time;

y =simout1.signals.values;

y=y(40000-1256*1+1:40000);

m=length(y);

Y=fft(y,m);

f=[0:m-1]*2*pi/m/0.005;

Y=Y/m;

n1=max(Y);

M=2*abs(Y);

n2=max(M)

stem((f(1:100)),(M(1:100)))

grid on
```

Time domain figure file

```
%fitted-based curve

t=simout.time(40000-1256*2+1:40000);

y=simout.signals.values(40000-1256*2+1:40000);

plot(t,y)
```

```
hold on

%OFRF-based curve
t1 =simout1.time(40000-1256*2+1:40000);
y1=simout1.signals.values(40000-1256*2+1:40000);
plot(t1,y1,'r')
xlabel('t(s)');ylabel('transmit force(N)');
title('transmit force in time domain magnitude=0.1');
```

Appendix D Graphical topology of the vehicle components

The connections of each subpart in the vehicle system can be indicated by the graphical topology. The graphical topology of each subpart in the vehicle dynamic model can be shown as follows

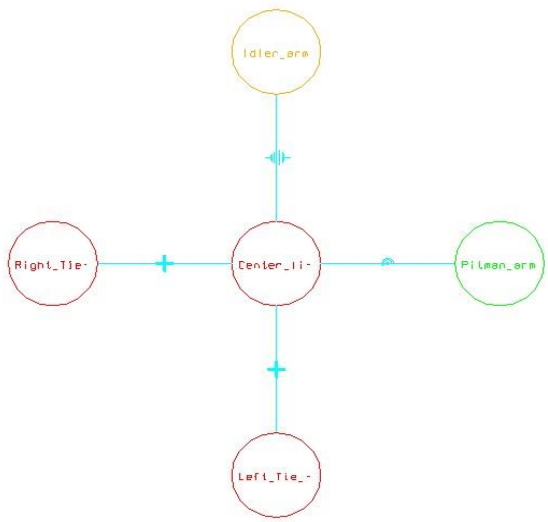

Figure A1 Graphical topology of center link

The connection between the center link and the idler arm is spherical joint; the connection between the center link and the right tie rod is Hooke joint; the connection between the center link and the center link and the Pitman arm is revolute joint; the connection between the center link and the left tie rod is the Hooke joint.

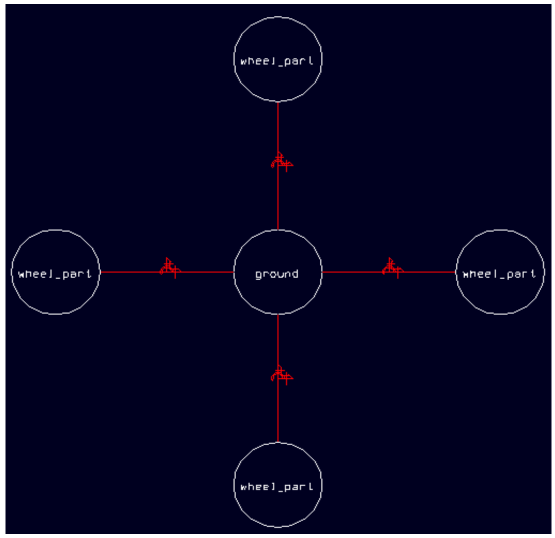

Figure A2 Graphical topology of ground

The connections between the ground and the four wheel parts are tires.

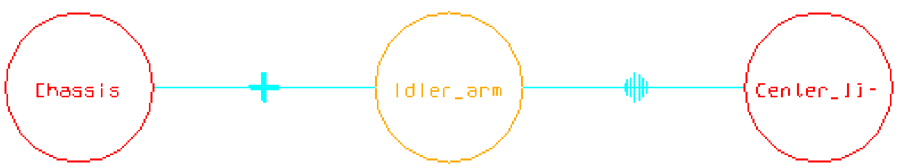

Figure A3 Graphical topology of idler arm

The connection between the idler arm and the chassis is the Hooke joint; the connection between the idler arm and center link is spherical joint.

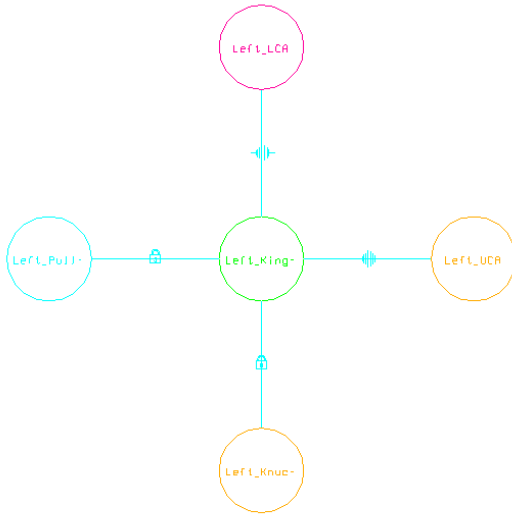

Figure A4 Graphical topology of left kingpin

The connection between the left kingpin and left low control arm is spherical joint; the connection between the left kingpin and the left pull arm is fixed joint; the connection between the left kingpin and the left up control arm is spherical joint; the connection between the left kingpin and the left knuckle is fixed joint.

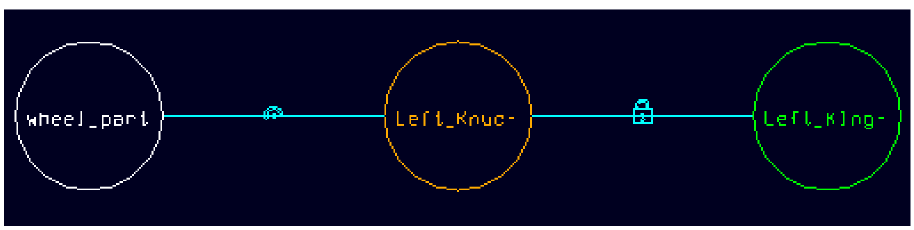

Figure A5 Graphical topology of left knuckle

The connection between the left front wheel and the left knuckle is the revolute joint; the connection between the left knuckle and the left kingpin is the fixed joint.

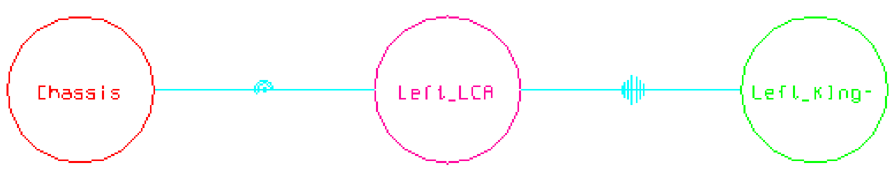

Figure A6 Graphical topology of left low control arm

The connection between the left low control arm and the chassis is the revolute joint; the connection between the left low control arm and the left kingpin is the spherical joint.

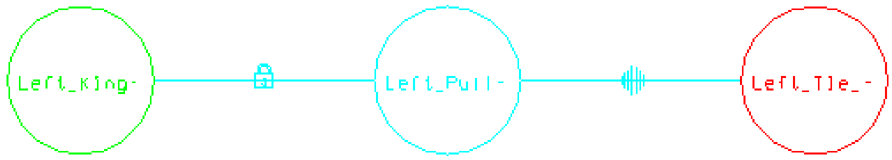

Figure A7 Graphical topology of left pull arm

The connection between the left pull arm and the left kingpin is the fixed joint; the connection between the left pull arm and the left tie rod is the spherical joint.

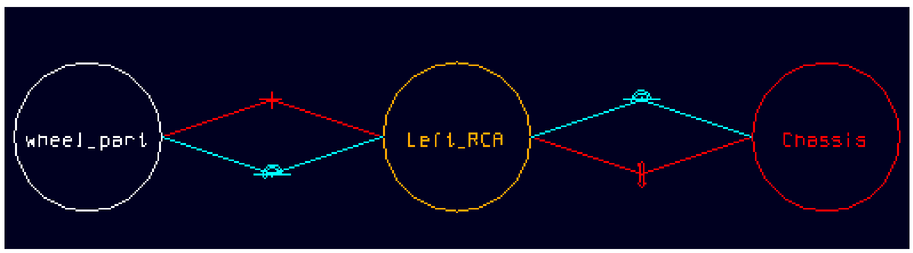

Figure A8 Graphical topology of left rear control arm

The connection between the left rear control arm and the left rear wheel is the revolute joint and the driving source; the connection between the left rear control arm and the chassis system is the revolute joint and the spring force.

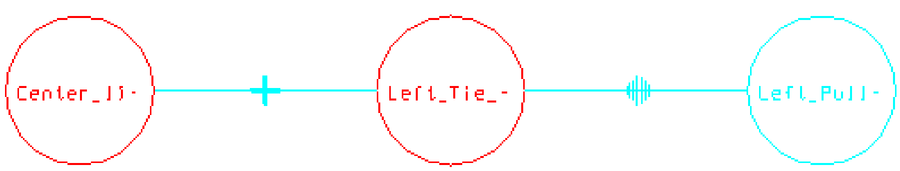

Figure A9 Graphical topology of left tie rod

The connection between the left tie rod and the center link is the Hooke joint; the connection between the left tie rod and the left pull arm is the spherical joint.

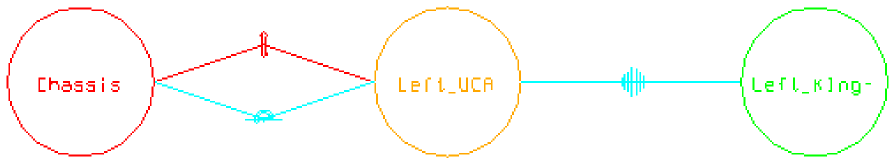

Figure A10 Graphical topology of left up control arm

The connection between the left up control arm and the chassis is revolute joint and spring force; the connection between the left kingpin and the left up control arm is spherical joint.

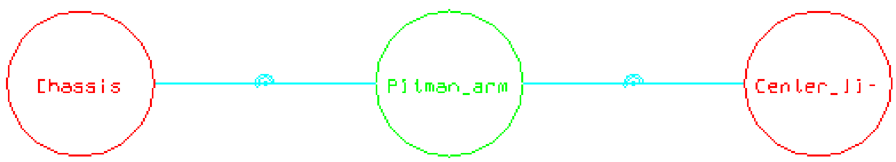

Figure A11 Graphical topology of pitman arm

The connection between the chassis and the pitman arm is revolute joint; the connection between the center link and the pitman arm is revolute joint.

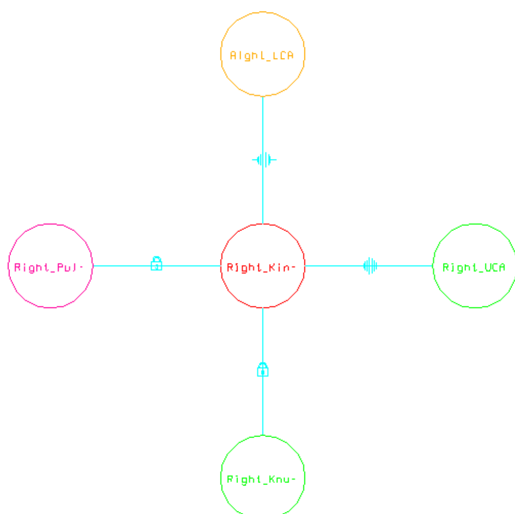

Figure A12 Graphical topology of right kingpin

The connection between the right kingpin and right low control arm is spherical joint; the connection between the right kingpin and the right pull arm is fixed joint; the connection between the right kingpin and the right up control arm is spherical joint; the connection between the right kingpin and the right knuckle is fixed joint.

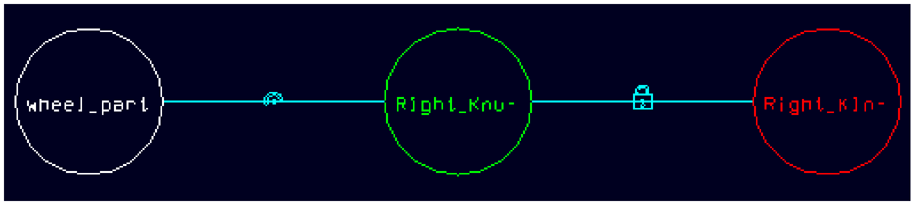

Figure A13 Graphical topology of right knuckle

The connection between the right front wheel and the right knuckle is the revolute joint; the connection between the right knuckle and the right kingpin is the fixed joint.

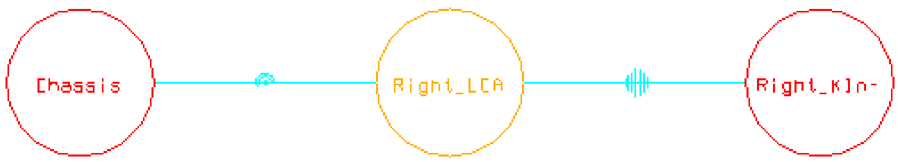

Figure A14 Graphical topology of right low control arm

The connection between the right low control arm and the chassis is the revolute joint; the connection between the right low control arm and the right kingpin is the spherical joint.

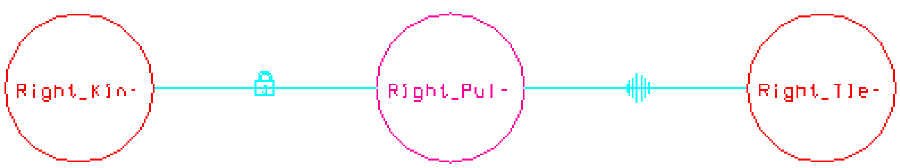

Figure A15 Graphical topology of right pull arm

The connection between the right pull arm and the right kingpin is the fixed joint; the connection between the right pull arm and the right tie rod is the spherical joint.

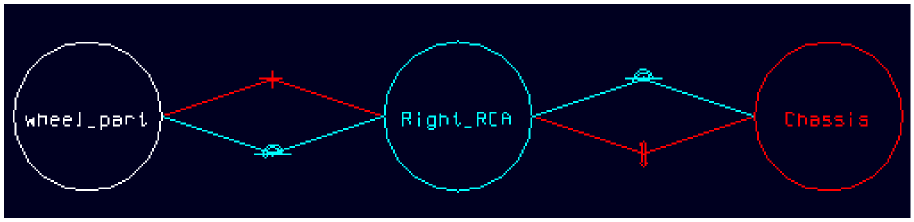

Figure A16 Graphical topology of right rear control arm

The connection between the right rear control arm and the right rear wheel is the revolute joint and the driving source; the connection between the right rear control arm and the chassis system is the revolute joint and the spring force.

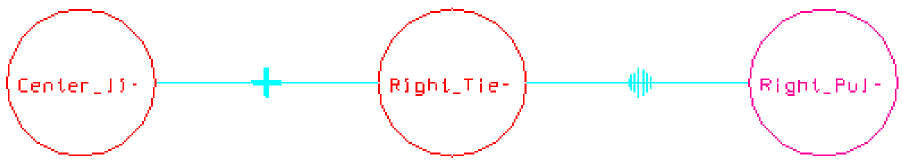

Figure A17 Graphical topology of right tie rod

The connection between the right tie rod and the center link is the Hooke joint; the connection between the right tie rod and the left pull arm is the spherical joint.

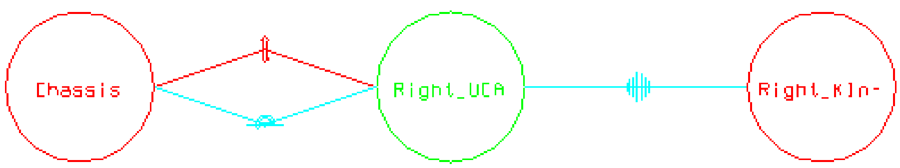

Figure A18 Graphical topology of right up control arm

The connection between the right up control arm and the chassis is revolute joint and spring force; the connection between the right kingpin and the right up control arm is spherical joint.

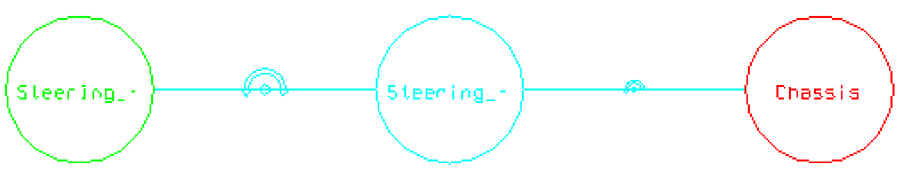

Figure A19 Graphical topology of steering gear

The connection between the steering gear and the steering shaft is the constant velocity joint; the connection between the steering gear and the chassis is the revolute joint.

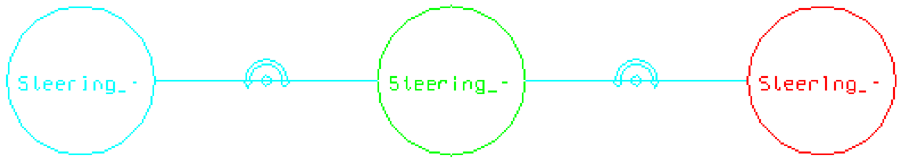

Figure A20 Graphical topology of steering shaft

The connection between the steering gear and the steering shaft is constant velocity joint; the connection between the steering gear and the steering wheel is the constant velocity joint.

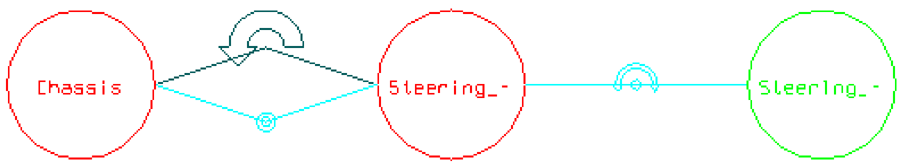

Figure A21 Graphical topology of steering wheel

The connection between the steering wheel and the chassis is the cylindrical joint and a driving motion; the connection between the steering wheel and the steering shaft is the constant velocity joint.

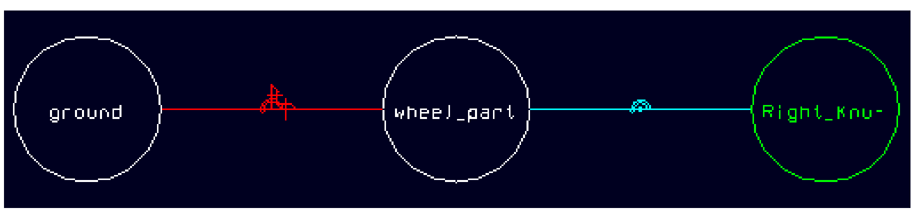

Figure A22 Graphical topology of right front wheel

The connection between the wheel part and the ground is the tire; the connection between the wheel part and the right knuckle is the revolute joint.

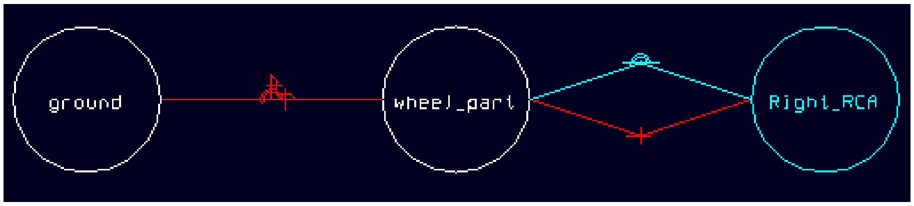

Figure A23 Graphical topology of right rear wheel

The connection between the wheel part and the ground is tire; the connection between the wheel part and the right rear control arm is the revolute joint and the driving source.

Appendix E Tire file in Adams/ View

```
$-------------------------------------------------------------------MDI_HEADER
[MDI_HEADER]
 FILE_TYPE     =  'tir'
 FILE_VERSION  =  2.0
 FILE_FORMAT   =  'ASCII'
(COMMENTS)
{comment_string}
'Tire      - XXXXXX'
'Pressure  - XXXXXX'
'Test Date - XXXXXX'
'Test tire'
'New File Format v2.1'
$------------------------------------------------------------------------units
[UNITS]
 LENGTH              = 'mm'
 FORCE               = 'newton'
 ANGLE               = 'degree'
 MASS                = 'kg'
 TIME                = 'sec'
$------------------------------------------------------------------------model
[MODEL]
!        use mode       1         2
!        -------------------------
!        smoothing                X
!
 PROPERTY_FILE_FORMAT    = 'FIALA'
 FUNCTION_NAME           = 'TYR902'
 USE_MODE                = 2.0
$--------------------------------------------------------------------dimension
```

```
[DIMENSION]
 UNLOADED_RADIUS         = 309.9
 WIDTH                   = 235.0
 ASPECT_RATIO            = 0.45
$-------------------------------------------------------------------parameter
[PARAMETER]
 VERTICAL_STIFFNESS      = 310.0
 VERTICAL_DAMPING        = 3.1
 ROLLING_RESISTANCE      = 0.0
 CSLIP                   = 1000.0
 CALPHA                  = 800.0
 CGAMMA                  = 0.0
 UMIN                    = 0.9
 UMAX                    = 1.0
$-----------------------------------------------------------------------shape
[SHAPE]
{radial width}
 1.0    0.0
 1.0    0.2
 1.0    0.4
 1.0    0.5
 1.0    0.6
 1.0    0.7
 1.0    0.8
 1.0    0.85
 1.0    0.9
 0.9    1.0
```

Appendix F Road file in Adams/ View

```
$------------------------------------------------------------------MDI_HEADER
[MDI_HEADER]
FILE_TYPE  =  'rdf'
FILE_VERSION  =  5.00
FILE_FORMAT  =  'ASCII'
(COMMENTS)
{comment_string}
'sine style road description'
$-----------------------------------------------------------------------UNITS
[UNITS]
 MASS              = 'kg'
 LENGTH            = 'mm'
 TIME              = 'sec'
 ANGLE             = 'degree'
 FORCE             = 'newton'
$-----------------------------------------------------------------------MODEL
[MODEL]
 METHOD            = '2D'
 FUNCTION_NAME     = 'ARC901'
 ROAD_TYPE         = 'sine'
$------------------------------------------------------------------PARAMETERS
[PARAMETERS]
 OFFSET                  =    0
 ROTATION_ANGLE_XY_PLANE =  180
 MU                      =  1.0
$
 START                   =  1000
 AMPLITUDE               =   50
 WAVE_LENGTH             =  2500
```

References

[1] N. Eslaminasab, "Development of a Semi-active Intelligent Suspension System for Heavy Vehicles, in Mechanical Engineering," PhD, Department of Mechanical Engineering, University of Waterloo, Waterloo, Ontario, Canada, 2008.

[2] H. P. Du, K. Y. Sze, and J. Lam, "Semi-active H-infinity control of vehicle suspension with magneto-rheological dampers," *Journal of Sound and Vibration,* vol. 283, pp. 981-996, May 20 2005.

[3] R. Rajamani, ed, *Vehicle dynamics and control*. New York: Springer press, 2006.

[4] C. Yue, "Control law designs for active suspensions in automotive vehicles," Master, Department of Mechanical Engineering, Massachusetts Institute of Technology, Cambridge,Massachusetts, U.S, 1987.

[5] J. Alanoly and S. Sankar, "A New Concept in Semi-Active Vibration Isolation," *Journal of Mechanisms Transmissions and Automation in Design-Transactions of the Asme,* vol. 109, pp. 242-247, Jun 1987.

[6] G. Z. Yao, F. F. Yap, G. Chen, W. H. Li, and S. H. Yeo, "MR damper and its application for semi-active control of vehicle suspension system," *Mechatronics,* vol. 12, pp. 963-973, Sep 2002.

[7] X. R. Zhang, H. Yamaguchi, X. D. Niu, and K. Nishioka, "Investigation of Impulse Response of an ER Fluid Viscous Damper," *Journal of Intelligent Material Systems and Structures,* vol. 21, pp. 423-435, Mar 2010.

[8] Y. Shen, M. F. Golnaraghi, and G. R. Heppler, "Semi-active vibration control schemes for suspension systems using magnetorheological dampers," *Journal of Vibration and Control,* vol. 12, pp. 3-24, Jan 2006.

[9] J. He, Y. K. Chen, C. H. Zhao, Z. G. Qi, and X. H. Ren, "Heavy truck suspension optimisation based on modified skyhook damping control," *International Journal of Heavy Vehicle Systems,* vol. 18, pp. 161-178, 2011.

[10] P. Kroneld, T. Liedes, and K. Nevala, "Optimal and skyhook - controlled suspension for a 4-axle heavy off-road vehicle," *Journal of Vibroengineering,* vol. 11, pp. 400-406, Sep 2009.

[11] S. B. Choi, D. W. Park, and M. S. Suh, "Fuzzy sky-ground hook control of a tracked vehicle featuring semi-active electrorheological suspension units," *Journal of Dynamic Systems Measurement and Control-Transactions of the Asme,* vol. 124, pp. 150-157, Mar 2002.

[12] M. Ahmadian and J. H. Koo, "A qualitative analysis of groundhook tuned vibration absorbers for controlling structural vibrations," *Proceedings of the Institution of Mechanical Engineers Part K-Journal of Multi-Body Dynamics,* vol. 216, pp. 351-359, 2002.

[13] C. Kim and P. I. Ro, "A sliding mode controller for vehicle active suspension systems with non-linearities," *Proceedings of the Institution of Mechanical Engineers Part D-Journal of Automobile Engineering,* vol. 212, pp. 79-92, 1998.

[14] C. Li, M. Liang, Y. X. Wang, and Y. T. Dong, "Vibration suppression using two-terminal flywheel. Part II: application to vehicle passive suspension," *Journal of Vibration and Control,* vol. 18, pp. 1353-1365, 2011.

[15] G. H. Donald Bastow, John P. Whitehead, Ed., *car suspensions and handling*. Pentech Press, London, 2004, p.^pp. Pages.

[16] L. Sun, "Optimum design of "road-friendly" vehicle suspension systems subjected to rough pavement surfaces," *Applied Mathematical Modelling,* vol. 26, pp. 635-652, May 2002.

[17] Z. Yu. (2009). *Vehicle Theory*.

[18] F. Gandhi and I. Chopra, "A time-domain non-linear viscoelastic damper model," *Smart Materials & Structures,* vol. 5, pp. 517-528, Oct 1996.

[19] G. M. Kamath and N. M. Wereley, "A nonlinear viscoelastic-plastic model for electrorheological fluids," *Smart Materials & Structures,* vol. 6, pp. 351-359, Jun 1997.

[20] Z. L. Fang Chang, "Air suspension performance analysis using nonlinear geometrical paramteres model," *SAE Technical Paper 2007-01-4270*, 2007.

[21] M. Berg, "A nonlinear rubber spring model for vehicle dynamics analysis," *Vehicle System Dynamics*, vol. 29, pp. 723-728, 1998.

[22] G. Litak, M. Borowiec, M. I. Friswell, and K. Szabelski, "Chaotic vibration of a quarter-car model excited by the road surface profile," *Communications in Nonlinear Science and Numerical Simulation,* vol. 13, pp. 1373-1383, Sep 2008.

[23] X. N. Xing and D. M. Zhang, "Realization of Nonlinear Describing Function Method Virtual Experiment System Based on LabVIEW," *International Conference of China Communication (Iccc2010),* pp. 211-213, 2010.

[24] M. Haeri, M. Attari, and M. S. Tavazoei, "Analysis of a fractional order Van der Pol-like oscillator via describing function method," *Nonlinear Dynamics,* vol. 61, pp. 265-274, Jul 2010.

[25] A. M. Elliott, M. A. Bernstein, H. A. Ward, J. Lane, and R. J. Witte, "Nonlinear averaging reconstruction method for phase-cycle SSFP," *Magnetic Resonance Imaging,* vol. 25, pp. 359-364, Apr 2007.

[26] A. N. Stanzhitskii and T. V. Dobrodzii, "Study of optimal control problems on the half-line by the averaging method," *Differential Equations,* vol. 47, pp. 264-277, Feb 2011.

[27] J. C. P. J. S.A. Billings, "Mapping nonlinear integro-differential equation into the frequency domain," *International Journal of Control*, vol. 54, pp. 863–879, 1990.

[28] Z. Q. Lang and S. A. Billings, "Output frequency characteristics of nonlinear systems," *International Journal of Control,* vol. 64, pp. 1049-1067, Aug 1996.

[29] X. J. Jing, Z. Q. Lang, and S. A. Billings, "Output frequency properties of nonlinear systems," *International Journal of Non-Linear Mechanics,* vol. 45, pp. 681-690, Sep 2010.

[30] S. A. B. R. Yue, Z.Q. Lang, "An investigation into the characteristics of non-linear frequency response functions. Part 1: understanding the higher dimensional frequency spaces," *International Journal of Control,* vol. 78, pp. 1031-1044, 2005.

[31] Z. Q. Lang, X. J. Jing, S. A. Billings, G. R. Tomlinson, and Z. K. Peng, "Theoretical study of the effects of nonlinear viscous damping on vibration isolation of sdof systems," *Journal of Sound and Vibration,* vol. 323, pp. 352-365, Jun 5 2009.

[32] X. J. Jing, Z. Q. Lang, and S. A. Billings, "Output frequency response function-based analysis for nonlinear Volterra systems," *Mechanical Systems and Signal Processing,* vol. 22, pp. 102-120, Jan 2008.

[33] X. J. Jing, Z. Q. Lang, and S. A. Billings, "Determination of the analytical parametric relationship for output spectrum of Volterra systems based on its parametric characteristics," *Journal of Mathematical Analysis and Applications,* vol. 351, pp. 694-706, Mar 15 2009.

[34] Z. K. Peng, Z. Q. Lang, S. A. Billings, and G. R. Tomlinson, "Comparisons between harmonic balance and nonlinear output frequency response function in nonlinear system analysis," *Journal of Sound and Vibration,* vol. 311, pp. 56-73, Mar 18 2008.

[35] X. J. Jing, Z. Q. Lang, S. A. Billings, and G. R. Tomlinson, "Frequency domain analysis for suppression of output vibration from periodic disturbance using nonlinearities," *Journal of Sound and Vibration,* vol. 314, pp. 536-557, Jul 22 2008.

[36] P. Eberhard, U. Piram, and D. Bestle, "Optimization of damping characteristics in vehicle dynamics," *Engineering Optimization,* vol. 31, pp. 435-455, 1999.

[37] D. Hrovat, "Survey of advanced suspension developments and related optimal control applications," *Automatica,* vol. 33, pp. 1781-1871, 1997.

[38] J. Wang and S. W. Shen, "Integrated vehicle ride and roll control via active suspensions," *Vehicle System Dynamics,* vol. 46, pp. 495-508, 2008.

[39] P. S. Els, "The applicability of ride comfort standards to off-road vehicles," *Journal of Terramechanics,* vol. 42, pp. 47-64, Jan 2005.

[40] Volterra, *Theory of functionals and of integral and integro-differential Equations*. New York: Dover Publications, 1959.

[41] X. J. Jing, Z. Q. Lang, and S. A. Billings, "Mapping from parametric characteristics to generalized frequency response functions of non-linear systems," *International Journal of Control,* vol. 81, pp. 1071-1088, 2008.

[42] Z. Q. Lang, Billings S A, Tomlinson G R, Yue R, "Analytical description of the effects of system nonlinearities on output frequency responses: A case study," *Journal of Sound and Vibration,* vol. 295, pp. 584-601, 2006.

[43] L. Z. Q. Jing X.J , S.A. Billings, "The parametric characteristics of frequency response functions for nonlinear systems," *International Journal of Control* vol. 79(12), pp. 1552–1564, 2006.

[44] R. Basso, "Experimental characterization of damping force in shock absorbers with constant velocity excitation," *Vehicle System Dynamics,* vol. 30, pp. 431-442, Dec 1998.

[45] C. C. Ward and K. Iagnemma, "Speed-independent vibration-based terrain classification for passenger vehicles," *Vehicle System Dynamics,* vol. 47, pp. 1095-1113, 2009.

[46] J. S. Lin and I. Kanellakopoulos, "Nonlinear design of active suspensions," *IEEE Control Systems Magazine,* vol. 17, pp. 45-59, Jun 1997.

[47] J. S. Lin and I. Kanellakopoulos, "Road-adaptive nonlinear design of active suspensions," *Proceedings of the 1997 American Control Conference, Vols 1-6,* pp. 714-718, 1997.

[48] I. Ballo, "Properties of air spring as a force generator in active vibration control systems," *Vehicle System Dynamics,* vol. 35, pp. 67-72, 2001.

[49] A. P. Fredrik Karlsson, "Modelling nonlinear dynamics of rubber bushinges- parameter identification and validation," Department of Structure Mechanics, Lund University, Lund, Scania, Sweden, 2003.

[50] C. Daniel, Wood, Fred S ; Gorman, John W, *Fitting equations to data : computer analysis of multifactor data*. New York: Wiley 1980.

[51] P. S. Hagan and G. West, "Interpolation methods for curve construction," *Applied Mathematical Finance,* vol. 13, pp. 89-129, 2006.

[52] W. Mathworld. (2012). *http://mathworld.wolfram.com/LeastSquaresFitting.html*.

[53] M. Software. (2010). *http://www.mscsoftware.com/Products/CAE-Tools/MD-Adams.aspx*.

[54] J. Li, *Adams shi li jiao cheng*. Beijing: Beijing Institute of Technology, 2002.

[55] D. H. Mike Blundell. (2004). *The Multibody Systems Approach to Vehicle Dynamics*.